Modelling the architecture of distal sand-rich lobe deposits: an example from Fan 2, Skoorsteenberg Formation, Tanqua Karoo, South Africa

by

Rochelle Steyn

Thesis presented in partial fulfilment of the requirements for the degree of Master of Science

at

Stellenbosch University

Department of Geology,
Geography and Environmental Studies

Supervisor: Dr H. de V. Wickens
Co-supervisor: Dr D. Hodgson

March 2009

Chapter 5

Stratigraphy and architectural elements

5. Stratigraphy and architectural elements

5.1. Stratigraphy

To simplify the lateral correlation of the vertical profiles, Middle Fan 2 was subdivided into three sandstone-lobe elements (designated 1, 2 and 3 from base to top) and two siltstone inter-lobe elements (designated A and B from base to top, Figure 77). There are also numerous siltstone intra-lobe elements found within the sandstone-lobe elements. They vary in thickness from less than a centimetre, thus a lamina, to 25 centimetres, thus a medium bed (Boggs, 2006), and are occasionally thicker than the siltstone inter-lobe elements, but not as laterally extensive.

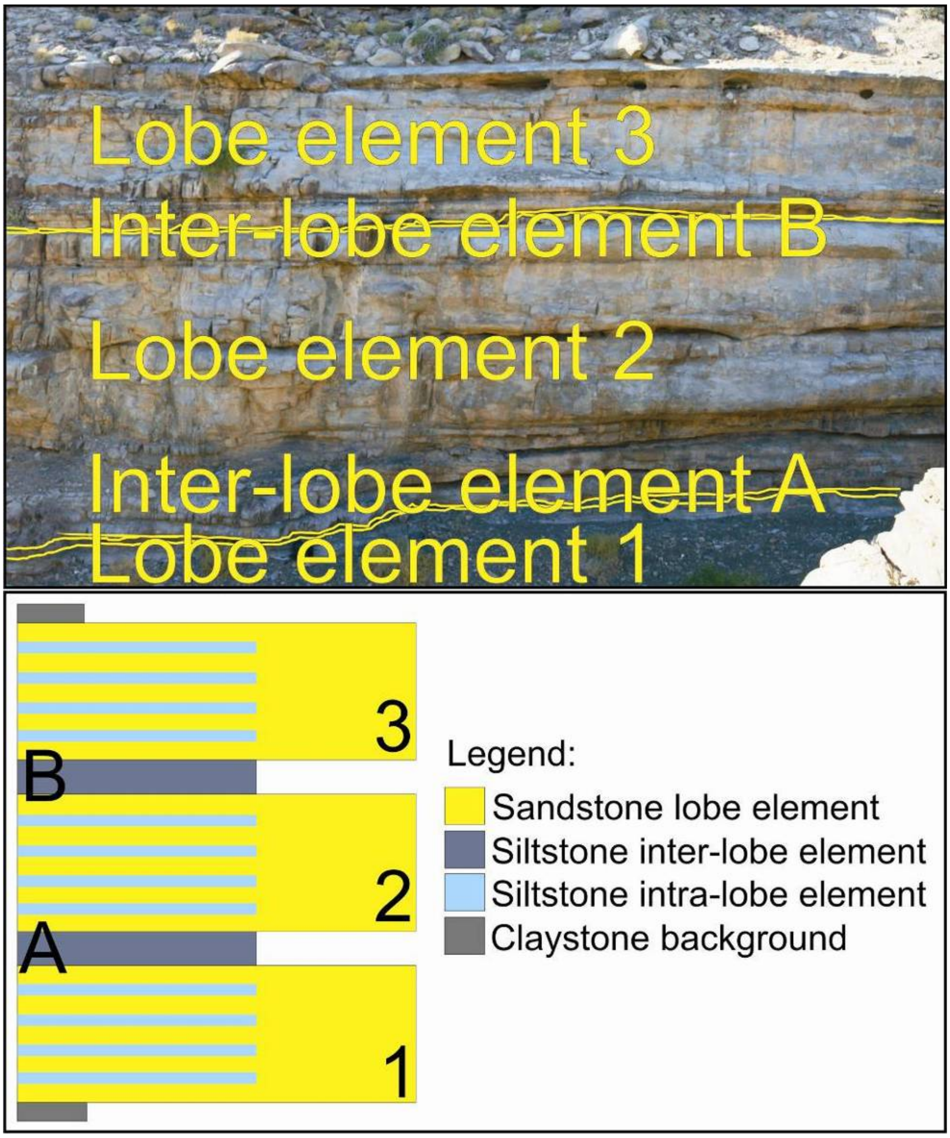

Figure 77: Diagram illustrating the internal stratigraphy of Middle Fan 2; photo location in the vicinity of vertical profile R00A (34H0399360/UTM6373789, on the farm Kleine Gemsbok Fontein 72).

5.2. Architectural elements

Only two types of architectural elements were recognised in the Middle Fan 2 outcrop, namely channel elements and sheet elements, making them the focus of this chapter. The outcrop data are represented as vertical profiles using CorelDraw (Figure 78).

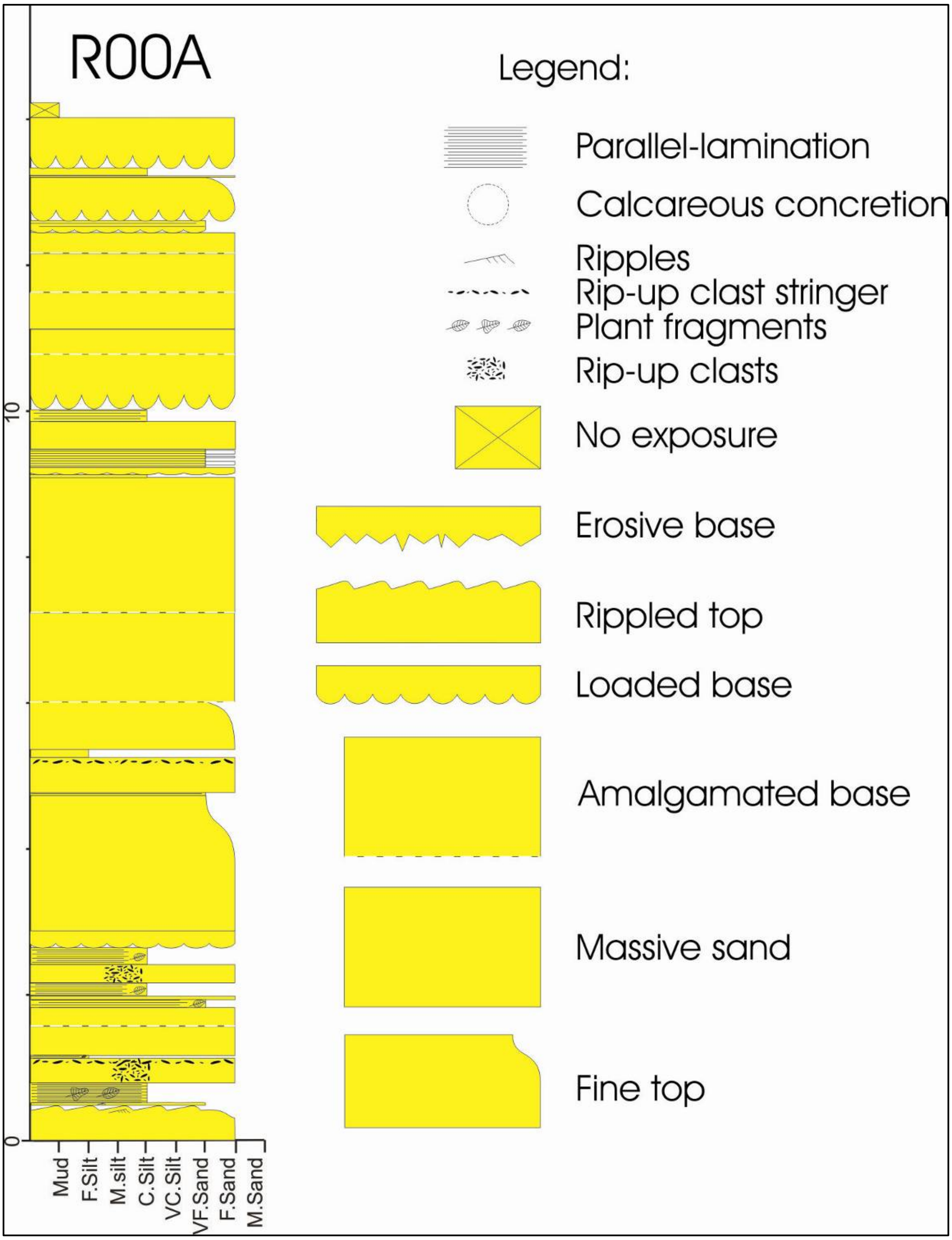

Figure 78: Profile R00A (34H0399360/UTM6373789) compiled in CorelDraw showing lithofacies and measured sedimentological features and a legend that includes all features that were used when creating the CorelDraw profiles.

5.2.1. Channel elements

Only two clear instances of channel elements were identified in strike sections in Middle Fan 2 (Figure 79). The lateral extent of the channels is 250 metres (Image B) and 100 metres (Image C). The channel elements are found in the same area as the proposed channel in the depositional model generated by Johnson *et al.,* (2001).

The geometry of the channel elements found in Middle Fan 2 can be described as “depositional and minor erosional” (Johnson *et al.,* 2001, p. 999). They are commonly found in mid-fan settings and are formed when a small amount of erosion at the base of the channel is followed by aggradational deposition. These channels change laterally into sheet deposits (Johnson *et al.,* 2001).

The channel elements are confined to the lobe-element scale, as they are found exclusively in sandstone-lobe-element 3. The channels erode into the underlying lobe-element 2, resulting in a thickened lobe-element 3 overlying a thinned lobe-element 2, which is an indication of compensational stacking.

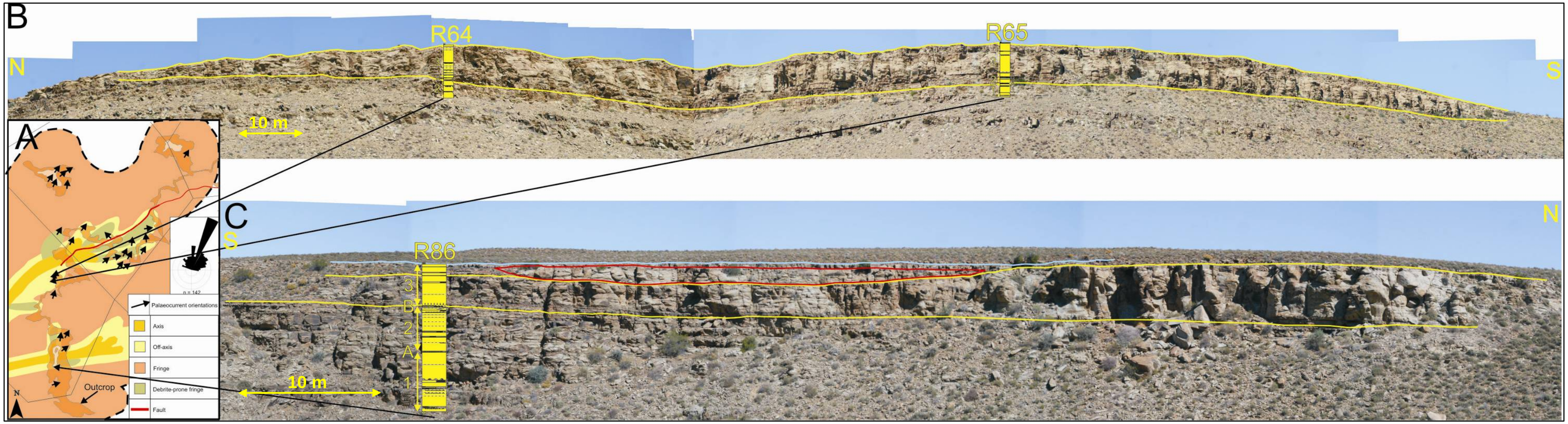

Figure 79: Image A shows the depositional model for Middle Fan 2 generated in this study.

Image B is a photomontage showing the positions of vertical profiles R64 (34H0396418/UTM6373257) and R65 (34H0396282/UTM6373117). It is viewed towards the east. The channel (outlined in yellow) can be seen to thin laterally to both the north and south. The sandstone beds in the channelised area thicken substantially towards the axis of the channel where they amalgamate to form a vertically stacked sandstone package. The lateral extent of the channelised area is 250 metres. The vertical scale equals the horizontal scale.

Image C is a photomontage showing the position of vertical profile R86 (34H0396326/UTM6368930). It is viewed towards the west. Two channel-fills (in yellow and red) can be seen. The channel-fill outlined in yellow comprises a sandstone bed that thickens laterally from south to north as the compactional drape probably obliterated the original channel shape. The channel-fill outlined in red thins laterally to the south and north. The sandstone bed indicated by the blue line is an overlying bed that retains the same thickness throughout. The lateral extent of the channelised area is 100 metres. The vertical scale equals the horizontal scale.

The outcrop locations of both the channels are on the farm Kleine Riet Fontein 88. The legend can be seen in Figure 78, page 74.

5.2.2. Sheet elements

Amalgamated sheets appear as massive sandstone, because less than 30% of the sediments are composed of siltstone or claystone. They occur in the mid- to outer regions of fans. Layered sheets incorporate more than 40% siltstone and claystone, and occur in mid- to upper regions of the fan (Johnson *et al.,* 2001). Examples of layered and amalgamated sheets can be seen in Figure 80.

The majority of sediments in the study area can be described as being deposited in a “transitional depositional style” (Johnson *et al.,* 2001, p. 999), mainly in the form of amalgamated and layered sheets. The sheets are described as tabular bodies with internal scouring and very few subordinate channel-fills. They commonly show compensational stacking and are composed of turbidite sandstone beds of varying thickness (Johnson *et al.,* 2001).

The amalgamated sheet elements are found at a lobe-element scale in all three sandstone-lobe elements. The sheet elements are also found at a lobe-element scale, but they are predominantly confined to lobe-element 3.

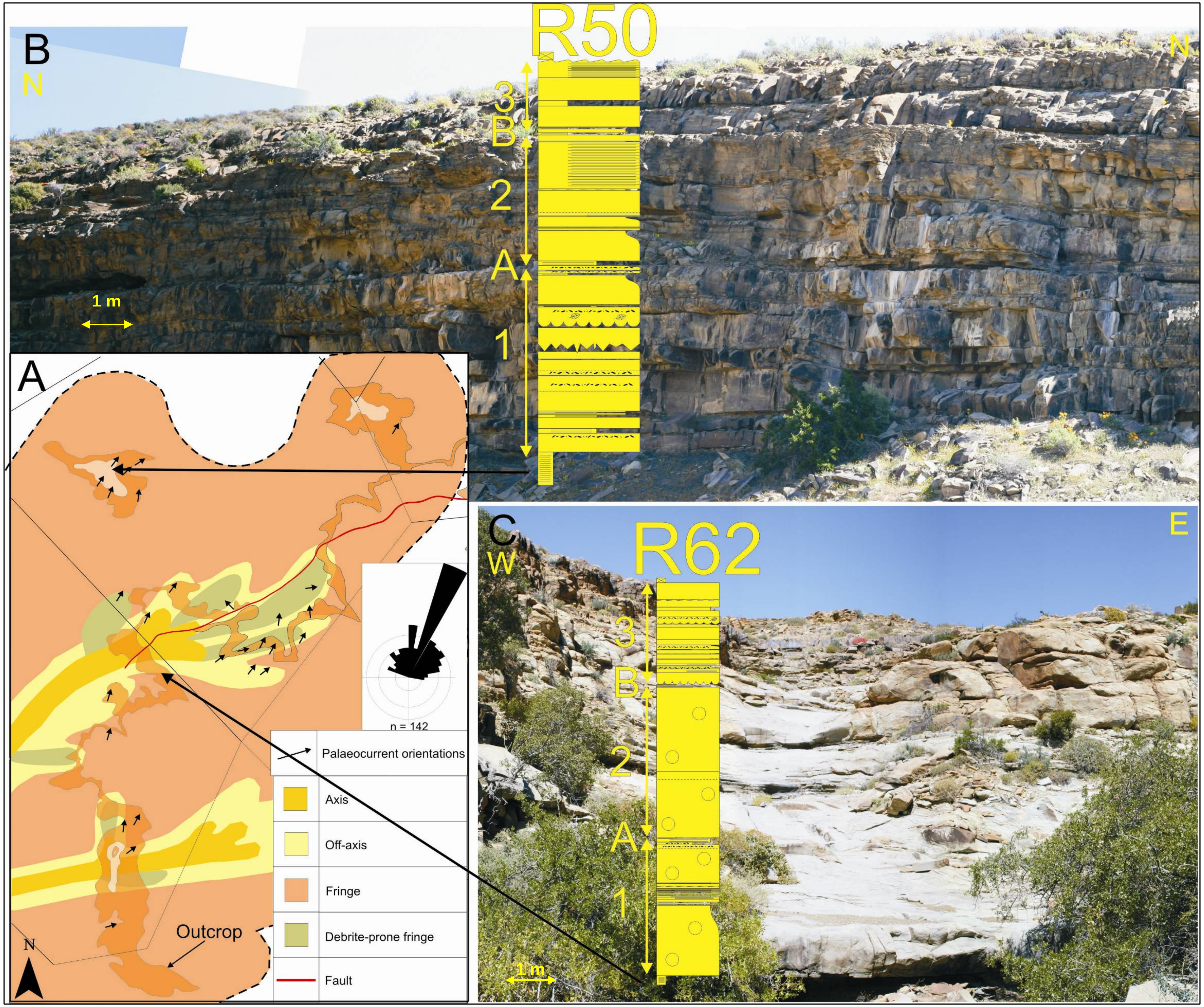

Figure 80: Image A shows the depositional model for Middle Fan 2 generated by this study.

Image B shows vertical profile R50 (34H0396732/UTM6376847) with layered sheets constituting the lobe elements. The sheets in this location are thinner than in the rest of the study area as each of the lobe elements are made up of numerous thin turbidite sandstone beds. This is due to the area being further away from the updip channelised area as it lies along the dip direction. The vertical scale equals the horizontal scale.

Note the parallel-laminated nature of beds in lobe elements 2 and 3, and the rip-up clasts at the base of sandstone beds in lobe-element 1.

Image C shows the position of vertical profile R62 (34H0396964/UTM6372859) with massive amalgamated sandstone beds forming the thick sandstone units. Very few siltstone beds are present. The vertical scale equals the horizontal scale.

Note the highly-amalgamated nature of the sandstone beds in lobe-element 2 and the profusion of secondary calcareous concretions. Rip-up clasts are found at the top of sandstone beds in lobe elements 1 and 3.

The legend can be seen in Figure 78, page 74.

5.3. Correlation panels

Complete correlation panels for the entire study area (Figure 81) incorporating Petrel panels, CorelDraw panels and descriptive photomontages were generated (Figure 82 – Figure 88). The locations of correlation panels 1 – 7 are delineated in an ArcView map (Figure 81).

The nature of the study area is such that the best outcrop exposure is found in the back of gullies with little or no outcrop linking them together that can be walked or traced out. It is often also impossible to see more than one vertical-profile location at any one time. As a result, the only lateral correlations that can be made with any certainty are the darker-weathering sandstone at the top of lobe-element 3 and the siltstone inter-lobe elements A and B (Chapter 1.4).

The presence of siltstone intra-lobe elements, which are occasionally thicker and may appear to be more laterally extensive than the siltstone inter-lobe elements, further decreases the reliability of lateral correlation, so that the correlation between these intra-lobe elements is most commonly inferred. An example of these inferred correlations can be seen in Correlation Panel 1 (Figure 82) between vertical profiles R00A, R01B and R01A. Co-genetic debrites (indicated in light green on Image B) pinch out within 10 to 15 metres, which makes it impossible for the debrites measured in vertical profiles R00A and R01A to cross over to profile R01B. However, there is an inferred link between the debrites and the intra-lobe siltstones in the neighbouring profiles that was retained for the purposes of simulating the internal variation within the lobe elements.

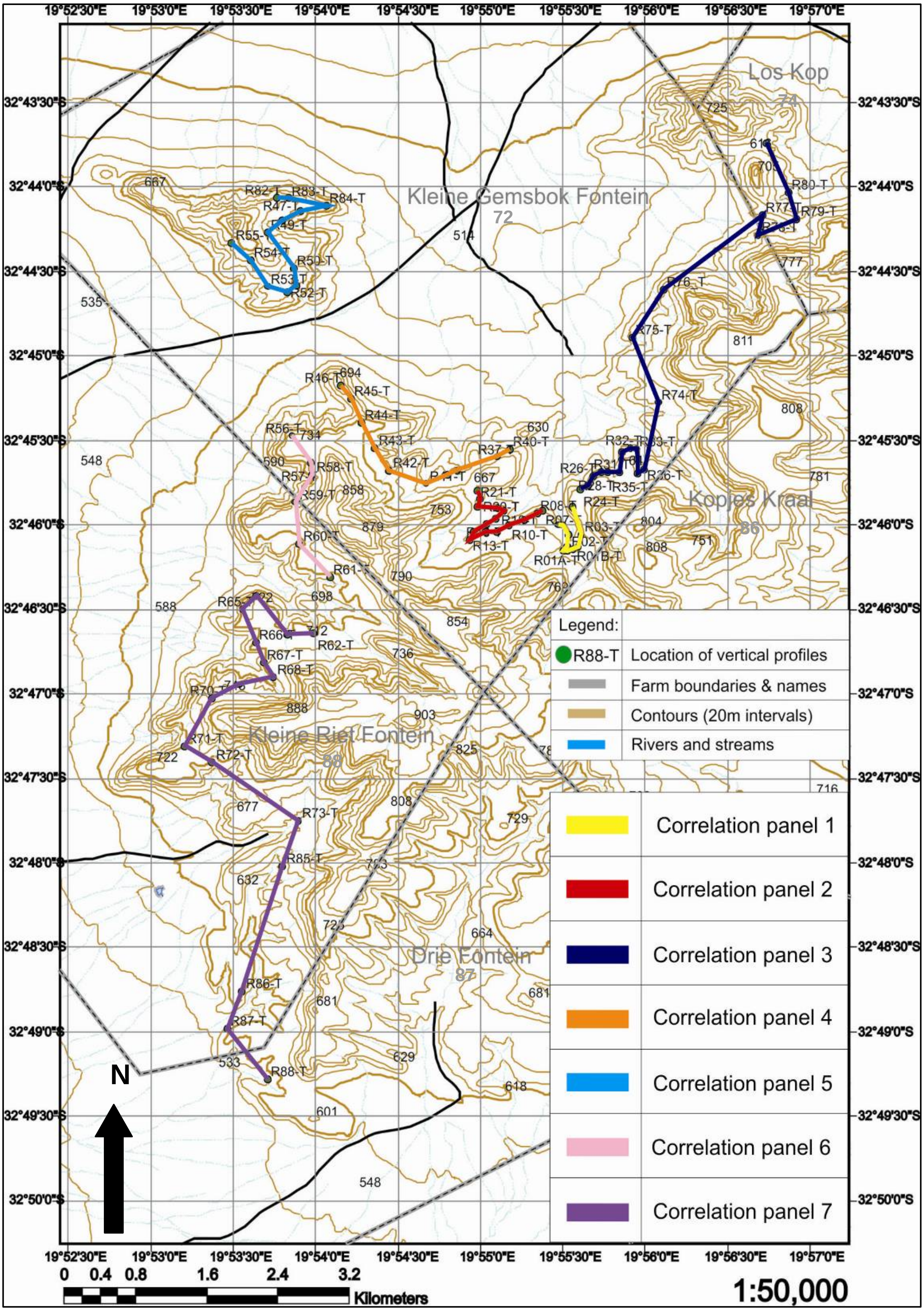

Figure 81: ArcView map of study area showing location of correlation panels 1 – 7.

Correlation panel 1 (Figure 82) represents the type locality of Middle Fan 2 (Image A). Twelve vertical profiles were measured, namely R06, R04, R03, R01A, R01B, R00A, R00B, R00C, R02, R05A, R05B and R07 (Image B), of which R00A, R00B, R00C, R01A, R01B and R02 offer the best-quality outcrop. The vertical thickness of the most complete profiles is approximately 17 metres. Other profiles, such as R03 and R05B, have sections with little or no exposure, limiting the vertical thickness to ~10 and ~14 metres, respectively.

Siltstone inter-lobe elements A and B are well-exposed throughout the area covered by the correlation panel, along with many siltstone intra-lobe elements. Some of the profiles contain massive sandstones formed due to amalgamation, such as profiles R00B and R00C. There are also instances of loading at the bases of massive sandstones and secondary concretions are commonly observed (Image B).

Lobe-element 1 is composed of mainly massive sandstone (dark yellow), whereas lobe elements 2 and 3 are composed of a mixture of massive sandstone (dark yellow), thin-bedded siltstone (blue) and thin-bedded sandstone (peach). The top of lobe-element 3 and the base of lobe-element 1 represent type 2 horizons or sequence boundaries, and siltstone inter-lobe elements A and B represent type 3 horizons. Lobe elements 1, 2 and 3 show compensational stacking across the area covered by the correlation panel as the lobe elements thicken and thin, but Middle Fan 2 retains the same average thickness throughout (Image B).

Petrel correlation panels (Image C) were generated to illustrate the differences between the measured vertical profiles (input data, left-hand column) and the up-scaled vertical-profile data generated by Petrel (output data, right-hand column). The input data were classified according to the original 17 DSL facies; the output data were reduced to 5 facies.

Correlation panel 1

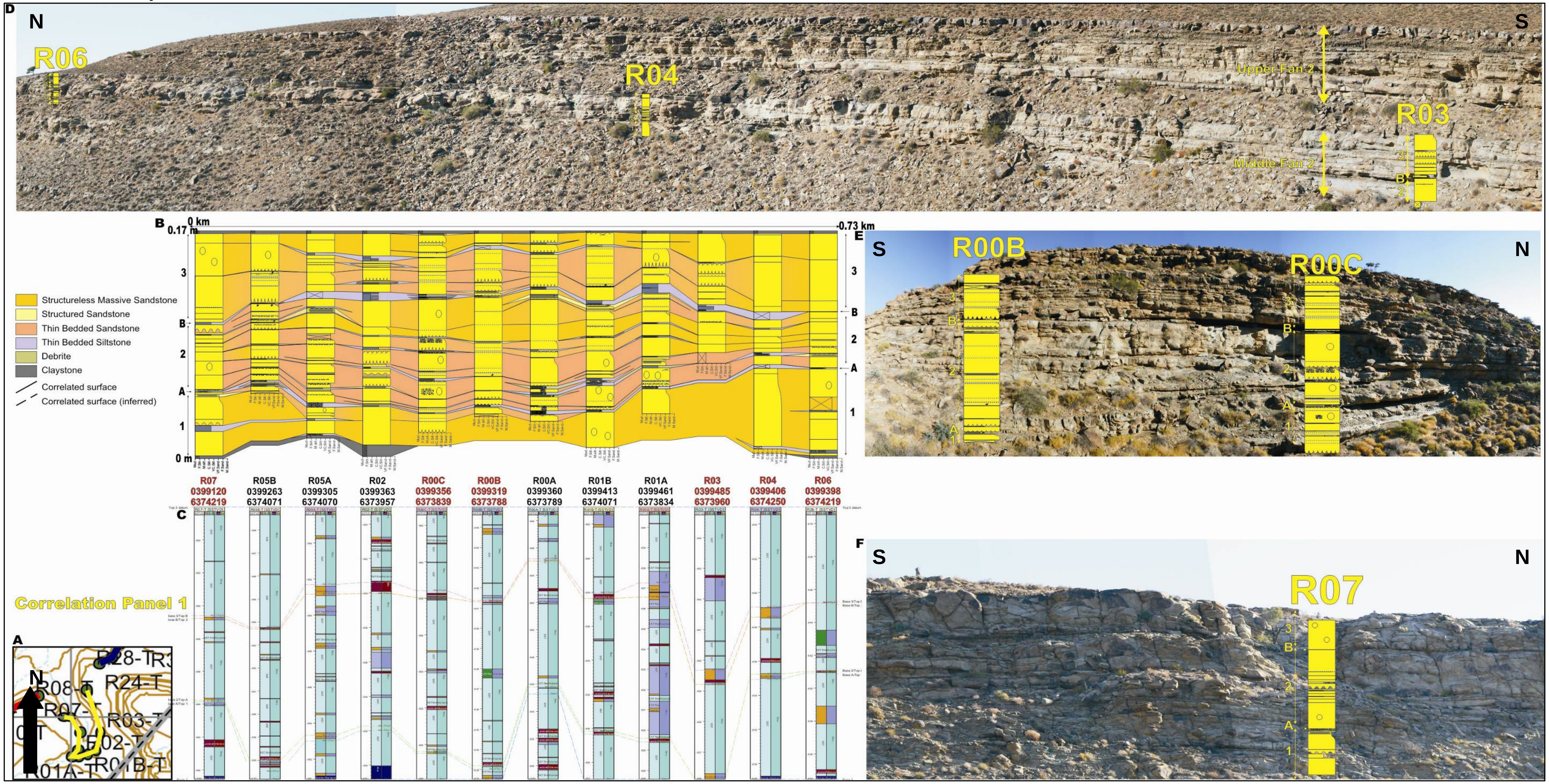

Figure 82: Correlation panel 1 of vertical profiles R06, R04, R03, R01A, R01B, R00A, R00B, R00C, R02, R05A, R05B and R07.

A: Location map of the profiles on the farm Kleine Gemsbok Fontein 72.

B: CorelDraw profiles were correlated to illustrate the largely massive sandstones of lobe-element 1, the thin-bedded sandstones of lobe-element 2 and the combination of the two facies in lobe-element 3.

C: Petrel profiles – note the dashed lines indicating the location of inter-lobe elements A and B throughout the panel, and in the process subdividing the lobe into lobe elements 1, 2 and 3.

D: The photopanel of R06, R04 andR03 illustrates that Middle and Upper Fan 2 are present in outcrop. Much of lobe-element 1 is obscured by scree or has been eroded away.

E: The photopanel of R00B and R00C illustrates the bedded nature of the lobe-element 3 and the poor exposure of lobe-element 1 due to obstruction by scree and sediment on the gully floor. Also note the amount of loading at the base of sandstone beds in this outcrop location.

F: The photopanel of R07 illustrates the amalgamated nature of the sandstone beds in lobe-element 3 and the top of lobe-element 2.

Panorama photomontages were taken of outcrop sections and the vertical profiles were superimposed over them. These include profiles R03, R04 and R06 (Image D), R00B and R00C (Image E) and R07 (Image F). Images E and F visually illustrate the massive amalgamated sandstones in outcrop with siltstones interspersed between them, as each of the deeper-weathering breaks between the sandstones. Also visible is the darker-weathering sandstone layer at the top of lobe-element 3.

Correlation panel 2 (Figure 83) represents 16 measured profiles, namely R08, R09, R10, R11, R12, R13, R14, R15, R16, R17, R18, R19, R20, R21, R22 and R23. Good vertical exposure of all the lobe elements can be seen from profiles R08 to R13, R15, R16 and R19. The remaining seven profiles have poor exposure at top or base due to scree-cover. The average thickness of Middle Fan 2 in this area is ~13 metres.

The area represented by correlation panel 2 is mostly composed of massive amalgamated sandstones (dark yellow) that show loading at the base and ripple cross-lamination at the top and compensational stacking. Concretions are also common. The thickness of Middle Fan 2 decreases from south-east to north-west across the correlation panel, which corresponds to a north-westerly direction on the outcrop map.

Panorama photomontages were taken of outcrop sections and the vertical profiles were superimposed over them. These include profiles R08, R09 and R06 (Image D), R00B and R00C (Image E) and R07 (Image F). Image E shows clearly defined massive amalgamated sandstones with interspersed siltstone breaks.

Correlation panel 2

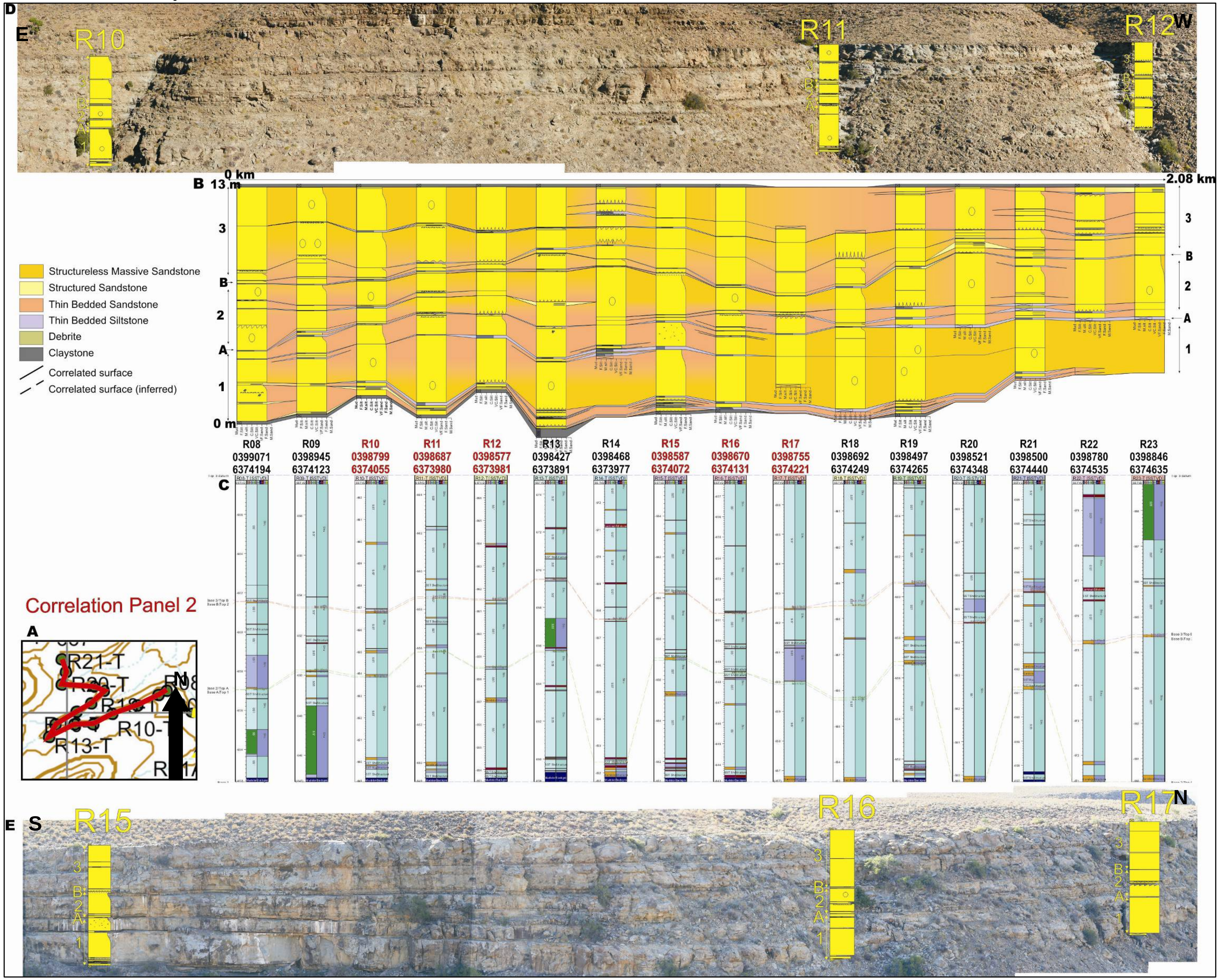

Figure 83: Correlation panel 2 of vertical profiles R08, R09, R10, R11, R12, R13, R14, R15, R16, R17, R18, R19, R20, R21, R22 and R23.

A: Location map of the profiles on the farm Kleine Gemsbok Fontein 72.

B: CorelDraw profiles were correlated to illustrate the variation from thin-bedded to massive sandstone from left (south-east) to right (north-west) across the panel for lobe-element 1, and the variation from massive to thin-bedded sandstone from left (east) to right (west) across lobe-element 3. Lobe-element 2 shows a combination of massive and thin-bedded sandstone. There is a zone of thin-bedded sandstones and siltstones at the bottom of lobe-element 1 (3 – 10 cm in thickness).

C: The Petrel profiles highlight the predominance of thin-bedded sandstones and siltstones at the base of lobe-element 1, and the location of structured sandstones (indicated in green and dark blue).

D: The photopanel of R08, R09, R10, R11, R12 shows the good quality outcrop enabling lobe elements to be traced out laterally. The photopanel is viewed to the south.

E: The photopanel of R15, R16, R17 shows the good quality outcrop, especially surrounding profile R15, enabling accurate lateral correlation. It also illustrates the bedded nature of the lobe elements in this location.

Correlation panel 3 (Figure 84) represents 20 measured profiles, namely R81, R80, R79, R78, R76, R75, R74, R36, R35, R34, R33, R32, R31, R30, R29, R28, R27, R26, R25 and R24. Vertical profiles R24, R25, R26, R34, R35, R36 and R74 show reasonably complete outcrop with all three lobe elements present. The remaining profiles, especially R30 through to R34, illustrate very incomplete outcrop, with sections of the lobe elements weathered or unexposed at base, top, or both. This leaves the outcrop with no definite frame of reference, making the correlation with surrounding profiles less accurate. The average thickness of Middle Fan 2 represented by this correlation panel is ~11 metres.

There is a decrease in thickness from right to left across the correlation panel, which corresponds to a decrease in thickness from south-west to north-east on the outcrop map (Image B).

The outcrop in this area is predominantly composed of amalgamated sandstone sheets (dark yellow) and sheets (peach), with the siltstone inter-lobe elements A and B (blue) present throughout all the profiles except R79, R80 and R81. The lobe elements are further sub-divided by siltstone intra-lobe elements of varying thickness (blue). Loading can be found at the bases of some of the amalgamated sandstone sheets; parallel- and ripple cross-laminations are less common. Many instances of rip-up clasts can be observed, although secondary concretions are less common.

Image D illustrates some of the poorer outcrop seen in this correlation panel, with the base of lobe-element 1 often obscured by scree. Image E has some of the better outcrop in this correlation panel, as is often found in the back of gullies. Note the bench-like appearance of the massive sandstones in profile R35 where the siltstone inter- and intra-lobe elements were eroded away.

Correlation panel 3

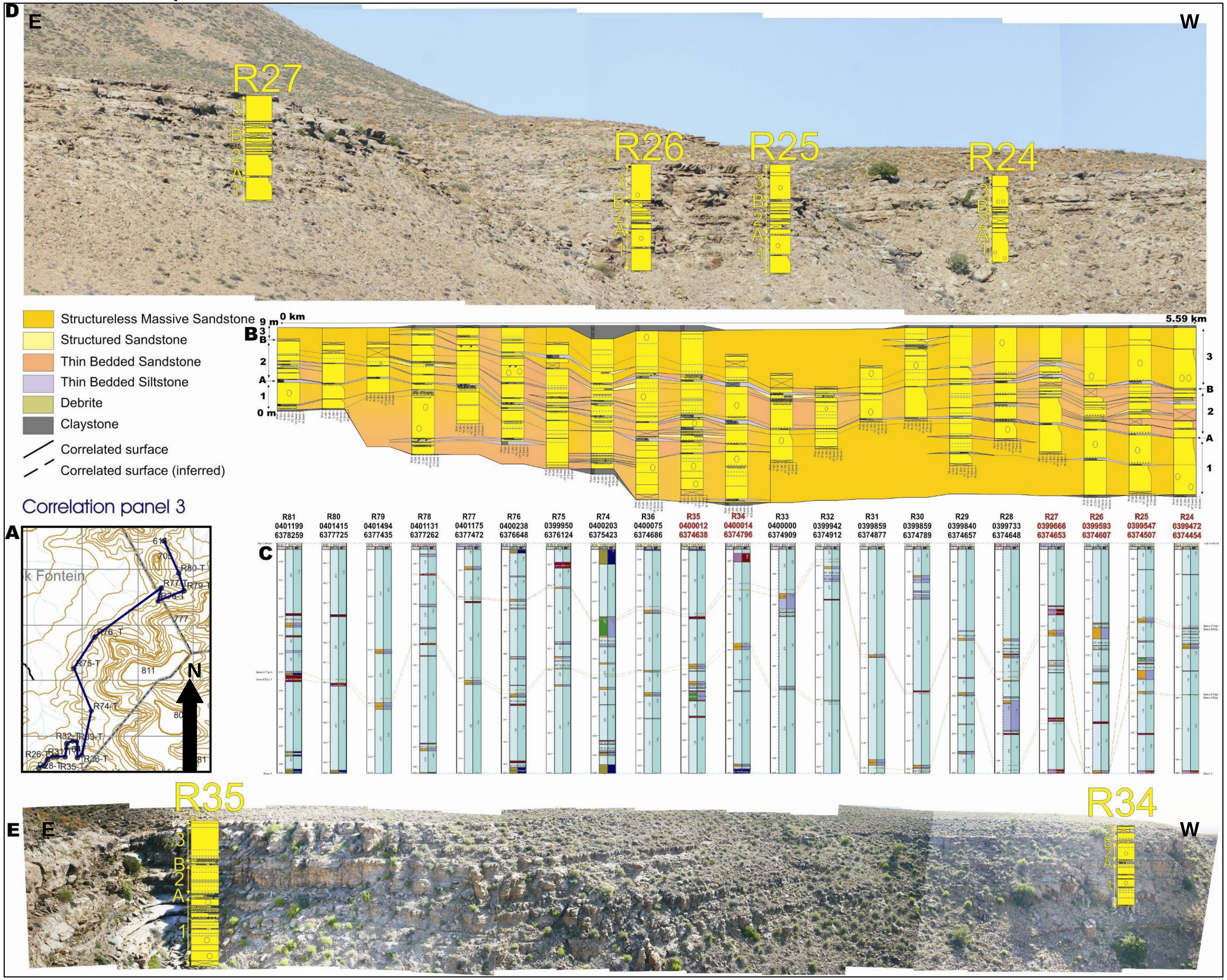

Figure 84: Correlation panel 3 of vertical profiles R81, R80, R79, R78, R76, R75, R74, R36, R35, R34, R33, R32, R31, R30, R29, R28, R27, R26, R25 and R24.

A: Location map of the profiles on the farms Kleine Gemsbok Fontein 72 and Los Kop 74.

B: CorelDraw profiles were correlated to illustrate the predominantly massive nature of the sandstone in lobe elements 1 and 3. It also highlights the structured, bedded nature of lobe-element 2. All three lobe elements thin significantly from right to left across the outcrop. This is equivalent to a thinning from west to east across the location map in the direction of the pinch out to the north-east. Also note the poor outcrop data available in profiles R31 to R33 due to erosion of lobe-element 3 and scree cover over lobe-element 1.

C: Petrel profiles – note the artificial exaggeration of the thickness of profiles R31 to R33 as Petrel stretches the available data of all the profiles to assume the same thickness.

D: The photopanel of R27, R26, R25, R24 illustrates some of the poorer outcrop quality encountered in the study area. Much of the outcrop is obscured by scree or eroded away. The photopanel is viewed towards the south.

E: The photopanel of R35 shows the typical good-quality outcrop in the back of a gully and the poor-quality outcrop outside of the gully, making correlation between profiles R35 and R34 more difficult. Note the ledge-like weathering of the massive sandstone in lobe-element 1 of profile R35.

Correlation panel 4 (Figure 85) represents 8 measured profiles, namely R38, R39, R41, R42, R43, R44, R45, and R46. Vertical profiles R38, R41, R42 and R43 illustrate complete outcrop for all the lobe elements. Profiles R39, R44, R45 and R46 have the base of lobe-element 1 obscured by scree.

The outcrop thins from east to west across the correlation panel, in a north-westerly direction on the outcrop map (Image A). The average thickness of the outcrop across this correlation panel is ~11 metres.

The outcrop (Image B) is predominantly composed of sheets (peach), but some amalgamated sheets (dark yellow) are also present. Loading and rip-up clasts are visible in some of the profiles. Parallel-lamination commonly occurs in lobe-element 3 (light yellow). Siltstone inter- and intra-lobe elements are present throughout (blue).

Images D, E and F, representing profiles R43, R41 and R42 respectively, illustrate the best outcrop in the correlation panel. Each of the sandstone-lobe elements can be clearly distinguished, as well as the various siltstone breaks.

Correlation panel 5 (Figure 86) represents 12 measured profiles, namely R55, R54, R53, R52, R51, R50, R49, R48, R47, R84, R83, and R82. Vertical profiles R55, R54, R52, R50, R49 and R48 illustrate complete outcrop for all the lobe elements. Profiles R47, R84, R83 and R82 are the least complete and lie furthest to the north.

The correlation panel arranges the outcrop in the shape of an “M”, with the middle sections of the “M” being thicker towards the east, and the legs of the “M” thinning towards the west (Image A). The average thickness of the outcrop across this correlation panel is ~9 metres. The outcrop is predominantly composed of amalgamated sandstone sheets (Image D), sandstone sheets (Image E), and parallel-laminated sandstones (Image F), represented in dark yellow, peach and light yellow, respectively, on Image B. Loading, rip-up clasts and plant fragments are commonly visible.

Correlation panel 4

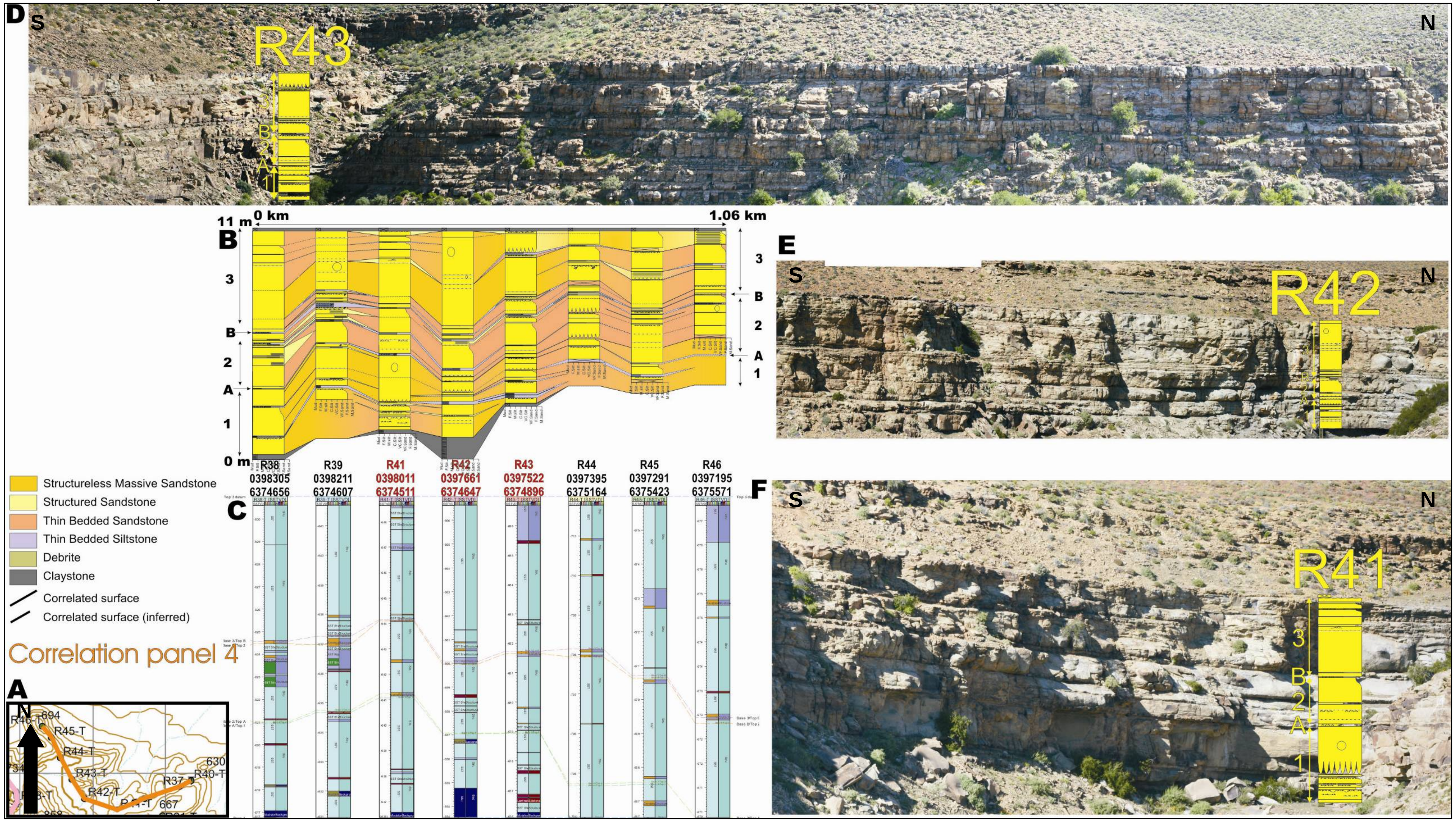

Figure 85: Correlation panel 4 of vertical profiles R38, R39, R41, R42, R43, R44, R45, and R46.

A: Location map of the profiles on the farm Kleine Gemsbok Fontein 72.

B: Correlated CorelDraw profiles illustrate the largely massive nature of the sandstone in lobe-element 3, the thin-bedded (3 – 10 cm) nature of sandstone in lobe-element 2, and the combination of the two facies in lobe-element 1. The correlation panel also illustrates the larger amount of siltstone intra-lobe elements present in this area.

C: Petrel profiles R38 and R39 mimic the thin-bedded nature of lobe-element 2.

D: The photopanel of R43 illustrates the excellent quality outcrop typical of the area covered by this correlation panel. Note the highly bedded areas interspersed with massive sandstone, and the lateral extent of lobe elements 2 and 3.

E: The photopanel of R42 highlights the thin-bedded sandstone nature of lobe-element 1, in comparison with F:, where the photopanel of R41 shows that only the lower half of lobe-element 1 is bedded, whereas the upper half is composed of massive sandstone. This change in facies occurs over a distance of 350 metres.

Correlation panel 5

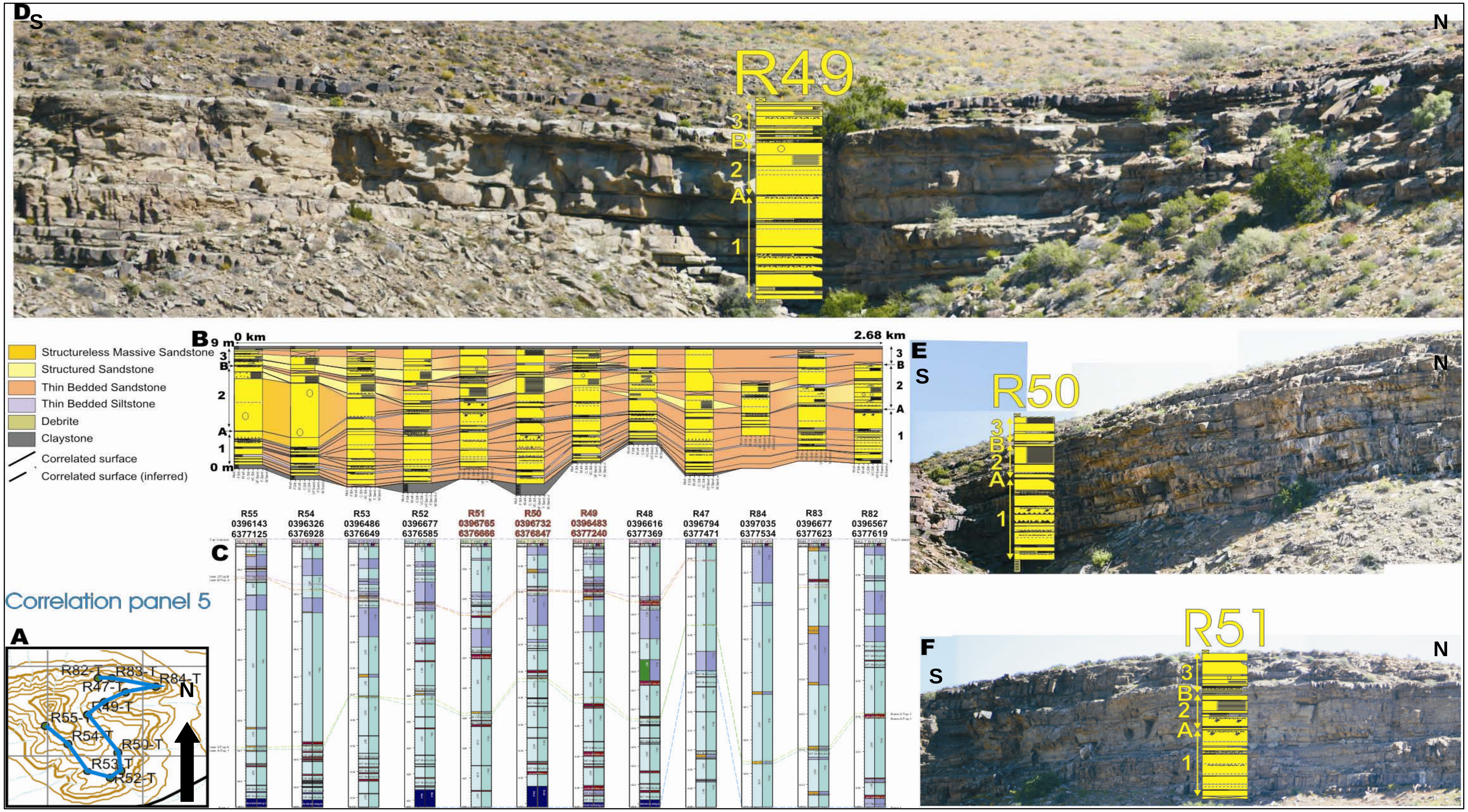

Figure 86: Correlation panel 5 of vertical profiles R55, R54, R53, R52, R51, R50, R49, R48, R47, R84, R83 and R82.

A: Location map of the profiles on the farm Kleine Gemsbok Fontein 72.

B: Correlated CorelDraw profiles illustrate the predominantly thin-bedded sandstone that predominates in this area. There are also many instances of structured sandstone, especially in lobe elements 2 and 3, which are predominantly composed of parallel-laminated sandstone. Note the large amount of siltstone intra-lobe elements.

C: The Petrel profiles in this correlation panel allow for the beds composed of structured sandstones to be clearly distinguished by their darker blue colour. They are commonly found in lobe-element 3 and the top half of lobe-element 2.

D: The photopanel of R49 shows the thin beds (3 – 10 cm) of lobe elements 1 and 3, and the amalgamated sandstones of lobe-element 3.

E: The photopanels of R50 and F: R51 illustrate the thin-bedded sandstones commonly found in this part of the study area. Note the parallel-laminated beds seen in lobe elements 2 and 3.

Correlation panel 6 (Figure 87) represents 6 measured profiles, namely R56, R57, R58, R59, R60, and R61. Only vertical profile R58 shows complete outcrop. Each of the other profiles has the lower half of lobe-element 1 obscured by scree.

The outcrop thickens from left (north-west) to right (south-east) across the correlation panel, in a south-easterly direction on the outcrop map (Image A). The average thickness of the outcrop across this correlation panel is ~12 metres. The outcrop varies from sheets (peach) to amalgamated sheets (dark yellow) from left to right across the panel. The amount of siltstone inter- and intra-lobe elements also decreases from left to right.

Images D and E represent a change-over from less-amalgamated to more-amalgamated sandstones as the outcrop area progresses from R58 to R60, in a south-easterly direction.

Correlation panel 7 (Figure 88) represents 6 measured profiles, namely R62, R63, R64, R65, R66, R67, R68, R69, R70, R71, R72, R73, R85, R86, R87 and R88. Seven profiles scattered throughout the correlation panel show complete outcrops; the remaining profiles are missing part of lobe-element 1 due to weathering or scree-cover. The outcrop shows a generally thickening trend from north north-west to south south-east across the correlation panel, in a south south-easterly direction on the outcrop map (Image A). The average thickness of the outcrop across this correlation panel is ~16.5 metres, making it the thickest correlation panel in the study area.

Two instances of channels can be seen in this correlation panel, namely the areas surrounding profiles R64 and R65, and the area around R86. Loading, parallel-lamination (light yellow), sandstone sheets (peach) and amalgamated sandstones (dark yellow) are common. There are fewer siltstone inter- and intra-lobe elements (blue) in this correlation panel than in the previous panels. All of these elements can be seen in Image E of profile R85.

Correlation panel 6

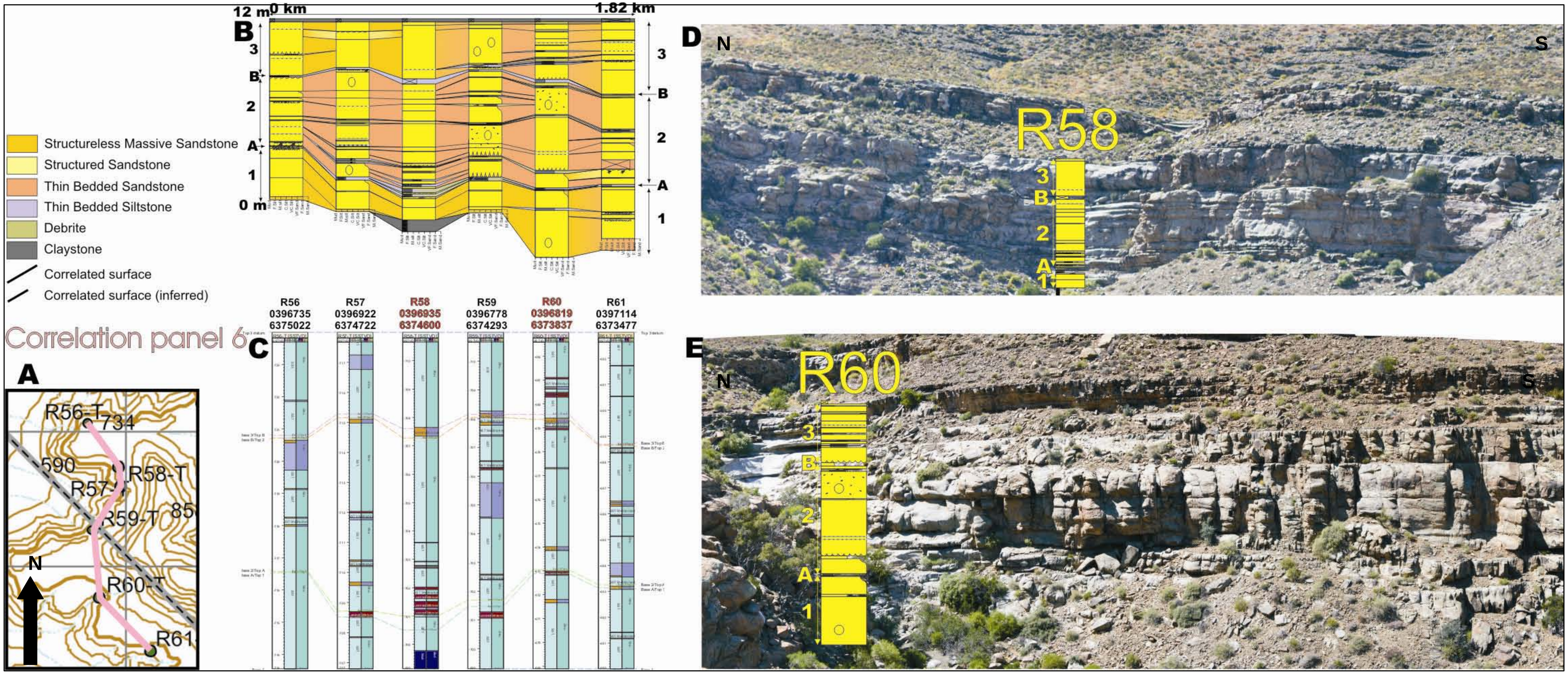

Figure 87: Correlation panel 6 of vertical profiles R56, R57, R58, R59, R60 and R61.

A: Location map of the profiles on the farms Kleine Gemsbok Fontein 72 and Kleine Riet Fontein 88.

B: Correlated CorelDraw profiles show that lobe elements 1 and 3 are largely composed of massive sandstone, but that it changes to thin-bedded sandstone to the right side (east side) of the panel. Lobe-element 2 is largely composed of thin-bedded sandstone, but changes to more amalgamated and massive to the right (south south-east) of the panel. This indicates a measure of compensational stacking between the lobes. Note the large amount of siltstone intra-lobe elements in lobe-element 2.

C: The Petrel profiles highlight siltstone inter-lobe element A (in red-brown) between lobe elements 1 and 2.

D: The photopanel of R58 illustrates the massive nature of lobe-element 3 in contrast with the thin-bedded nature of lobe-element 2 directly below it towards the left side (west) of the panel.

E: The photopanel of R60 illustrates the more thin-bedded lobe-element 3 and the more massive lobe-element 2 found to the right side (south south-east) of the panel.

Correlation panel 7

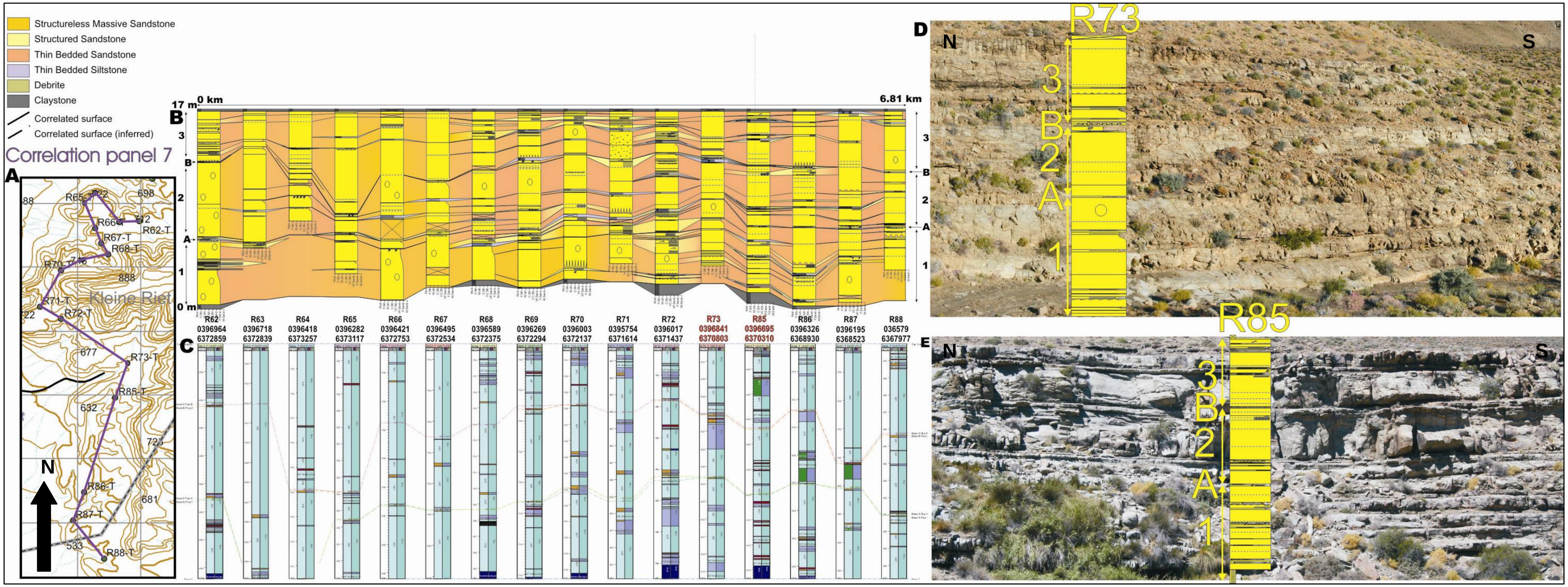

Figure 88: Correlation panel 7 of vertical profiles R62, R63, R64, R65, R66, R67, R68, R69, R70, R71, R72, R73, R85, R86, R87 and R88.

A: Location map of the profiles on the farms Kleine Riet Fontein 88 and Drie Fontein 87.

B: Correlated CorelDraw profiles illustrate the predominantly massive sandstone composition of lobe elements to the left (corresponding to north on the map) of the panel and predominantly thin-bedded sandstone to the right (corresponding to south on the map) of the panel. Profiles R64, R65 and R86 were measured in channelised areas. Note the significant thickening of lobe-element 3 from profile R64 to R65 and the thinning of lobe-element 2.

C: The Petrel profiles show the gradual change-over from massive to structured sandstone from left (north) to right (south) across the correlation panel.

D: The photopanel of R73 illustrates a combination of amalgamated massive sandstone in lobe-element 2 and the top of lobe-element 1, and thin-bedded sandstone at the base of lobe-element 1.

E: The photopanel of R85 illustrates good quality outcrop that highlights the thin-bedded nature of lobe-element 1 and the more amalgamated nature of lobe-element 2.

5.4. Lobe geometry

According to Rozman (2000) the Lower, Middle and Upper units of Fan 2 are stacked progressively eastwards as each overlying unit is affected by the topography of the underlying unit, which can be illustrated by the location of the depositional axes of each of the units (Figure 89).

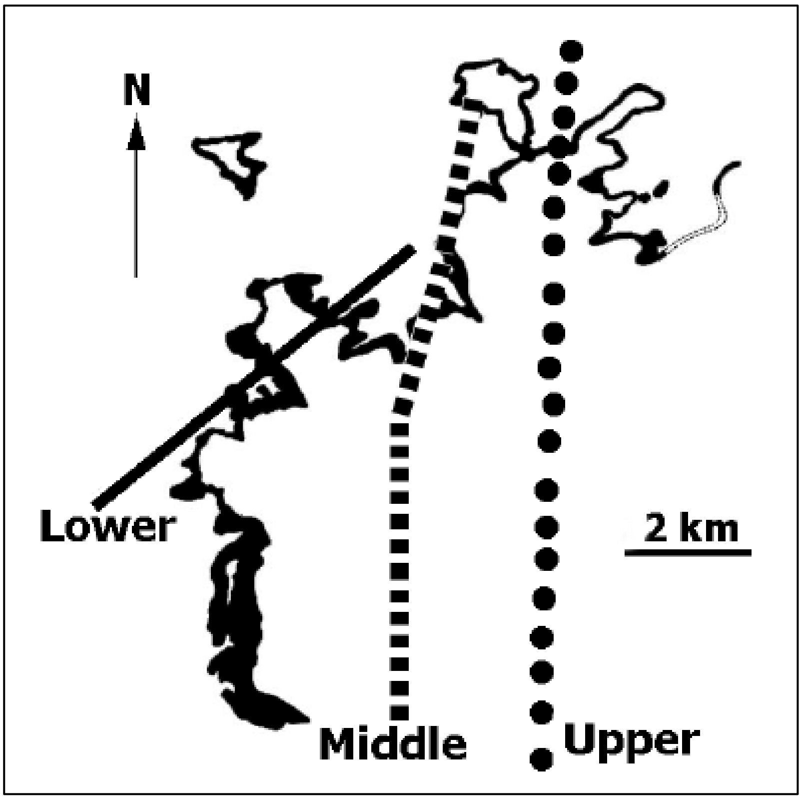

Figure 89: Lateral stacking of the Lower, Middle and Upper units of Fan 2, illustrating the eastward shift of depositional axes (after Rozman, 2000).

Following this model, and from observations in the field, the lobe elements of Middle Fan 2 are seen to stack progressively eastward in a similar manner as the Lower, Middle and Upper units of Fan 2, with all three of the lobe elements pinching out laterally within 1 km (Figure 90). The location of the pinch out in relation to the study area can be seen in plan view in Figure 91.

The stacking of lobes and lobe elements can be influenced by the underlying topography during deposition, thus falling under autogenic control. As a result, each consecutive lobe or lobe-element is positioned in a slight topographic low left by the previously deposited lobe or lobe-element.

Avulsion of distributive channels up-dip of the study area towards the north-west can also have an influence on the stacking of lobes and lobe elements (Prélat *et al*., in review).

Lobe-element 1 (indicated in yellow) is the lowermost and oldest of the lobe elements. It pinches out first, both to the north-east on the farm Los Kop 74 (Figure 92, Image A), and the south-southwest on the farm Drie Fontein 87 (Figure 92, Image B). The base of lobe-element 1 is often obscured by scree, making it difficult to trace out in outcrop. Lobe-element 2 (indicated in orange) is stacked on top of lobe-element 1, but is slightly offset to the east. It pinches out between 200 and 400 metres further east than lobe-element 1. Lobe-element 3 (indicated in red) is stacked on top of lobe-element 2 and is also offset to the east. It pinches out approximately 300 metres further east than lobe-element 2.

Vertical profiles were not measured in the areas represented by Figure 92 as the lobe elements were commonly only visible in outline, if at all. The thickness of the lobe elements rarely exceeds half a metre, and they are generally obscured by scree or are highly weathered.

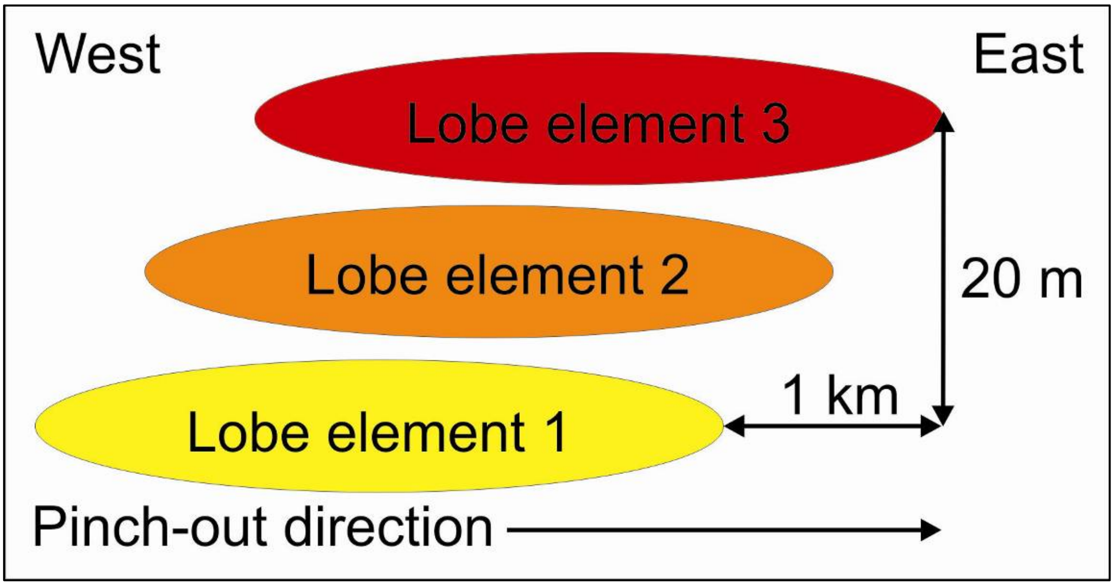

Figure 90: Stacking of sandstone-lobe elements 1, 2 and 3 in relation to each other.

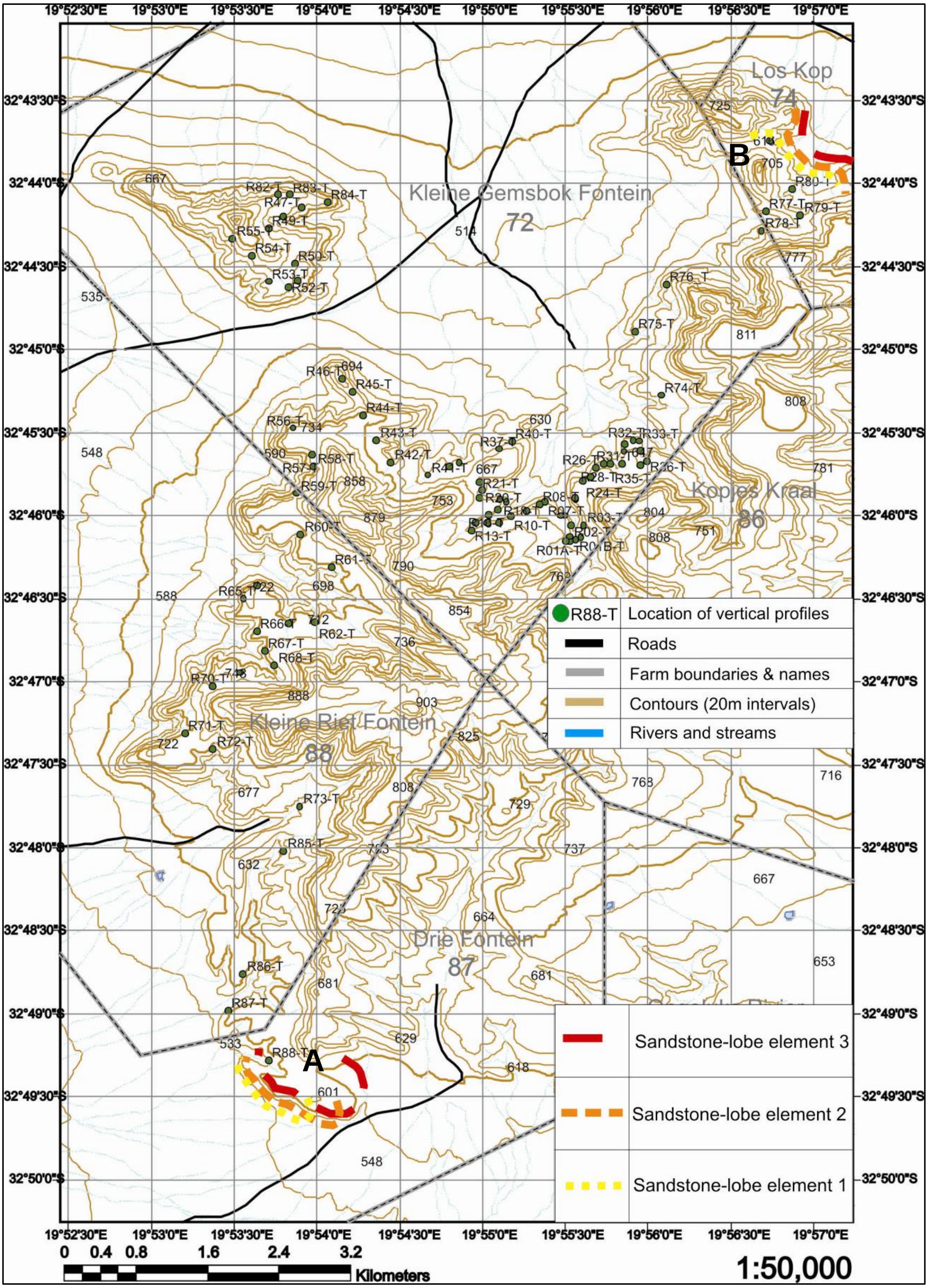

Figure 91: ArcView map showing the location of the up-dip (A) and down-dip (B) pinch out of lobe-element 1 (yellow), 2 (orange) and 3 (red) in relation to the study area.

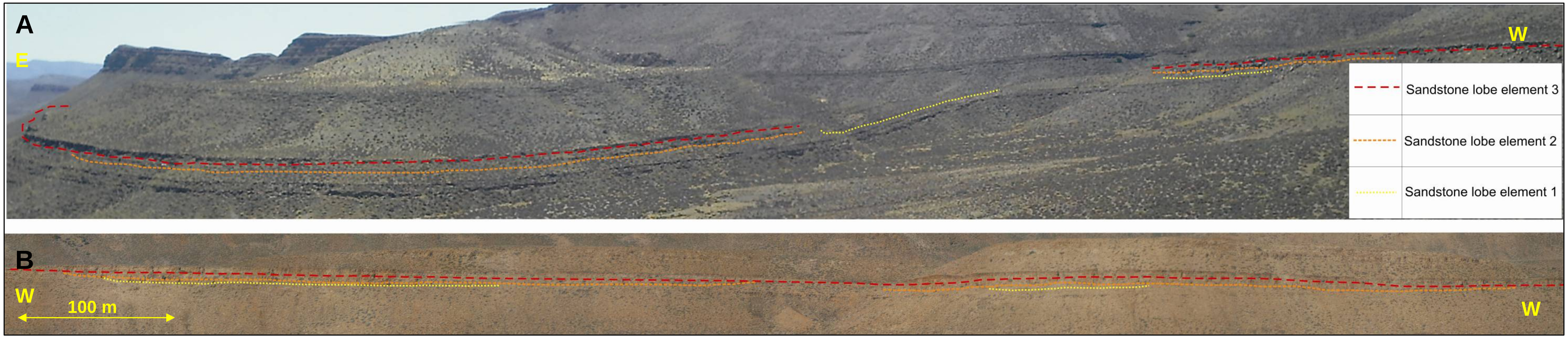

Figure 92: Panorama photomontage illustrating the pinch-out of lobe elements 1 (yellow), 2 (orange) and 3 (red) on the farms Los Kop 74 (Image A) in the north-east (down-dip) and the farm Drie Fontein 87 (Image B) in the south-southwest (up-dip). Lobe-element 1 pinches out first in both locations, followed by lobe-element 2, and finally by lobe-element 3.

5.5. Sequence stratigraphy

5.5.1. Introduction

Sedimentary successions can be grouped into depositional systems tracts that together make up a depositional sequence. A depositional sequence is bound at its top and bottom by unconformities, and is formed during a single cyclic rise and fall of relative sea level, which equates to a rise and fall in the base level of the depositional basin (Boggs, 2006).

A eustatic rise or fall in sea level, coupled with a period of tectonic uplift or subsidence, changes the relative sea level, and can cause an increase or decrease in accommodation, in turn making more or less space available for sediments to accumulate. If the sediment supply exceeds the relative sea-level rise, the basin will become shallower resulting in a regression. If the relative sea-level rise exceeds the sediment supply the basin will become deeper, causing a transgression. Erosion of the sediments can occur if the sediment supply exceeds the accommodation space to such an extent that it reaches sea level. A drop in relative sea level will expose the sediments, allowing them to be eroded away (Boggs, 2006). This causes an unconformity that may represent a considerable period of geological time that has been lost. Unconformities can also form when a period of non-deposition occurs.

Deep-water turbidites are deposited in parts of a basin that always have available accommodation. This implies that a relative change in sea-level has less influence on the development of the fan system than the amount and type of the sediments that are available to be deposited (Johnson *et al.,* 2001).

5.5.2. The Tanqua sub-basin

Each fan in the Tanqua sub-basin is interpreted to be a low-frequency lowstand systems tract. Each of the 20 to 60 metre thick claystone intervals between the fans has been interpreted to represent transgressive and highstand systems tracts (Goldhammer *et al*., 2000; Johnson *et al.,* 2001)

By applying the hierarchies suggested by Mutti & Normark (1987), Deptuck *et al*. (2008) and Prélat *et al*. (in review), the Tanqua fan complex can be seen as a 1st order fan complex, and Fan 2 can be seen as a 2nd order fan. Middle Fan 2 can be seen as a 3rd order lobe. It is subdivided into lobe elements (1, 2 and 3) that classify as 4th order, bed-sets that classify as 5th order and individual 6th order sandstone beds.

5.5.3. Middle Fan 2

The sandstone intervals make up the biggest part of Middle Fan 2 and represent active fan growth due to high sediment supply. The siltstone and claystone intervals represent a period of fan retreat due to low sediment supply (Johnson *et al.,* 2001; Hodgson *et al.,* 2006).

The most effective way to perform a sequence stratigraphic analysis on the Tanqua sub-basin, and Middle Fan 2, is by using condensed intervals. According to Johnson *et al*. (2001), Type 1 horizons represent the 20 to 60 metre thick claystone packages that are found between Fans 1, 2 and 3. They are indicative of “transgressive and highstand systems tracts of low-frequency sequences” (Johnson *et al.*, 2001, p. 1006) and can be interpreted as “the deep-basin equivalent of the maximum flooding surface on the coeval shelf” (Johnson *et al.*, 2001, p. 1006).

Hemipelagic claystone background deposition is found between the Lower, Middle and Upper units of Fan 2. They can be described as Type 2 condensed intervals that represent intrafan packages that are between 0.2 and 3 metres thick (Johnson *et al*., 2001; Hodgson *et al*., 2006), and are deposited across the lobe complex during periods of reduced sand supply (Prélat *et al*., in review).

The Type 2 horizons are found throughout the outcrop area and are interpreted to be indicative of allocyclic controls on the basin, for example sea-level changes (Hodgson *et al*., 2006), and tectonic- and climate changes (Prélat *et al*., in review). Type 2 horizons represent “transgressive and highstand systems tracts to high-frequency sequences" (Johnson *et al*., 2001, p. 1007). In the study area, the change from an underlying Type 2 horizon to overlying sandstone is interpreted as a sequence boundary (SB).

However, a different interpretation invokes autocyclic control of deposition as a result of intrabasinal aspects such as channel meander, avulsion, and the underlying topography during deposition. According to this interpretation, the fine-grained deposition between lobes represents the lateral fringes of extra lobes that lie to the east or west of the studied outcrop, with avulsion of these lobes occurring at a scale of more than 10 km (Prélat *et al*., in review).

The siltstone inter-lobe elements are found between the sandstone-lobe elements. They can be described as Type 3 condensed intervals that represent thin-bedded, commonly amalgamated siltstones with a thickness of less than 30 centimetres. They are found throughout the outcrop area and are interpreted to represent allocyclic switching within the fans that is caused by "very high-frequency, parasequence-scale, shelf-flooding events" (Johnson *et al.,* 2001, p. 1007). The application of sequence stratigraphy to Middle Fan 2 can be seen in Figure 93.

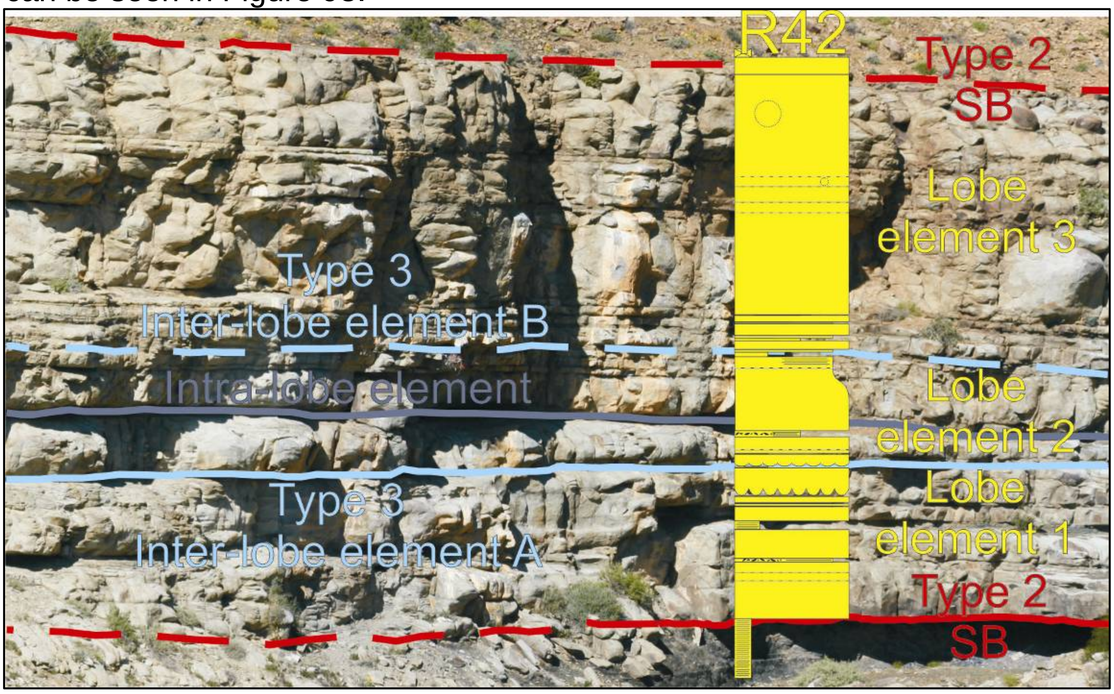

Figure 93: Photomontage of profile R42 (34H0397661/UTM6374647) illustrating the position of Type 2 horizons (sequence boundaries, in red), Type 3 horizons (siltstone inter-lobe elements, in light blue), lobe elements 1, 2 and 3 (in yellow, separated by the Type 3 boundaries) and a prominent siltstone intra-lobe element (in dark blue).

Chapter 6

Palaeocurrent analysis

6. Palaeocurrent analysis

6.1. Introduction

Palaeocurrent measurements were taken using a Krantz geological compass with magnetic declination set at 21° W of N. In total, 142 measurements were taken, of which 134 were in sandstone and 8 in siltstone.

The measurements in sandstone were of ripple cross-lamination, flute casts and groove casts, and the measurements in siltstones were of ripple cross-lamination. Palaeocurrent measurements from ripple cross-lamination were taken where the latter occurs in plan view. The dip of the beds was negligibly small, and as such there was no need to correct for dip.

The distribution of palaeocurrent measurements within the three different lobe elements of Middle Fan 2 are as follows: 57 measurements in lobe-element 1, 30 in lobe-element 2 and 47 in lobe-element 3. Five palaeocurrent measurements were taken from inter-lobe element siltstone A and three measurements were taken from inter-lobe element siltstone B. Ripple cross-lamination provided 115 palaeocurrent measurements, and flute- and groove casts provided 27 measurements.

6.2. Flute casts

Flute casts commonly occur at the bases of turbiditic sandstones. They are formed as sandstone casts of a hollow which is created by powerful turbidity current eddies that scoop out mud from the sea floor. Turbidity currents can reach velocities of 60 – 70 km/h. The cast has a rounded nose that points upstream and becomes shallower downstream which means flute casts can be used to determine palaeocurrent directions (Potter *et al.,* 1977; Pettijohn *et al*., 1987). Flute casts are formed by unimodal currents.

6.3. Groove casts

Groove casts (Figure 24 & Figure 94) are also common on the bases of turbidite beds. They are ridges created when a furrow, formed by an object being dragged across unconsolidated mud by a turbidity current, is filled up when a layer of sand is deposited in the furrow. They are also used as palaeocurrent indicators, but only indicate the orientation of the flow (Boggs, 2006), and are thus ambiguous, as the flow is from one of two opposing directions. The measured palaeocurrent direction was selected to coincide with the overall palaeocurrent direction determined by Rozman (2000).

Figure 94: Groove casts at the base of a massive sandstone bed (R34, 34H0400014/UTM6374796, Klein Gemsbok Fontein).

6.4. Ripple cross-lamination ("Rib and furrow")

The ripple cross-lamination in the sand- and siltstones resulted from migrating linguoid ripples with amplitude of no more than 5 centimetres. The ripples form parallel to the general direction of flow of the water mass due to traction of the sand grains and development of foreset beds (Allen, 1966; Pettijohn *et al*., 1987) (Figure 95), and they are thus formed by unimodal currents.

Figure 95: Ripple cross-lamination seen from above (arrow) (near vertical profile R01B, 34H0399413/UTM6373810, Klein Gemsbok Fontein).

Results

Rose diagrams were compiled for Middle Fan 2, incorporating all the measurements taken in the study area (Figure 96), and separately for each of the lobe and inter-lobe elements (Figure 97). The diagrams were created using the computer program EZ-ROSE, Version 1.0 created by J.H. Baas of the Department of Earth Sciences, University of Leeds (Baas, 2000). No mean vector calculations were undertaken for the palaeocurrent orientations.

The general trend for Middle Fan 2 is to the north north-east, with a second smaller peak to the north. In the individually-generated rose diagrams, lobe elements 2 and 3 have a general trend to the north-east, and lobe-element 1 to the north-northeast. However, some variation can be seen between 0 and 90 degrees.

Few palaeocurrent measurements were taken for inter-lobe elements A and B, as the siltstones are mostly badly weathered, making it difficult to take accurate readings.

Ripple cross-lamination and flute casts have unimodal palaeocurrent orientation, whereas groove casts are ambiguous. Despite this, all the palaeocurrent measurements were represented as unimodal on the rose diagrams generated below as the major palaeocurrent trend provided by the 115 measurements taken from ripple cross-lamination is to the north north-east.

A single figure would be desirable, derived by calculation (Tucker, 1982) to complement the visually successful, but numerically inadequate rose diagram.

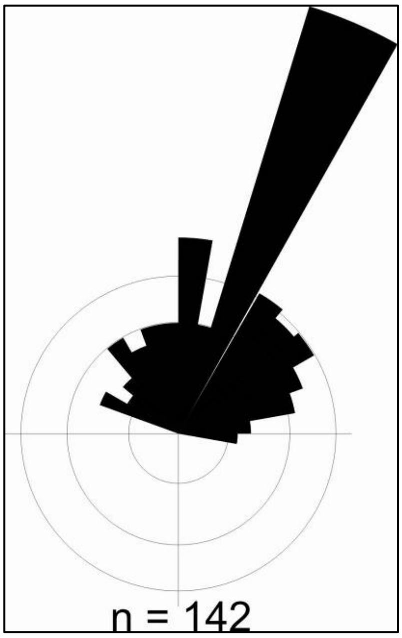

Figure 96: Rose diagram of 142 palaeocurrent measurements representing the entire Middle Fan 2.

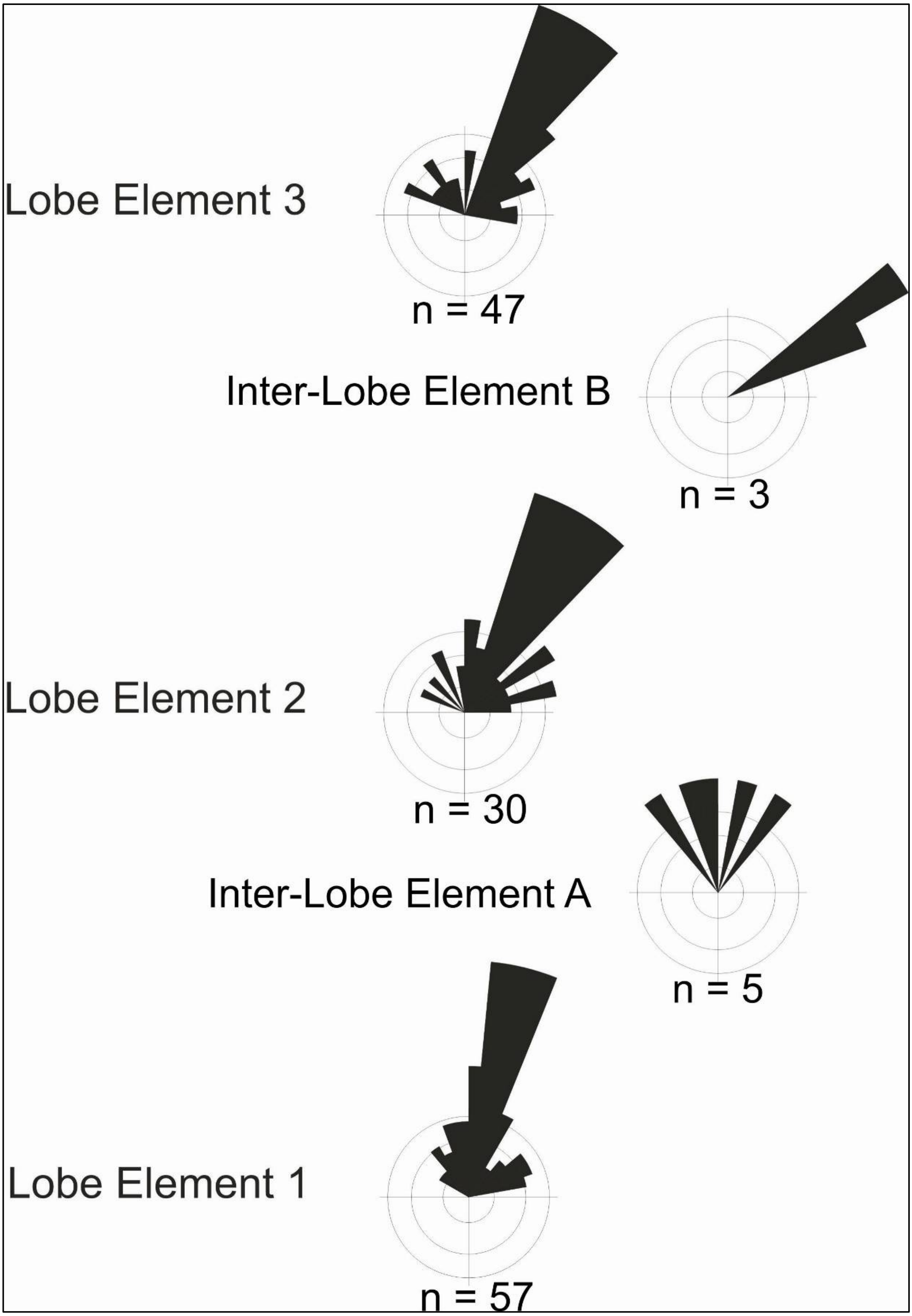

Figure 97: Rose diagrams depicting palaeocurrent measurements of the lobe and inter-lobe elements.

Chapter 7

Depositional model

7. Depositional model

A data-driven depositional model of Middle Fan 2 is presented that integrates measured vertical profiles, the distribution of lithofacies, bed thickness, stratigraphy and architectural elements (channels, sheets and amalgamated sheets).

Previous depositional models for the entire fan have been created (Johnson *et al*., 2001; Bouma 2000). Here, a new depositional model for the pinch out of Middle Fan 2 is presented (Figure 98), which took the ratio of architectural elements into account for each of the vertical profiles or group of vertical profiles in the study area.

Yellow squares represent channels, light blue represents amalgamated sheets and dark blue represents sheets. The size of the square indicates the predominant architectural element. For example, a yellow square followed by a light blue and a dark blue square indicates a channelised area mostly comprised of amalgamated sheets, with a smaller amount of sheets. The red squares always indicate the presence of one or more co-genetic debrite beds, regardless of the size of the square or its order relative to the other squares.

Outlines were drawn to indicate areas that were populated by the different architectural elements (Figure 98). Some of the outlines are based on little data, e.g. in the south of the study area, where the. The geometry of the outlines indicate finger-like thickening across the outcrop area that coincides with a facies change. Channellised massive sandstone changes to amalgamated sheeted massive sandstone, which, in turn, changes to sheeted massive- and structured sandstone (predominantly composed of parallel- and ripple cross-laminated sandstone). The co-genetic debrite beds are most commonly found in the amalgamated sheet area. Middle Fan 2 is interpreted to be a lobe (Rozman, 2000). Each of the three lobe elements is present throughout the study area, apart from the pinch-out areas to the north-east and south-southwest.

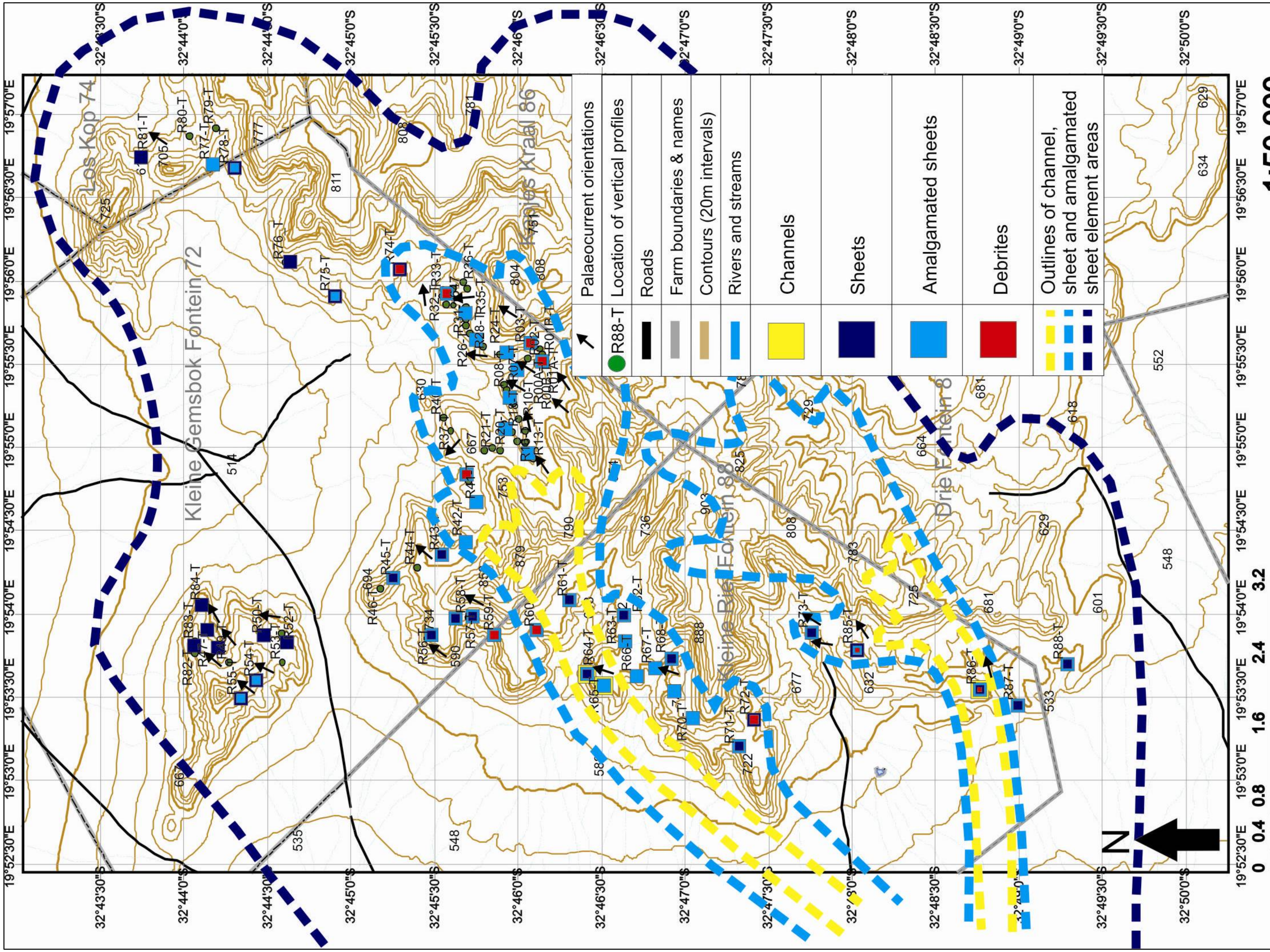

Figure 98: Depositional model for Middle Fan 2 generated using outcrop.

Only two channels are present in the study area, and they only display minimal erosion (approximately 30 cm) into the underlying substrate. This indicates that the velocity of the turbidity current was already reduced by the time it flowed through the channels.

The channel deposits change laterally into amalgamated sheet deposits, and then transform into non-amalgamated sheet deposits. No levee deposits were found in the study area. Leveed channels and levee deposits are generally found in the middle fan on the basin plain (Bouma, 2000), where there are still high-velocity feeder currents that can force the flow over the margins. This is an indication that the amalgamated sheet and sheet deposits were formed in a comparatively low-energy area of the submarine fan.

The Grand Banks earthquake off Nova Scotia, (U.S.A.) in 1929, triggered a turbidity current that travelled at speeds of up to 67 km/h, timed by breaks in submarine telegraph cables. The velocity of a turbidity current decrease as the flow spreads out over the basin or ocean floor at the base of slope (Boggs, 2006). The energy decrease from channels to amalgamated sheets to sheets also occurs in a north-easterly direction, which is also the main palaeotransport direction.

If the two channels in the study area are classified as distributary channels that are found in the lower fan on the basin plain (Bouma, 2000), they would feed directly into sheet-sand lobes, which would explain the absence of leveed channels and deposits. Close to the distributary channels, the turbidity currents would still retain enough energy to form amalgamated sheets co-genetic debrites. However, farther away from the distributary channels, the turbidity current would quickly dilute, forming progressively thinner sheets until they pinched out and there would be less chance of co-genetic debrites being formed.

Middle Fan 2 is interpreted as a lower-fan, sand-rich lobe fed by a distributary channel that is hypothetically positioned to the west-southwest of the study area. The limited amount of channels present may be a function of the relatively low-energy origins of the deposits in the study area. The higher the available energy, the more channelised areas would be created.

A variation on the first depositional model was created using a facies map developed from Fan 3 (Figure 99, Strat Group, 2008). This lithofacies model (Figure 100) defines the axis, off-axis and fringe zones. These zones are comparable to the channel, amalgamated sheet and sheet zones defined for the first depositional model (Figure 98), and zones depicting the debrite-prone fringe were also added.

The finger-like shapes of the facies map (Figure 99) and the Fan 2 depositional model (Figure 98) shows great similarity, although the measured outcrop data are less symmetrical than those of the theoretical model. Unlike the cartoon, the depositional model does not include a distal fringe, as the pinch-out ends abruptly with fringe deposits. The debrite-prone fringe seen in the depositional model also originates out of the axis deposits, instead of the off-axis deposits as represented by the cartoon.

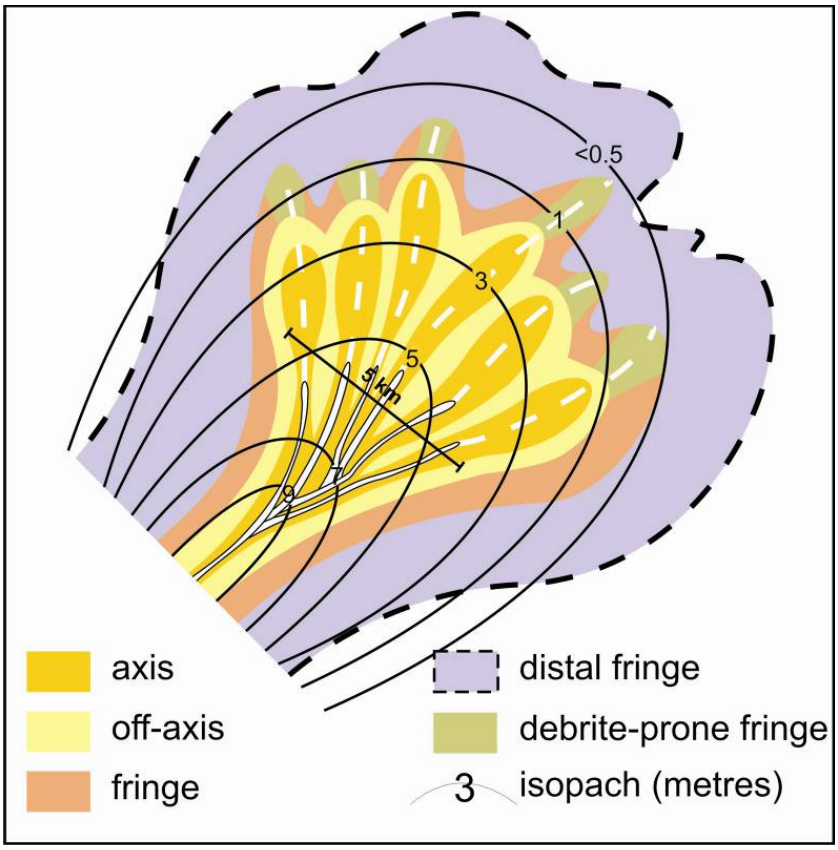

Figure 99: Facies distributions in a lobe developed from observations in Fan 3 (Strat Group, 2008).

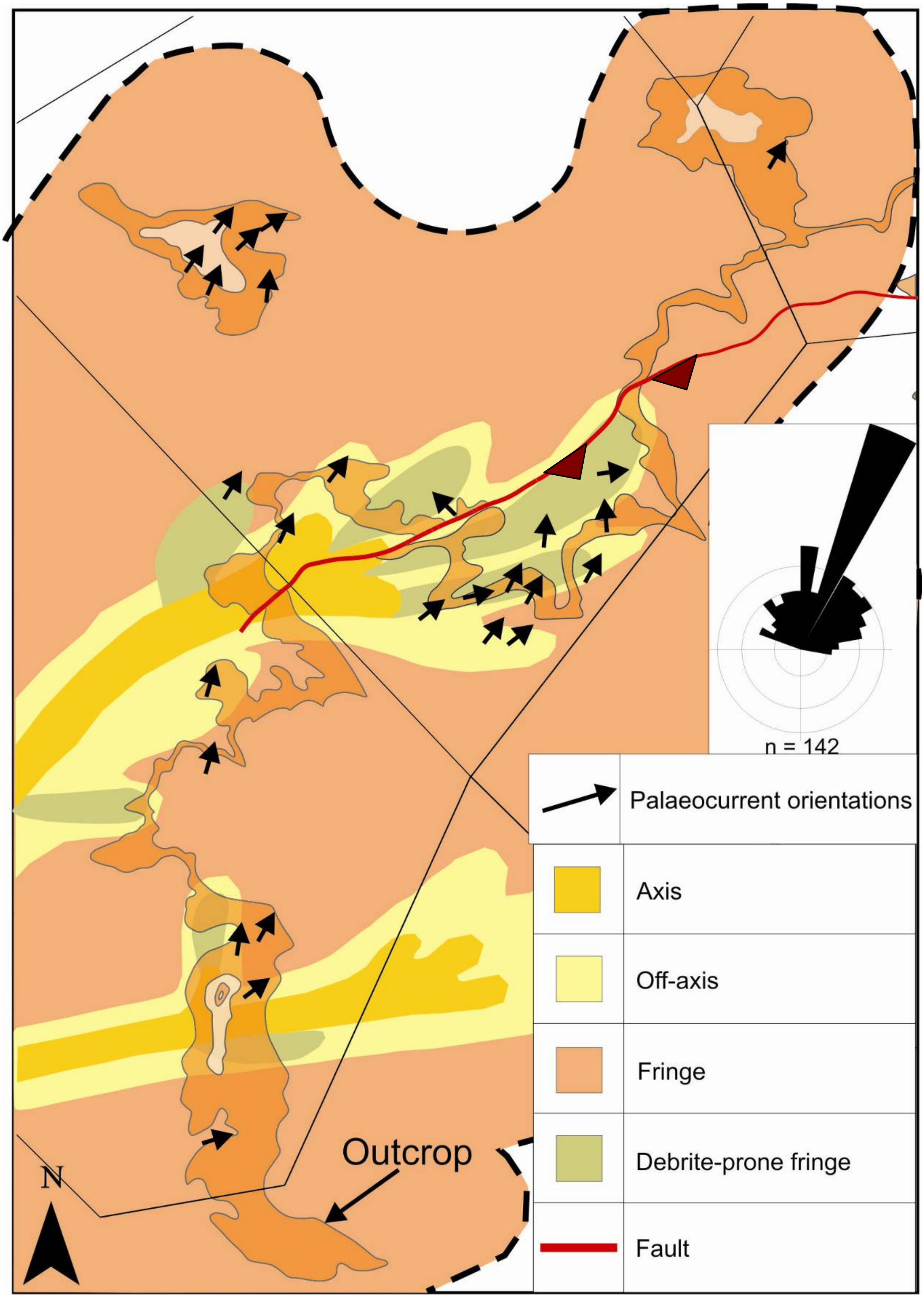

Figure 100: Depositional model illustrating axis and fringe zones of Middle Fan 2.

Chapter 8

Discussions and conclusions

8. Discussion and conclusions

This chapter discusses the aims set at the start of this thesis and the results of the study.

Aims and results:

1. *To document the precise changes in lithostratigraphy and sedimentology towards a submarine fan pinch-out within a distal fan setting;*

The detailed vertical profiles allowed for the characterisation and interpretation of the stratigraphic and sedimentological changes across Middle Fan 2. The outcrop changes from a relatively high-energy channelised area in the south-west to a relatively low-energy sheet-dominated area in the north and north-east. The total vertical thickness of the Middle Fan 2 outcrop decreases from channelised to amalgamated sheet areas, and again from amalgamated sheet to sheet areas. Despite the lateral down-system thinning of the lobe, all the lobe elements are still present throughout the outcrop. The lobe elements pinch out towards the the north-east and south-southwest of the study area.

a. *To define and interpret lithofacies characteristics accurately for Middle Fan 2 across the study area;*

Six lithofacies were described based on grain size and primary sedimentary structures. Massive sandstones are predominantly found in the higher-energy areas, close to the distributary channels and in the amalgamated sheet area of the lower fan. Ripple cross- and parallel laminated sandstones are found in the amalgamated sheet and lower-energy sheet areas of the lower fan. Siltstones and claystones are found throughout the lower-fan study area. Co-genetic debrites are generally found in the amalgamated sheet area.

b. To determine, define and interpret the architectural elements of Middle Fan 2;

Three architectural elements were identified in Middle Fan 2. They are channels, amalgamated sheets and sheets. The two cases of channels are confined to the south-western area of the outcrop. The amalgamated sheets and sheets extend laterally with a roughly finger-shaped geometry away from the channelised area in a north-easterly direction. The feeder channels originate from a south-westerly direction, and transport sediments in a north-easterly direction. The energy available in the system decreases in a north-eastern direction. This results in the transition from channels to amalgamated sheets to sheets.

c. To define and interpret the internal stratigraphy of Middle Fan 2 by designating lobe and inter-lobe elements;

Fan 2 can be interpreted as a lobe complex or fan. It is subdivided into three lobes, namely Lower, Middle and Upper Fan 2. Middle Fan 2 is further subdivided into three lobe elements, which are each made up of various bed-sets and beds.

The sandstone-lobe elements, designated 1, 2 and 3, are separated by siltstone inter-lobe elements, designated A and B. The three sandstone-lobe elements are found throughout the study area and pinch out to the north-east and south-southwest.

The average thickness for the sandstone-lobe elements is approximately four metres, with a minimum thickness of ~1 metre and a maximum thickness of ~6 metres, classifying them as very thick beds. The average thickness for the siltstone inter-lobe elements is approximately 0.1 metres with a minimum thickness of ~0.03 metres and a maximum thickness of ~0.3 metres, classifying them as medium to thick beds.

The siltstone inter-lobe elements are frequently eroded away by overlying sandstone-lobe elements, and the lobe elements thin progressively further away from the distributary channels in the direction of the sheets. The average vertical thickness for Middle Fan 2 in the channelised area is ~16 metres; in the amalgamated sheet area it decreases to ~14 metres; in the sheet area it decreases to ~8 metres.

d. To determine and illustrate possible palaeocurrent patterns;

One-hundred-and-forty-two palaeocurrent measurements were gathered throughout the study area. Rose diagrams were generated for each of the lobe and inter-lobe elements, and for Middle Fan 2 as a whole. The palaeocurrent orientation shows some variation, but the average was not calculated. The predominant direction of transport is in a north-easterly direction.

e. To apply sequence stratigraphy concepts to Middle Fan 2;

The interfan successions between the fans in the Tanqua fan complex can be described as Type 1 condensed intervals. The claystone intrafan successions that are found between the Lower, Middle and Upper units of Fan 2 can be interpreted as Type 2 condensed intervals. They are indicative of allocyclic controls on the basin, and the change from an underlying Type 2 horizon to overlying sandstone indicates a sequence boundary.

The siltstone inter-lobe elements A and B found between the sandstone-lobe elements 1, 2 and 3 can be described as Type 3 condensed intervals that most likely represent autocyclic switching, meaning that these intervals are the lateral (marginal) facies of similar lobe intervals elsewhere in the fan system.

2. *To determine the regional extent of co-genetic debrites (sensu Haughton et. al., 2003), and the possible significance thereof when compiling a depositional model;*

Co-genetic debrites are found throughout the study area. They are not laterally extensive as they generally pinch out within ten metres and they do not form a distinct layer that can be followed out in outcrop. They are predominately associated with the amalgamated sheet areas as they require more energy for formation and transport than is available in the sheet areas. The locations of vertical profiles that contain measured co-genetic debrites are arrayed as a debrite-prone fringe, of which each lobe-like protuberance originates in an axis zone.

3. *To generate a depositional model for Middle Fan 2*

The relevant data from the preceding chapters were used to generate a depositional model for Middle Fan 2. Of particular importance were the measured vertical profiles and the architectural elements, as well as palaeocurrent data and the location of co-genetic debrites in the study area.

The resultant depositional model indicates that Middle Fan 2 has a distributary channel as a feeder system that changes laterally into amalgamated sheets and sheets as the sediments move downslope from a higher-energy to a lower-energy area. There are neither levee channels nor levee deposits, indicating that Middle Fan 2 was formed as a lower-fan sand-rich lobe.

A second depositional model was generated, which designates the channel, amalgamated sheet and sheet areas as axis, off-axis and fringe deposits, respectively. This depositional model allows for the placement of a debrite-prone fringe in the locations where co-genetic-debrites were measured in outcrop, with the debrites originating from the axis zone.

4. *To apply 1-, 2- and 3-dimensional manipulation of the vertical profile data to visually illustrate gradual changeover to pinch-out;*

Data manipulation was effectively applied to all the outcrop data to generate digitised databases for use in DSL and Petrel. Digitised vertical profiles were also successfully superimposed onto photomontages of the outcrop to enable the accurate delineation of lobe and inter-lobe elements and the interpretation of architectural elements and the application of sequence stratigraphy. Seven correlation panels were generated using the results of the data manipulation and digitisation.

5. *To generate surfaces, isopach maps, static model grids and facies models using Petrel software to illustrate the sedimentological and stratigraphical changes visually towards the pinch-out, and to determine the efficacy of detailed measured vertical profile data for use with Petrel software;*

The outcrop data was effectively incorporated into Petrel for the creation of surfaces, isopach maps, static-model grids and facies models. The process was very iterative, as the outcrop data had to be manipulated in such a way as to enable them to be incorporated into Petrel. Limitations of the outcrop data include areas where no outcrop data were available or where significant amalgamation of lobe elements generated incomplete “wells”. Some of the detailed small-scale variations in facies were lost as vertical profiles measured too closely together caused a radius of influence on adjacent “wells”. Isopach maps were compared with the first depositional model, and reiterated the placement of the designated channel, amalgamated sheet and sheet zones.

9. References

Allen, J.R.L., 1966. On bedforms and palaeocurrents. *Sedimentology* Vol. 6, pp. 153 – 190.

Baas, J.H., 2000. EZ-ROSE: a computer program for equal-area circular histograms and statistical analysis of two-dimensional vectorial data. *Computers & Geosciences* Vol. 26, pp. 153 – 166.

Baas, J.H., 2004. Conditions for formation of massive turbiditic sandstones by primary depositional processes. *Sedimentary Geology* Vol. 166, pp. 293 – 310.

Basu, D. & Bouma, A.H., 2000. Thin-bedded turbidites of the Tanqua Karoo: physical and depositional characteristics. In: Fine-grained turbidite systems, Bouma & Stone (eds.). *American Association of Petroleum Geologists Memoir 72/SEPM Special Publication* Vol. 68, pp. 263 – 278.

Boggs, S., Jr., 2001. *Principles of Sedimentology and Stratigraphy*, 3rd ed. Prentice-Hall, Inc., New Jersey, USA, 726 pp.

Boggs, S., Jr., 2006. *Principles of Sedimentology and Stratigraphy*, 4th ed. Prentice-Hall, Inc., New Jersey, USA, 662 pp.

Booth, P.W.K., Brunsdon, G. & Shone, R.W., 2004. A duplex model for the Eastern Cape Fold Belt? Evidence from the Palaeozoic Witteberg and Bokkeveld Groups (Cape Supergroup), near Steytlerville, South Africa. *Gondwana Research* Vol. 7, No. 1, pp. 211 – 222.

Bouma, A.H., 1962. *Sedimentology of Some Fflysch deposits: A Graphic Approach to Facies Interpretation*. Elsevier, Amsterdam, 168 pp.

Bouma, A.H., 2000. Coarse-grained and fine-grained turbidite systems as end member models: applicability and dangers. *Marine and Petroleum Geology* Vol. 17, pp. 137 – 143.

Bouma, A.H. & Wickens, H. de V., 1991. Permain passive margin submarine fan complex, Karoo Basin, South Africa: possible model to Gulf of Mexico. *Gulf Coast Association of Geological Societies Transactions* Vol. 41, pp. 30 – 42.

Dasgupta, P., 2003. Sediment gravity flow – the conceptual problems. *Earth-Science Reviews* Vol. 62, pp. 265 – 281.

De Beer, C.H., 1990. Simultaneous folding in the western and southern branches of the Cape Fold Belt. *South African Journal of Geology* Vol. 93, No. 4, pp. 583 – 591.

De Beer, C.H., 1992. Structural evolution of the Cape Fold Belt syntaxis and its influence on syn-tectonic sedimentation in the SW Karoo. *In: Inversion tectonics of the Cape Fold Belt, Karoo and Cretaceous basins of Southern Africa*, De Wit M.J. & Ransome I.G.D. (eds.). A.A. Balkema, Rotterdam, pp. 197 - 206.

Deptuck, M.E., Piper, D.J.W., Savoye, B. & Gervais, A., 2008. Dimensions and architecture of late Pleistocene submarine lobes off the northern margin of East Corsica. *Sedimentology* Vol. 55, No. 4, pp. 869 - 898.

De Wit, M.J. & Ransome, I.G.D., 1992. Regional inversion tectonics along the southern margin of Gondwana. *In: Inversion Tectonics of the Cape Fold Belt, Karoo and Cretaceous Basin of southern Africa*, De Wit M.J. & Ransome I.G.D. (eds.). A.A. Balkema, Rotterdam, pp 15 – 21.

Fildani, A., Drinkwater, N.J., Weislogel, A., McHargue, T., Hodgson, D.M. & Flint, S.S., 2007. Age controls on the Tanqua and Laingsburg deep-water systems: new insights on the evolution and sedimentary fill of the Karoo

Basin, South Africa. *Journal of Sedimentary Research* Vol. 77, pp. 901 – 908.

Fouché, J., Bate, K.J. & Van der Merwe, R., 1992. Plate tectonic setting of the Mesozoic Basins, southern offshore, South Africa: A review. *In: Inversion Tectonics of the Cape Fold Belt, Karoo and Cretaceous basins of Southern Africa,* De Wit M.J. & Ransome I.G.D. (eds.). A.A. Balkema, Rotterdam, pp 33 – 48.

Gardner, M.H., Borer, J.M., Melick, J.J., Mavilla, N., Dechesne, M. & Wagerle, R.N., 2003. Stratigraphic process-response model for submarine channels and related features from studies of the Permian Brushy Canyon outcrops, West Texas. *Marine and Petroleum Geology* Vol. 20, pp. 757 – 787.

Goldhammer, R.K., Wickens, H. De V., Bouma, A.H. & Wach, G., 2000. Sequence stratigraphic architecture of the Late Permian Tanqua Submarine Fan Complex, Karoo Basin, South Africa. In: Fine-grained turbidite systems, Bouma & Stone (eds.). *American Association of Petroleum Geologists Memoir 72/SEPM Special Publication* Vol. 68, pp. 165 – 172.

Google, 2007. Google Earth. http://earth.google.com/.

Grecula, M., Flint, S.S., Wickens, H. De V. & Johnson, S.D., 2003. Upward-thickening patterns and lateral continuity of Permian sand-rich turbidite channel fills, Laingsburg Karoo, South Africa. *Sedimentology* Vol. 50, pp. 831 – 853.

Haughton, P.D.W., Barker, S.P. & Mcaffrey, W.D., 2003. “Linked” debrites in sand-rich turbidite systems – origin and significance. *Sedimentology* Vol. 50, pp. 459 – 482.

Hodgson, D.M., Flint, S.S., Hodgetts, D., Drinkwater, N.J., Johannessen, E.J. & Luthi, S.M., 2006. Stratigraphic evolution of fine-grained submarine fan systems, Tanqua Depocenter, Karoo Basin South Africa. *Journal of Sedimentary Research* Vol. 76, pp. 19 – 39.

Johnson, M.R., 1991. Sandstone petrography, provenance and plate tectonic setting in Gondwana context of the southeastern Cape-Karoo Basin. *South African Journal of Geology* Vol 94, pp. 137 – 154.

Johnson, S.D., Flint, S., Hinds, D. & De Ville Wickens, H., 2001. Anatomy, geometry and sequence stratigraphy of basin floor to slope turbidite systems, Tanqua Karoo, South Africa. *Sedimentology* Vol. 48, pp. 987 – 1023.

Johnston, S.T., 2000. The Cape Fold Belt and Syntaxis and the rotated Falkland Islands: dextral transpression tectonics along the southwestern margin of Gondwana. *Journal of African Earth Sciences* Vol. 31, No. 1, pp. 51 – 63.

King, R., Van Lente, B., Potts, G., Hodgson, D.M., Andersson, P.O.D., Worden, R.H., Flint, S.S. & Wickens, H. de V. (2004). Extra-foreland source to turbidite sink in the early Karoo Basin, South Africa. *AAPG Annual Meeting 2004: Embrace the Future, Celebrate the Past Technical Program.*

Lowe, D.R., 1976. Subaqueous liquefied and fluidized sediment flows and their deposits. *Sedimentology* Vol. 23, pp. 285 – 308.

Lowe, D.R., 1982. Sediment gravity flows: II – depositional models with special reference to the deposits of high-density turbidity currents. *Journal of Sedimentary Petrology* Vol. 52, pp. 279 – 297.

Luthi, S.M., Hodgson, D.M., Geel, C.R., Flint, S.S., Goedbloed, J.W., Drinkwater, N.J. & Johannessen, E.P., 2006. Contribution of research borehole data to modelling fine-grained turbidite reservoir analogues, Permian Tanqua-Karoo basin-floor fans (South Africa). *Petroleum Geoscience* Vol. 12, pp. 175 – 190.

MacRae, C.S., 1999. *Life Etched in Stone: Fossils of South Africa*. The Geological Society of South Africa, Johannesburg, South Africa, 305 pp.

Middleton, G.V., 1993. Sediment deposition from turbidity currents. *Annual Reviews of Earth Planet Sciences* Vol. 21, pp. 89 – 114.

Mulder, T. & Alexander, J., 2001. The physical character of subaqueous sedimentary density flows and their deposits. *Sedimentology* Vol. 48, pp. 269 – 299.

Mutti, E. & Normark, W.R., 1987. Comparing examples of modern and ancient turbidite systems: Problems and concepts. In: Marine Clastic Sedimentology: Concepts and Case Studies, Leggett & Zuffa (eds.). Graham and Trotman, London, pp. 1 – 38.

Mutti, E. & Ricci-Lucchi, F., 1972. Turbidites of the Northern Apennines: Introduction to facies analysis*. International Geology Review* Vol. 20, pp. 125 – 166.

Mutti, E., Tinterri, G.B., Di Biase, D. & Cavanna, G., 2003. Deltaic, mixed and turbidite sedimentation of ancient foreland basins. *Marine and Petroleum Geology* Vol. 20, pp. 733 – 755.

Nguema-Mve, O., 2005. Petrology, geochronology and provenance of the Laingsburg and Tanqua Karoo submarine fan systems, Ecca Group, South Africa. Unpublished M.Sc. Thesis, Department of Geology, Geography and Environmental Sciences, University of Stellenbosch, 229 pp.

Normark, W.R. & Reid, J.A., 2003. Extensive deposits on the Pacific Plate from Late Pleistocene North American glacial lake outbursts. *The Journal of Geology* Vol. 111, No. 6, pp. 1 - 25.

Parsons, J.D., Schweller, W.J., Stelting, C.W., Southard, J.B., Lyons, W.J. & Grotzinger, J.P., 2002. A preliminary experimental study of turbidite fan deposits. *Journal of Sedimentary Research* Vol. 72, No. 5, pp. 619 – 628.

Paulissen, W., 2007. The Geometry of Lobe Elements in Basin-Floor Fan 4, Tanqua Karoo Basin, South Africa: Unpublished M.Sc. Thesis, Department of Geotechnology, Delft University of Technology, The Netherlands, 98 pp.

Pettijohn, F.J., Potter, P.E. & Siever, R., 1987. *Sand and Sandstone*. Springer-Verlag, New York, 553 pp.

Posamentier, H.W. & Kolla, V., 2003. Seismic geomorphology and stratigraphy of depositional elements in deep-water settings. *Journal of Sedimentary Research* Vol. 73, No. 3, pp. 367 – 388.

Potter, P.E. & Pettijohn, F.J., 1977. *Palaeocurrents and Basin Analysis*, 2nd ed. Springer-Verlag, Berlin, 413 pp.

Prélat, A., 2006. *Sedimentology and Stratigraphy of Unit B around the Heuningberg Anticline, Permian Laingsburg Formation, Southwestern Karoo Basin, South Africa*. Unpublished M.Sc. Thesis, Department of Geology, Geography and Environmental Studies, University of Stellenbosch, South Africa, 160 pp.

Prélat, A., Hodgson, D.M. & Flint, S.S. Evolution, architecture and hierarchy of distributary deep-water deposits: a high-resolution outcrop investigation of submarine lobe deposits from the Permian Karoo Basin, South Africa. *MPG Lobe Special Publication* (in review).

Reading, H.G. & Richards, M., 1994. Turbidite systems in deep-water basin margins classified by grain size and feeder system. *American Association of Petroleum Geologists Bulletin* Vol. 78, pp. 792 – 823.

Remacha, E. & Fernandez, L.P., 2003. High-resolution correlation patterns in the turbidite systems of the Hecho Group (South-Central Pyrenees, Spain). *Marine and Petroleum Geology* Vol. 20, pp. 711 – 726.

Rozman, D.J., 2000. Characterization of a fine-grained outer submarine fan deposit, Tanqua-Karoo Basin, South Africa. In: Fine-grained turbidite systems, Bouma & Stone (eds.). *American Association of Petroleum Geologists Memoir 72/SEPM Special Publication* Vol. 68, pp. 279 – 290.

Saito, T. & Ito, M., 2002. Deposition of sheet-like turbidite packets and migration of channel-overbank systems on a sandy submarine fan: an example from the Late Miocene-Early Pliocene forearc basin, Boso Peninsula, Japan. *Sedimentary Geology* Vol. 149, pp. 265 – 277.

Scott, E.D. (1997). Tectonics and Sedimentation: Evolution, Tectonic Influences and Correlation of the Tanqua and Laingburg Sub-Basins, Southwest Karoo Basin. Unpublished Ph.D thesis, Louisiana State University. 234 pp.

Seilacher, A., 2001. Concretion morphologies reflecting diagenetic and epigenetic pathways. *Sedimentary Geology* Vol. 143, pp. 41 – 57.

Shanmugam, G., 1997. The Bouma Sequence and the turbidite mind set. *Earth-Science Reviews* Vol. 42, pp. 201 – 229.

Shanmugam, G., 2000. 50 years of the turbidite paradigm (1950s – 1990s): deep-water processes and facies models – a critical perspective. *Marine and Petroleum Geology* Vol. 17, pp. 285 – 342.

Shanmugam, G., 2002. Ten turbidite myths. *Earth Science Reviews* Vol. 58, pp. 311 – 341.

Sixsmith, P.J. (2000) Stratigraphic Development of a Permian Turbidite System on a Deforming Basin Floor: Laingsburg Formation, Karoo Basin, South Africa: Unpublished Ph.D Thesis, Department of Earth and Ocean Sciences, University of Liverpool, 229 pp.

Sixmith, P.J., Flint, S.S., Wickens, H. de V., Johnson, S.D., 2004. Anatomy and stratigraphic development of a basin floor turbidite system in the Laingsburg Formation, main Karoo Basin, South Africa. *Journal of Sedimentary Research*, Vol. 74, No. 2, pp. 239 – 254.

South-Africa 1: 50 000 Sheet 3219DB Kapelsfontein Second Edition.

South-Africa 1: 50 000 Sheet 3219DD Kareekolk Second Edition.

Stephen, K.D., Clark, J.D. & Gardiner, A.R., 2001. Outcrop-based stochastic modelling of turbidite amalgamation and its effects on hydrocarbon recovery. *Petroleum Geoscience* Vol. 7, pp 163 – 172.

Stow, D.A.V. & Shanmugam, G., 1980. Sequence of structures in fine-grained turbidites: comparison of recent deep-sea and ancient flysch sediments. *Sedimentary Geology* Vol. 25, pp. 23 – 42.

Stow, D.A.V. & Johansson, M., 2000. Deep-water massive sands: nature, origin and hydrocarbon implications. *Marine and Petroleum Geology* Vol. 17, pp. 145 – 174.

Stow, D.A.V. & Mayall, M., 2000. Deep-water sedimentary systems: New models for the 21st century. *Marine and Petroleum Geology* Vol. 17, pp. 125 – 135.

Stow, D.A.V., Huc, A.-Y. & Bertrand, P., 2001. Depositional processes of black shales in deep water. *Marine and Petroleum Geology* Vol. 18, pp. 491 – 498.

Strat Group, 2004. *Karoo Basin Slope Project – Final Report*, The Stratigraphy Group, Department of Earth and Ocean Sciences, University of Liverpool, United Kingdom.

Strat Group, 2008. Hodgson, D.M., Prélat, A., Groenenberg, R., Paulissen, W.E., Luthi, S.M., Neethling, J., Steyn, R. & Wickens, DeV. Poster series: AAPG Conference, Cape Town 2008. *Geological reservoir modelling and process-based numerical modelling of deep-water distributive systems from detailed outcrop data: examples from the Tanqua depocentre, South Africa.* The Stratigraphy Group, Department of Earth and Ocean Sciences, University of Liverpool, United Kingdom

Sullivan, M.D., Foreman, J.L., Jennette, D.C., Stern, D., Jensen, G.N. & Goulding, F.J., 2004. An integrated approach to characterization and modelling of deep-water reservoirs, Diana field, western Gulf of Mexico. In: Integration of outcrop and modern analogs in reservoir modelling. *American Association of Petroleum Geology Memoir* Vol. 80, pp. 215 – 234.

Talling, P.J., Amy, L.A., Wynn, R.B., Peakall, J. & Robinson, M., 2004. Beds comprising debrite sandwiched within co-genetic turbidite origin and widespread occurrence in distal depositional environments. *Sedimentology* Vol. 51, pp. 163 – 194.

Tucker, M.E., 1982. *Field Description of Sedimentary Rocks*. Open University, M. Hon Keynos, 128 pp.

Van der Merwe, W.C., 2005. *Stratigraphy and Facies Architecture of the Uppermost Fan System in the Tanqua Sub-Basin, Permian Ecca Group, South Africa*. Unpublished M.Sc. Thesis, Department of Geology, Geography and Environmental Studies, University of Stellenbosch, South Africa, 197 pp.

Van der Werff, W. & Johnson, S., 2003. High resolution stratigraphic analysis of a turbidite system, Tanqua Karoo Basin, South Africa. *Marine and Petroleum Geology* Vol. 20, pp. 45 – 69.

Van Lente, B., 2004. *Chemostratigraphic Trends and Provenance of the Permian Tanqua and Laingsburg depocentres, South Western Karoo Basin, South Africa*. Unpublished Ph.D. Thesis, Department of Geology, Geography and Environmental Studies, University of Stellenbosch, South Africa, 339 pp.

Veevers, J.J., Cole, D.I. & Cowan, E.J., 1994. Southern Africa: Karoo Basin and Cape Fold Belt. In: Permian-Triassic Pangean basins and foldbelts along the Panthalassan margin of Gondwanaland, Veevers & Powell (eds.). *Geological Society of America Memoir* Vol. 184, pp. 223 – 279.

Viljoen, J.H.A. & Wickens, H. de V., 1992. Lithostratigraphy of the Vischkuil Formation (Ecca Group). *Geological Survey of South Africa, Lithostratigraphic Series* No. 19, 7 pp.

Visser, J.N.J., 1993. Sea-level changes in a back-arc forearc transition – The Late Carboniferous-Permian Karoo Basin of South Africa. *Sedimentary Geology* Vol. 83, pp. 115 – 131.

Wickens, H. de V., 1984. *Die Stratigrafie en Sedimentologie van die Groep Ecca Wes van Sutherland*. Unpublished MS.c. Thesis, Department of Geology, University of Port Elizabeth, South Africa, 86 pp.

Wickens, H. de V., 1994. *Basin Floor Fan Building Turbidites of the Southwestern Karoo Basin, Permian Ecca Group, South Africa*. Unpublished Ph.D. Thesis, Department of Geology, University of Port Elizabeth, South Africa, 233 pp.

Wickens, H. de V. & Bouma, A.H., 1991a. A passive margin-type submarine fan complex, Permian Ecca Group, South Africa. *American Association of Petroleum Geologists Bulletin*, Vol. 75, p. 693.

Wickens, H. de V. & Bouma, A.H., 1991b. The Tanqua submarine fan complex, Permian Ecca Group, South Africa. *American Association of Petroleum Geologists Bulletin*, Vol. 75, p. 522.

Wickens, H. de V. & Bouma, A.H., 2000. The Tanqua fan complex, Karoo Basin, South Africa – Outcrop analog for fine-grained, deepwater deposits, In: Fine-grained turbidite systems, Bouma & Stone (eds.). *American Association of Petroleum Geologists Memoir 72/SEPM Special Publication* Vol. 68, pp. 153 – 164.

Wickens, H. de V., Brink, G.J., Basson, W.A. & Van Rooyen, W., 1990. *The Sedimentology of the Skoorsteenberg Formation and its Applicability as a Model for Submarine Fan Turbidite Deposits in the Bredasdorp Basin*. Unpublished Report, Soekor, Parow, 47 pp.

Wild, R., King, R., Van Lente, B., Flint, S., Hodgson, D., Potts, G. & Wickens, H. de V. (2004). *Slope project first year report and field guide*. The Stratigraphy Group, Department of Earth and Ocean Sciences, University of Liverpool, United Kingdom & Department of Geology, University of Stellenbosch, South Africa. Part A, 65 pp.

Wild, R.J., Hodgson, D.M. & Flint, S.S., 2005. Architecture and stratigraphic evolution of multiple, vertically-stacked slope channel complexes, Tanqua depocenter, Karoo Basin, South Africa. In: Submarine Slope Systems, Processes and Products, Hodgson & Flint (eds.). *Geological Society, London, Special Publications*. Vol. 244, pp. 89 – 112.

Appendix A Poster presented at the AAPG conference in Cape Town, 26 – 29 October 2008.

Geological reservoir modelling and process-based numerical modelling of deep-water distributive systems from detailed outcrop data:

examples from the Tanqua depocentre, South Africa

Hodgson, D.M.[1], Prelat, A[1]., Groenenberg, R.[2], Paulissen, W.E.2, Luthi, S.M.[2], Neethling, J.[3], Steyn, R.[3], Wickens, DeV.[3]

[1] Stratigraphy Group, Department of Earth and Ocean Sciences, 4 Brownlow Street, University of Liverpool, Liverpool, UK
[2] Department of Geotechnology, Delft University of Technology, The Netherlands
[3] Department of Geology, Geography, and Environmental Studies, Cnr Ryneveld and Merriman Streets, Stellenbosch, Western Cape, South Africa

A. Introducing the problem and the tools used

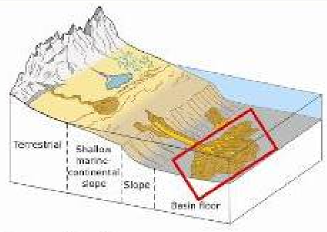

Terminal submarine fan lobes are distributive systems at the most down-dip depositional position of terrigenous sediment transported by gravity flows through basin margins. As such, they form an important, if cryptic, record of the interplay between climatic, eustatic and tectonic controls on the transfer of sediment from land to ocean. Distributive systems are dominated by depositional processes, although erosional processes are still important.

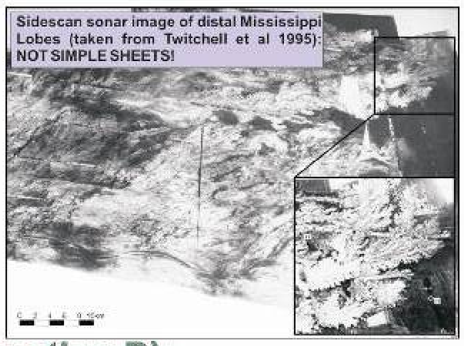

Sidescan sonar image of distal Mississippi Lobes (taken from Twitchell et al 1995): NOT SIMPLE SHEETS!

A1. Key questions:

On the shape, dimensions and geometries of lobe deposits (section B):

- What is the architectural hierarchy of elements in distributive systems?
- What is the depositional shape, dimensions and stacking patterns of lobe deposits?

On the prediction of the subsurface (section C):

- Can small-scale outcrop data be effectively imported and represented in 3D modeling software?
- Does the resulting output data remain true to the input data after upscaling of facies?

On the control on geometry and stacking patterns of the lobe deposits (section D):

- What controls the stacking of lobes and lobe elements?
- Are the stacking patterns and hierarchy identified at outcrop possible to simulate using a forward modelling approach?
- What is the interplay of autogenic and allogenic controls required to produce the lobe geometries, stacking patterns and volumes observed in the Karoo deposits?

A2. Tools for answering:

B. Geological model

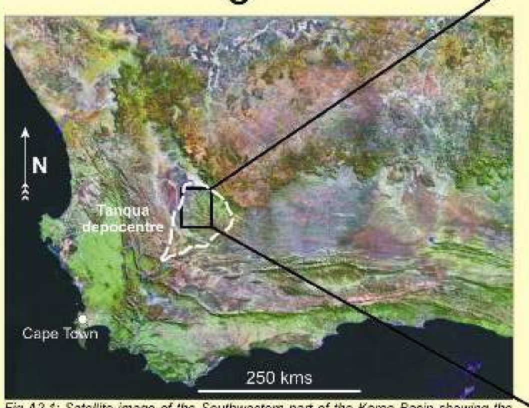

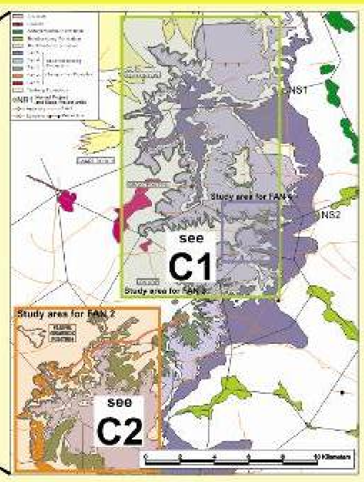

Fig A2.1: Satellite image of the Southwestern part of the Karoo Basin showing the location of the Tanqua Depocentre. Geological map of the Skoorsteenberg Fm. (adapted from Wickens 1994)

Outcrops of the Permian Tanqua depocentre were chosen because of their strike and dip continuity and good accessibility. They allow detailed study from bed to system scale.

The **Tanqua depocentre** is situated in the southwestern corner of the Karoo Basin and records sedimentation ins a retroarc forewland basin during the late Paleozoic and early Mesozoic. The Skoorsteenberg Formation (**~255 Ma; Fildani et al. 2007**), the focus of this study, consists of four basin floor fans and one lower slope to base of slope unit.

- **Fan 2** was studied to document the changes in stratigraphy and sedimentology towards a fan pinch-out within a distal fan setting *(MSc work of Rochelle Steyn in* **POSTER C2)**
- **Fan 3** was studied in its most distal areas (starting 15 km from frontal pinchout). The aim is to document the evolution, architecture and hierarchy of lobe deposits *(MSc work of Jaco Neethling in* ***POSTER C1****/ PhD work of Amandine Prélat in* ***POSTER B****.)*
- Two static reservoir models were built for **Fan 4** from 49 sedimentary logs and the NB2 boreholes *(MSc work of Wieske Paulissen in* ***Poster E****).*

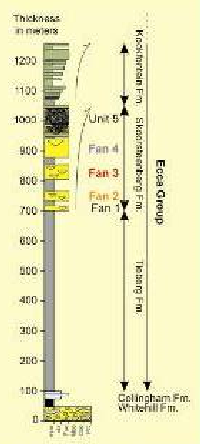

Fig A2.2: Schematic stratigraphic column of the Tanqua depocentre.

C: Reservoir modelling: *Petrel*

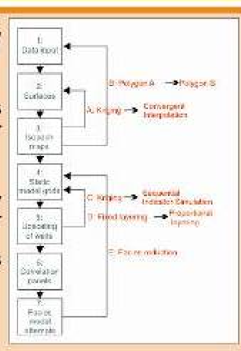

Petrel is used to build a 3D view of the studied geobodies. Fans 2, 3 and 4 were investigated and static reservoir models were built for each from sedimentary logs collected in the field:

- The data from 91 sedimentary logs were collected over the Fan 2 study area of 12 x 5 km. The data was used to generate a facies model for sandstone lobe- and siltstone inter-lobe elements for Middle Fan 2.
- The data from 72 sedimentary logs collected in the Fan 3 study area of 8 x 6 km was used to generate a facies model of 6 sandstone lobes.
- The data from 49 sedimentary logs in Fan 4 was also investigated.

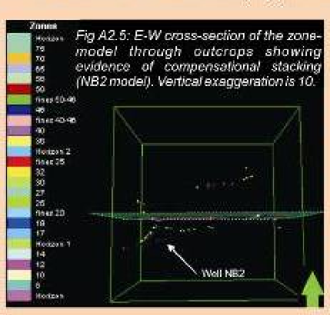

Fig A2.5: E-W cross-section of the zone-model through outcrops showing evidence of compensational stacking (NB2 model). Vertical exaggeration is 10.

Isopach thickness maps:

Isopach maps are generated by subtracting surfaces from each other. Often, geobodies have a larger extent than the isopachs map boundaries. Generally, trends can be drawn when coupled with palaeocurrents.

Simple grids:

Grids were created to define a 3D frame of reference for the study areas using surfaces. The grid allows each of the lobes or lobe elements defined at outcrop to be described as a zone in Petrel. Each zone is further subdivided into layers to simulate internal variation. The zone models represent several levels in the hierarchy of the lobe complex, and may provide insights into the trends of the zones and their stacking patterns.

Facies Modelling:

Based on the upscaled well-logs containing facies and facies associations, facies distributions can be visualized in 3D. Correlation panels, a 2D representation, can illustrate the differences between input and output data.

D: Process-based modelling: *FanBuilder*

The aim is to test some of the concepual models derived from outcrop observations, and to try and constrain some of the input parameters that governed the flow of the turbidity currents and the depositional architecture observed in the ancient distributive system.

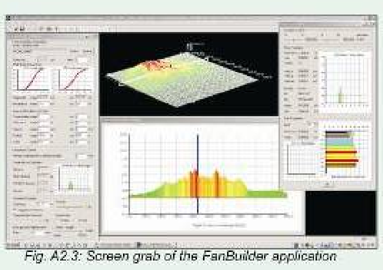

Fig. A2.3: Screen grab of the FanBuilder application

FanBuilder is a generic 3D process-based model capable of simulating the construction of fan stratigraphy by sequential turbidity-current events.

The core of the FanBuilder application patterns a process-based model capable of simulating turbidity-current flow behaviour and resulting sedimentation.

Input parameters are: initial topography, tectonic activity, grain size distribution, concentrations, magnitude and frequency of the flows.

The validation step is an essential step in the development of any model. During validation, the quality of the model is assessed and, preferably, quantified by comparing simulated results to a truth-case. Here, the truth-case is a laboratory experiment (Luthi, 1981), in which a mixture of water and suspended sediment flows out from a supply channel onto an expansion table (see Figure 4A) in the form of a small-scale turbidity current. The experiment itself may be considered to represent a downscaled version of turbidity currents that occur in nature, with a scaling of 1:103 to 1:105.

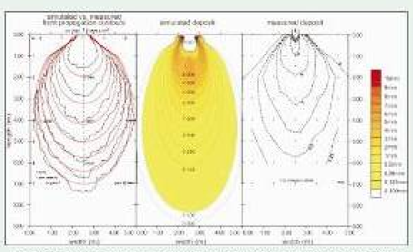

Fig. A2.4: Comparison of simulated flow behaviour and deposition vs. experimental data (Luthi, 1981)

B. INTERNAL ARCHITECTURE AND ORGANISATION OF TERMINAL LOBE DEPOSITS

B1. Hierarchy

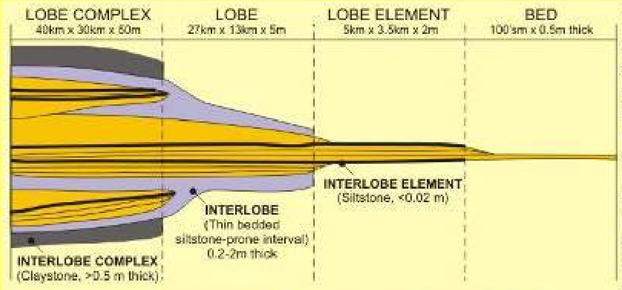

Fig. B1.1:Hierarchical element scheme for distributive systems based on Fan 3.

The development of a hierarchy of architectural elements that stack to construct a distributive deep-water system begins with identification of different types of bounding surfaces and/or fine-grained units.

- The fundamental building block in the stratigraphy of a distributive system is the ***bed***, which represents a single depositional event.
- One or more beds or bedsets stack to form a sand-rich ***lobe element***, which is separated from another lobe element by a locally eroded <0.02 m thick siltstone.
- One or more genetically related lobe elements stack to form a ***lobe***, which are typically 4-10 m thick, and several kilometres long and wide, and elongate in a downstream direction.
- Lobes are separated by fine-grained thin-bedded intervals that maintain similar facies and thickness for >8km in dip and strike sections, and are referred to as ***interlobes.***
- One or more genetically-related lobes stack to form a ***lobe complex*** (eg Fan 3). Lobe complexes are typically 30-60 m thick and bounded by 2-20 m thick claystones.

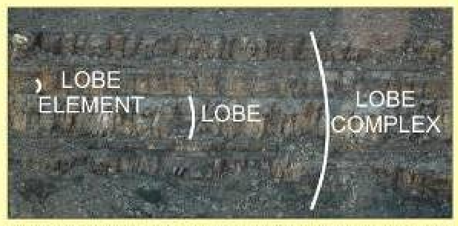

Fig. B1.2: Outcrop photograph of the Fan 3 showing the hierarchy of lobe element, lobe and lobe complex.

B2. Facies Distribution

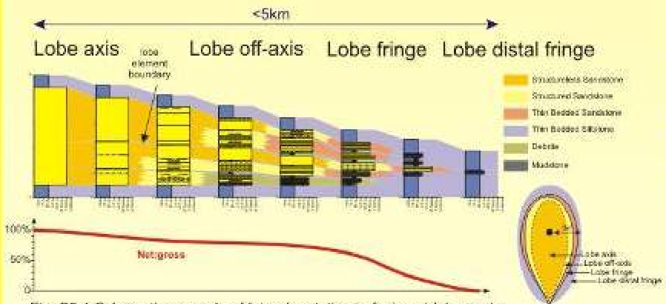

Fig. B2.1:Schematic example of lateral variation in facies at lobe scale. Lobes are seen to thin and fine from lobe axis to lobe fringe becoming more structured with the occurrence of debrites in the lower part.

- Facies transitions in lobes generally show an increase in bed stratification and tractional structures from axial to fringe settings. However, this is not a linear transition because multiple zones of increased bed amalgamation are identified along strike. In general, net:gross decreases from axis to fringe as the lobe thins. However, not all lobes pass from axis to fringe in the same manner. No clear pattern in the style of thinning has been documented, although we speculate that lobes that thin and fine are less confined by underlying topography than those that maintain a structureless sandstone facies.

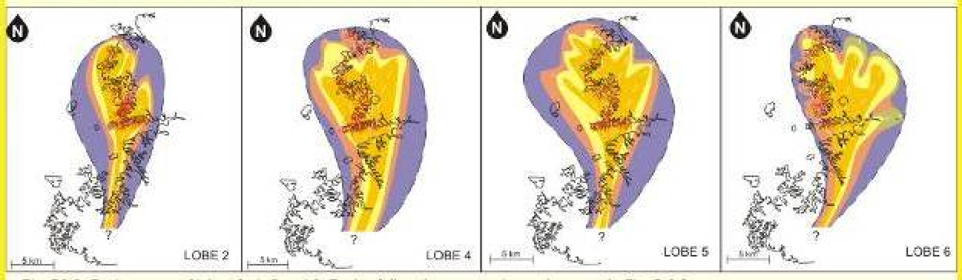

Fig. B2.2: Facies maps of lobes 2, 4, 5 and 6. Facies follow the same colour scheme as in Fig. B.2.2

Four broad environments of deposition in distributive systems have been identified for each element in the hierarchy: axis, off-axis, fringe, and distal fringe. Margin is avoided as this term has connotations with a confining surface.

- ***Axis settings*** are represented by >80% net: gross successions comprising amalgamated sandstone with local dewatering features, but no erosional confinement
- ***Off-axis settings*** are represented by 60-80% net: gross succession comprising stratified medium-bedded facies with Ta, Tab, and local Tc intervals, and some amalgamation. Some lenticular bedforms are identified here.
- ***Fringe settings*** are represented by 40-60% net: gross with medium- to thin-bedded successions of current ripple-laminated and/or bipartite and tripartite hybrid beds (linked debrites)
- ***Distal fringe settings*** are represented by <40% net: gross successions with thin-bedded very fine-grained sandstone and siltstone intervals that are commonly graded and ripple laminated.

B3. Shape

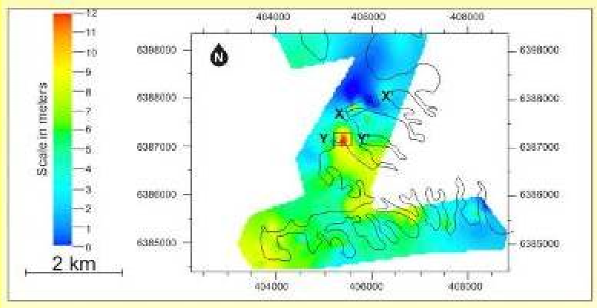

Fig. B3.1: ***Isopach maps*** were created from logged sections collected throughout the study area. Compilation of isopachs maps for each lobe and interlobe allow analysis of thickness variation, and construction of isopach maps.

Lobes are not simple radial bodies thinning evenly from the centroid (volumetric centre) as in an ellipsoid. Lobe 2, for example, in distal reaches is characterised by abrupt changes in thickness across strike.

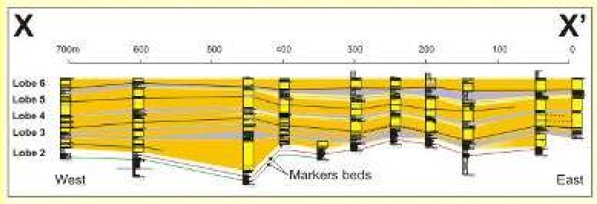

Fig. B3.2: **XX'** Lobe 2 thins from 3 m in the west to 0.1 m and then thickens back to 3 m moving east along strike. The cross-sectional geometry of this feature at outcrop is channel-form (base concave-up). Underlying marker beds are not truncated and follow the concave-up base of the lobe.

Fig. B3.3: **YY'** Up dip (500 m to the SW) along the same finger, Lobe 2 thickens to 14 m with a concave-up basal surface. Changes in thickness are abrupt and perpendicular to flow direction. Lobes that overlie the fingered basal lobe display minimal thickness variations.

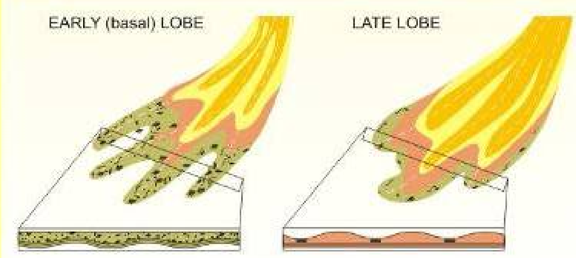

Fig. B3.4:Cartoon of early and late lobe and cross section through distal positions.

The pinchout pattern of Lobe 2 described above has a multiple finger-like expression. A similar pattern has been identified in basal lobes in Fan 3 in the Klipfontein area (lobe 4, this study), Fan 2 (Rozman 2000) and Fan 4 (Bouma and Rozman 2000). ***This finger-like pinchout pattern is particularly evident in basal lobes***, and indicates that the map view shape of lobes is not as smooth and radial as previously envisaged but can be much more irregular across strike. In contrast, the lateral fringe of lobe 6 is smooth and is parallel to the direction of thinning of the lobe, oriented N165. Away from its western fringe, lobe 6 thickens consistently at 2m/km.

B4. Stacking patterns

Local compensational stacking patterns

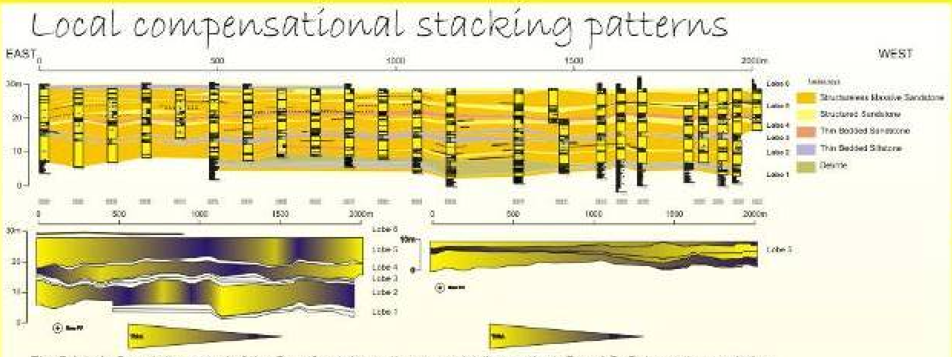

Fig. B4.1: A. Correlation panel of the Grootfrontein south outcrop (strike section). B and C. Schematic correlation panels highlighting compensational stacking pattern of lobes and lobe elements.

- At outcrop, the compensational stacking of lobes is most apparent in strike orientated sections and can be demonstrated along a 2 km strike section in the Grootfontein area by the thickening and thinning patterns of lobes (2, 4 and 5).
- The maximum depositional relief is calculated by assuming that thickness change is due to seabed topography, and these estimates are presented as angles.
- From east to west, lobe 2 thins from 7.8 m to 4.2 m over 700 m (angle of 0.29°), thickens back to 10 m in 500 m (angle of 0.66°) and, at the western end, thins to 6.7m in 600m (angle of 0.32°). Locally, lobe 4 is thickest overlying the thinner parts of lobe 2, and thins from 5.4 m to 3.2 m over 1000 m to the east (angle of 0.13°). Finally, lobe 5 has two loci of thickening situated at either end of the panel and thickens from 6 m to 9 m in 1000 m towards the east and the west (angle of 0.17°).

Fig. B4.2: Diagram of compensational cycles after Mutti and Sonnino, 1981. Scale is indicative.

Planform stacking patterns

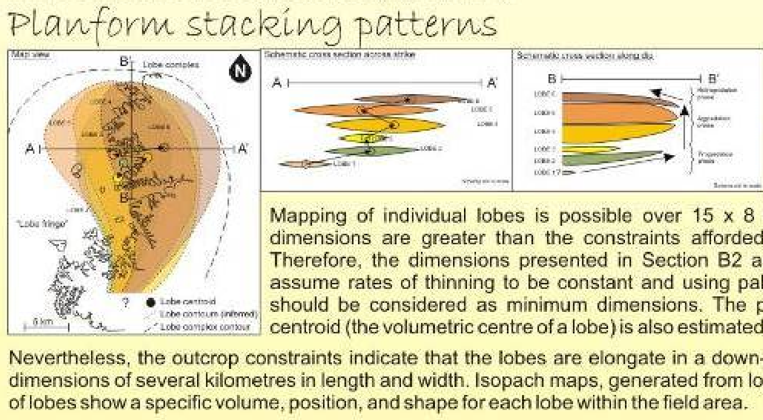

Fig. B4.3: Geometry of lobes within Fan 3 and stacking patterns of Lobes 2 to 6. Schematic cross section across strike and and along dip through the 6 lobes of Fan 3

Mapping of individual lobes is possible over 15 x 8 km, but a lobe's dimensions are greater than the constraints afforded by the outcrop. Therefore, the dimensions presented in Section B2 are estimates that assume rates of thinning to be constant and using palaeocurrents, and should be considered as minimum dimensions. The position of a lobe centroid (the volumetric centre of a lobe) is also estimated.

Nevertheless, the outcrop constraints indicate that the lobes are elongate in a down-dip direction with dimensions of several kilometres in length and width. Isopach maps, generated from logged thicknesses of lobes show a specific volume, position, and shape for each lobe within the field area.

B5. Dimensions

Methodology:

2D data, such as the lengths of surfaces, beds, bedsets, or 'shales', can be extracted easily from outcrop panels, but need to be reoriented from their outcrop lengths to be tied to local palaeocurrent directions.

Key conclusions:

- Interlobe low permeability intervals (thin-bedded fine-grained facies) were deposited as a blanket over lobes to form significant barriers to vertical fluid flow that are cut out locally

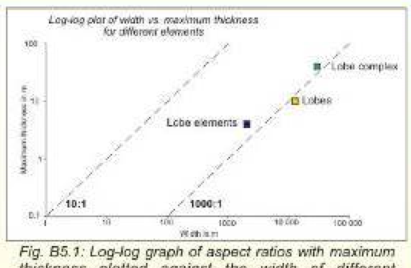

Fig. B5.1: Log-log graph of aspect ratios with maximum thickness plotted against the width of different architectural elements from Tanqua.

- Bed thickness distributions form segmented power laws, which is related to bed amalgamation and lobe element confinement
- Width to length ratios show a linear relationship across the hierarchy of lobe components (Fig. B2.2.)
- A non-linear relationship exists between lobe element thickness and lobe element area, which indicates the presence of a process that limits lobe element thickness to <3m (Fig. B2.3.)
- Aspect ratios (width to thickness) of lobe elements, lobes, and lobe complexes are comparable (1000:1)
- Estimates of typical turbidity current volumes and number of beds that comprise lobe elements have been calculated and used to help constrain process-based numerical models (Poster D)

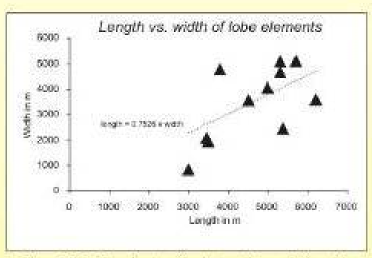

Fig. B5.2.:Graph to illustrate the relationship between the lengths and widths of several lobe elements identified in the Tanqua depocentre.

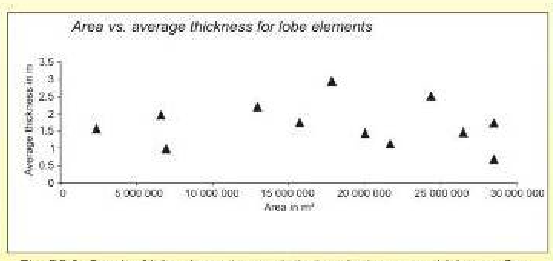

Fig. B5.3.:Graph of lobe element area plotted against average thickness. See Poster D for an explanation. Note the low variability in lobe element thickness, but wide range of lobe element area.

C. RESERVOIR MODELLING AND SUBSURFACE APPLICATION

Why geological reservoir modelling?
Modelling allows the visualisation of subsurface data in 3D that would not normally be visible in seismic data. Lateral facies variations is highlighted by the process, making the simulation of fluid flow possible. Digital outcrop models (DOM) provide a means to capture quantitative 1D, 2D ,and rarely 3D, data collected at outcrop.

1. Input data: vertical profiles measured in the study area includes information on sedimentary structures, architectural elements, bed thickness, facies, etc. This data can be visually represented as sedimentary logs and correlation panels in CorelDraw to highlight variation in stratigraphy, architecture and facies distribution.

2. Output data: input data is imported and manipulated in Petrel to build a 3D representation of the 2D outcrop data. The accuracy of the representation is dependant on the efficacy of the outcrop data for use in modelling software.

The work presented below forms part of theses by Jaco Neethling (C1) and Rochelle Steyn (C2), University of Stellenbosch.

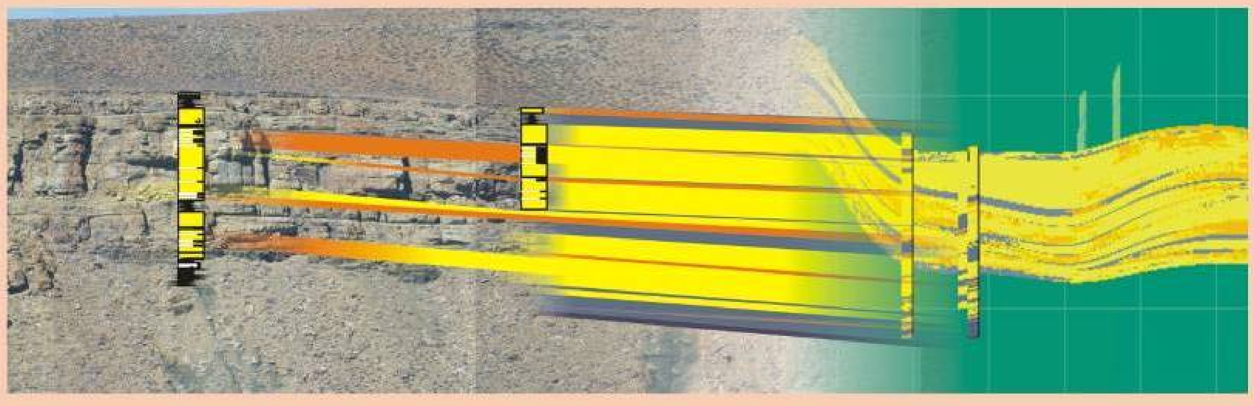

C1. lobe complex axis (Fan 3)

Outcrop observation

Outcrops of the **Fan 3 lobe complex** in medial axial position show a slightly different pattern to the outcrops studies to the north (Poster B). Lobe 3 is not present, and two additional lobes are present beneath Lobe 1. Lobes 2, 4 and 5 can be divided into **Upper** and **Lower lobe elements**, each exhibiting significantly different behaviour. For instance, Upper Lobe 5 pinches out 4 kilometres before Lower Lobe 5, and has a different palaeoflow direction. The outcrop below (Fig C1.1) represents the **southern Gemsbok valley**. Beneath are two correlation panels, one created in **CorelDraw** and the other a **Petrel** generated panel, both indicating facies variation across the 3800km long outcrop.

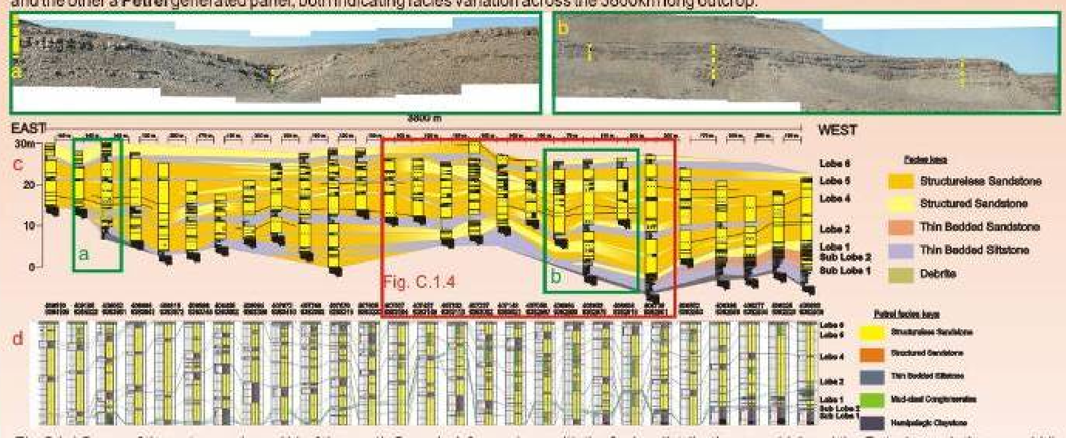

Fig.C1.1 Some of the outcrops (a and b) of the south Gemsbok face, along with the facies distribution panel (c) and the Petrel correlation panel (d).

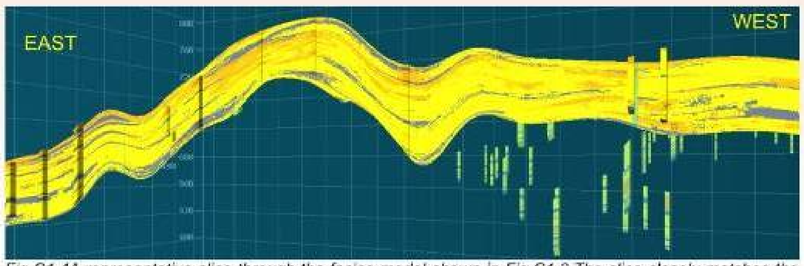

Fig.C1.4A representative slice through the facies model shown in Fig.C1.3.The slice closely matches the boxed section to the east of the correlation panel.

3D Geological model

A **conceptual depositional model** was constructed using outcrop data and **isopachs** created in Petrel. The conceptual model was converted into a **grid** in Petrel and divided into 19 **zones** based on the **top and base surfaces** of lobes and lobe elements. The internal variation was simulated using **proportional layering**. Surface **topography** was left unchanged.

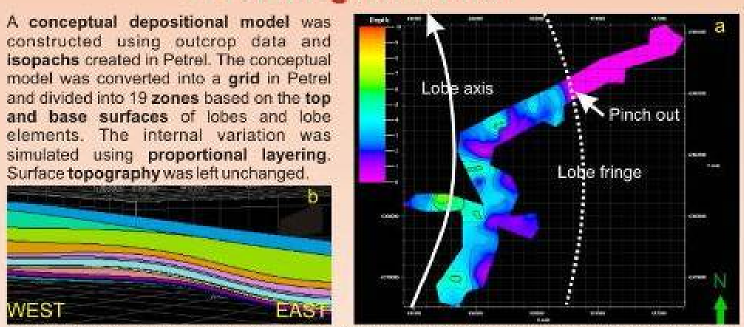

Fig.C1.2 (a) is an isopach of Upper Lobe 2 created in Petrel. (b) is an example of the 19 zones created. The zones represent 4 lobes, with 6 lobe elements (upper and lower lobes) and 9 interlobe units).

Reservoir model

The wells were upscaled into the 20mx20m **cells** of the grid, and the 3D distribution was simulated in 3D by using the **sequential Gaussian algorithm**.
The model is shown in Fig C1.3

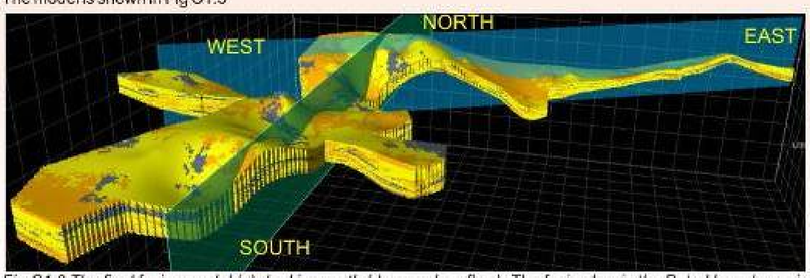

Fig.C1.3 The final facies model (a) looking north (down palaeoflow). The facies key is the Petrel key shown in Fig. C1.1.d.

C2. Lobe axis to fringe (Middle Fan 2)

Outcrop observation

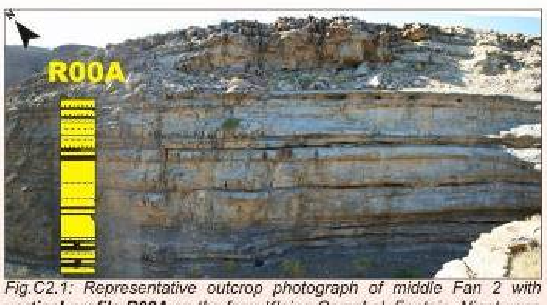

*Fig.C2.1: Representative outcrop photograph of middle Fan 2 with **vertical profile R00A** on the farm Kleine Gemsbok Fontein. Ninety-one vertical profiles were measured, representing Middle Fan 2 outcrop across the study area. Each profile depicts observations on sedimentary structures, facies and architectural elements.*

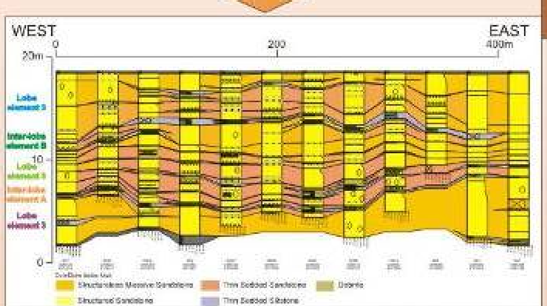

*Fig.C2.2: Correlation panel created using **CorelDraw,** illustrating the internal variation between 12 vertical profiles measured adjacent to each other on the farm Kleine Gemsbok Fontein. Middle Fan 2 is subdivided into three sandstone lobe elements separated by siltstone inter-lobe elements.*

3D geological model

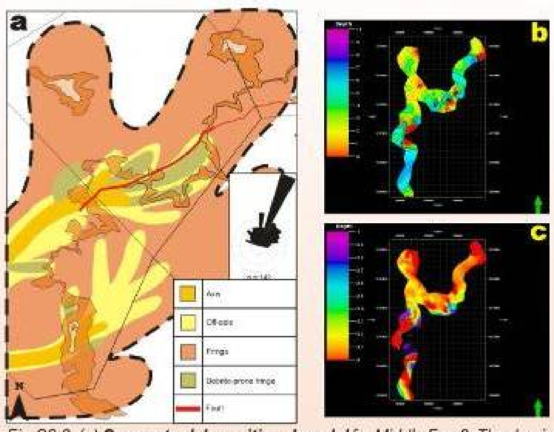

*Fig.C2.3: (a) **Conceptual depositional model** for Middle Fan 2. The dominant palaeocurrent indicates flow to the north-east. Isopach thickness maps were created for lobe element 1 (b) and inter-lobe element B (c), with hot colours indicating **thinner** elements .*

*Fig.C2.4: Correlation panel created using **Petrel,** illustrating the difference between input outcrop data (left) and output upscaled data (right). Input data represents 17 original facies, output data represents facies reduced to 5.*

Reservoir model

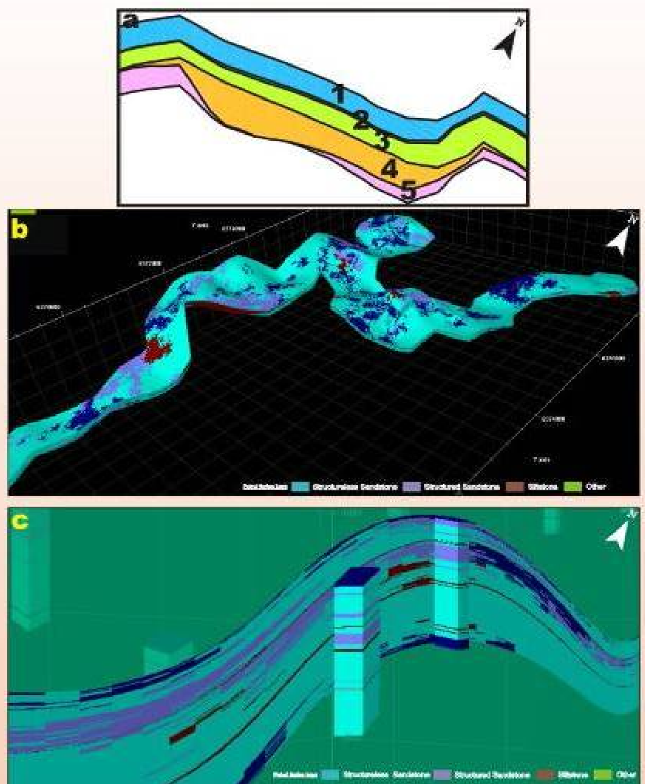

*Fig.C2.5: **Reservoir model** for Middle Fan 2 indicating the lobe elements and inter-lobe elements represented by 5 zones, each subdivided into layers (a), (b and c) the facies model for Middle Fan 2 and detail of the upscaled facies in the facies model.*

D. AUTOGENIC CONTROLS ON THE GEOMETRY AND STACKING PATTERN OF TERMINAL LOBE DEPOSITS

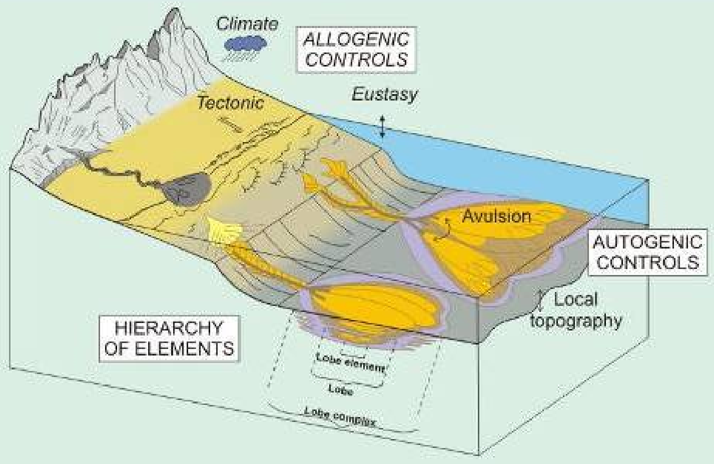

The architecture of submarine fans is governed by a multitude of processes, some of which may be classified as allogenic to a fan system, whereas others are considered autogenic.

Allogenic, or extrinsic, controls are those that force change in the architecture of the fan system *from the outside*. Examples of allogenic controls are mostly related to changes in the sediment supply signal (volume and frequency of flows, grain size of the source sediment), e.g., due to changes in relative sea level and climate, and changes in seafloor shelf-slope morphology due to tectonic activity.

Autogenic, or intrinsic, controls are those that cause changes in architecture due to processes occurring *in the fan system itself*. Autogenic behaviour in submarine fans is intimately related to the interplay between turbidity-current flow and sedimentation, which causes a subtle but complicated and dynamic depositional topography that strongly impacts the loci of erosion and deposition of subsequent flows and, therefore, the facies and thickness distributions of architectural elements.

D1. Finger like lobe geometry

Outcrop observation

Outcrops of Fan 3 demonstrate that planform geometries of lobes are not simple radial fan shapes. Commonly, lobes have finger-like projections near their termination, particularly basal lobes on a muddy substrate (see Section B3).

Interpretation

This cartoon map represents facies and thickness distributions within a typical Tanqua lobe. It attempts to **synthesise outcrop observations, isopach maps, and correlation panels.** There are no 'hard' lines between facies as these are transitional, and dotted lines represent axial pathways and indicate that there is not a single axis to a lobe. Smooth radial isopach contour lines are sketched here although in reality they are more complicated, particularly in areas close to pinchout.

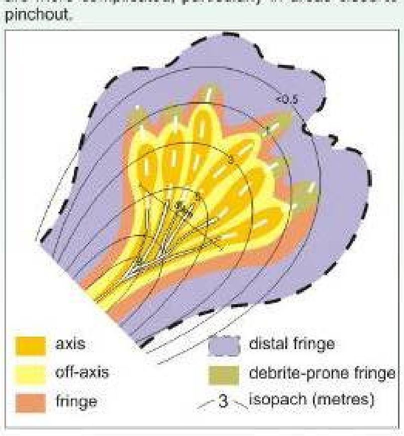

Fig D.1.1.:Cartoon map to represent facies and thickness distributions within a typical Tanqua lobe.

Process-based realisation

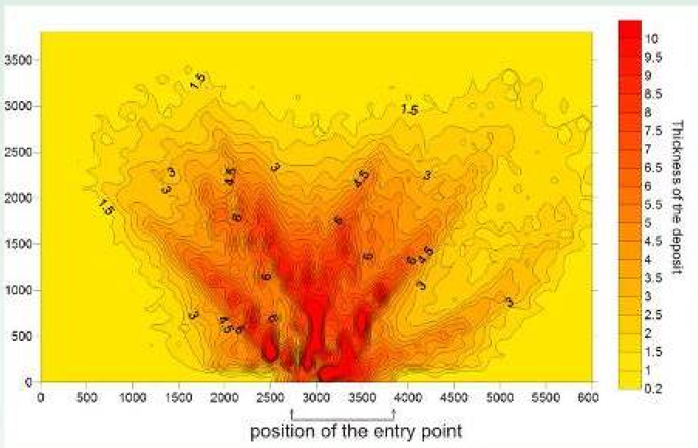

Aim:
To mimic the lateral shifts in the position of the mouth of a distributary channel due to avulsion, or a change in the axis of flow through a (depositional) shallow conduit. The position of the entry point of the flows into the model domain was varied on a flow-by-flow basis and in a disorganized manner.

Inflow position:
Inflow positions were randomly assigned from a distribution with a mean of 3000m and a standard deviation of 200 m. As such, all flows entered the domain of interest roughly between 2400 and 3600m.

Result:
Clearly, the disorganized shift in entry point results in an asymmetric stacking of beds which causes the depositional relief to be undulating, with elongated highs and lows in-between that widen downstream. Properties of this simulated lobe, such as the number of beds, overall thickness, volume and geometry, are in agreement with those observed at lobe scale in outcrop.

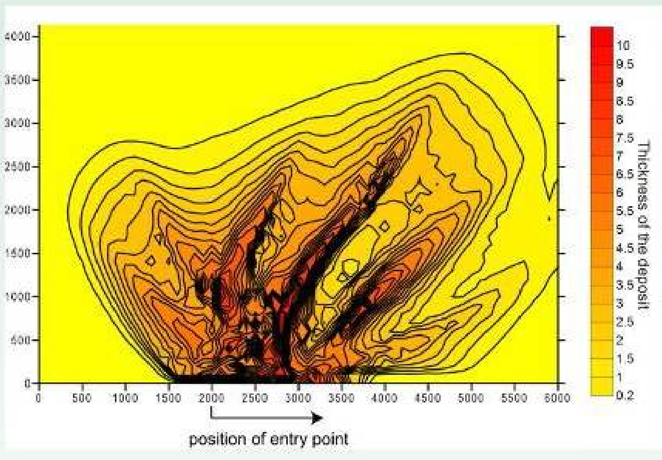

Aim:
To assess the influence of a more organized way of entry point switching, both in time and in space.

Inflow position:
The input parameters values are the same than in the previous example, but with flow entry points shifting from 2000 m to 3400 m and with steps of 100 m. Timing of the shifts was defined such that a shift occurred every three to four flows, depending on size and recurrence interval, which are randomly drawn from user-defined log normal distributions.

Result:
Elongate ridges now vary in length, and curve towards the right, i.e., in the direction of lateral shift of the entry point. Furthermore, flows seem to have preferentially followed one particular conduit, which therefore has resulted in bounding highs left and right that are more pronounced than the other highs, and also in transport of sediment further downstream. Evidently, the more organized shift of entry point, both in time and space, has resulted in a depositional relief with more pronounced highs with lows in-between that serve as pathways for several consecutive flows, which increases the distance over which sediment is transported.

D2. Compensational stacking patterns

Outcrop observation

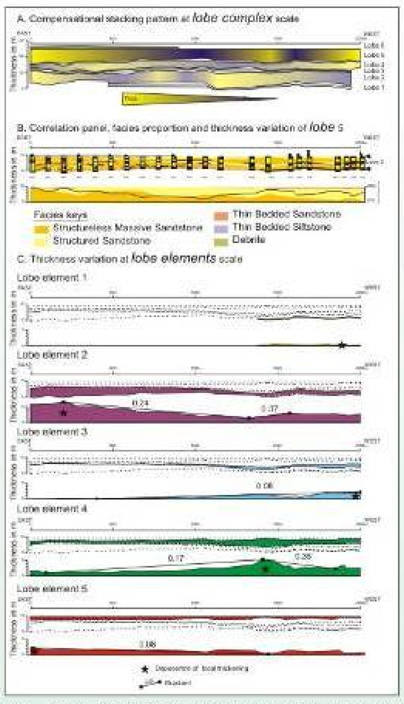

Fig. D2.1: Correlation panel of Lobe 5 in the Grootfontein area (strike section) and schematic correlation panels of individual lobe elements, highlighting distinct local thickening and thinning at lobe element scale, which is interpreted to result from the interaction of flows with depositional relief (compensational stacking).

Interpretation

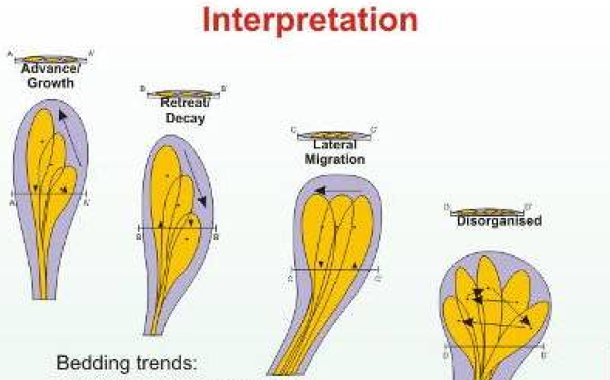

Fig. D2.2: Illustration of the conceptual models of stacking patterns of beds and lobe elements within lobes.

Four simple conceptual models of different lobe element stacking styles that can occur during the formation of a lobe, advance, retreat, lateral, disorganised.

Stacking Style 1: Advancement or Growth
This style could develop where the up-dip distributary channel is increasing in efficiency (channel lengthening) and/or sediment supply rate increases, although it could develop as an autogenic response to dynamic underlying topography.

Stacking Style 2: Retreat or Decay
This style could develop where the up-dip distributary channel is decreasing in efficiency (channel shortening) and/or sediment supply rate decreases, although it could develop as an autogenic response to dynamic underlying topography.

Stacking Style 3: Lateral Migration
This style could develop where sediment supply is quasi-stable, but the position of the distributary channel moves laterally (avulsion or open channel migration).

Stacking Style 4: Disorganised
This style could develop where the position of the up-dip distributary channel and/or the rate of sediment supply are unstable, although it could develop as an autogenic response to the developing underlying topography.

Process-based realisation

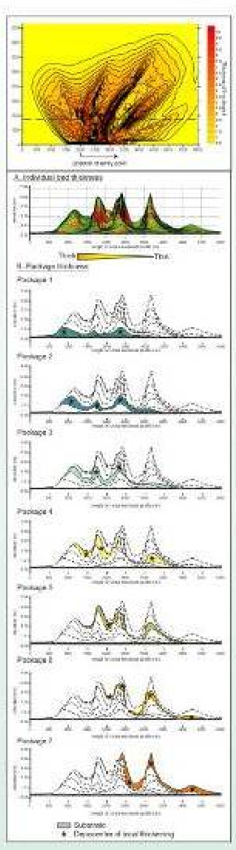

Fig. D2.3: The cross-section is located at 900 m downstream of the entry point of the flows. The cross-section at the top displays the stratigraphy, with colour coding representing individual bed thickness. In the other cross-sections, individual beds have been grouped into 7 packages, based this time on the position of the entry point of the flows that deposited them, to highlight the effect of a systematic change in the position of a distributary channel-mouth or depositional conduit on the distribution of sediment and, consequently, organised stacking pattern at the scale of packages of beds. Each package is roughly equivalent in number of beds and volume to two lobe elements.

Fig. D2.4:
The cross-section is located at 2200 m downstream of the entry point of the flows. The cross-section A displays the stratigraphy, with colour coding representing individual bed thickness. In the other cross-sections (B), individual beds have been grouped into four packages, based on spatial trends in bed thickness and grain size to illustrate lateral shifts in the locus of deposition due to the disorganized shift in entry points and the interaction of flows with depositional relief. Packages are equivalent in volume and number of beds to two to three outcrop-defined lobe elements. After Package 1, at any given time, deposition never occurs in a single area, i.e., it occurs simultaneously both to the left and right of Package 1, although at different rates.

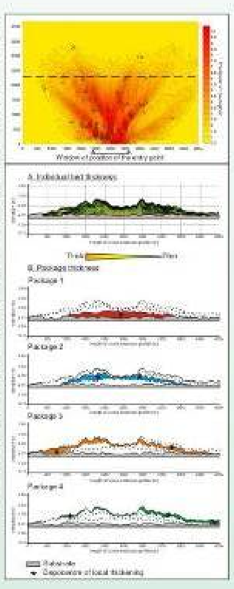

E. DISCUSSIONS AND CONLUSIONS

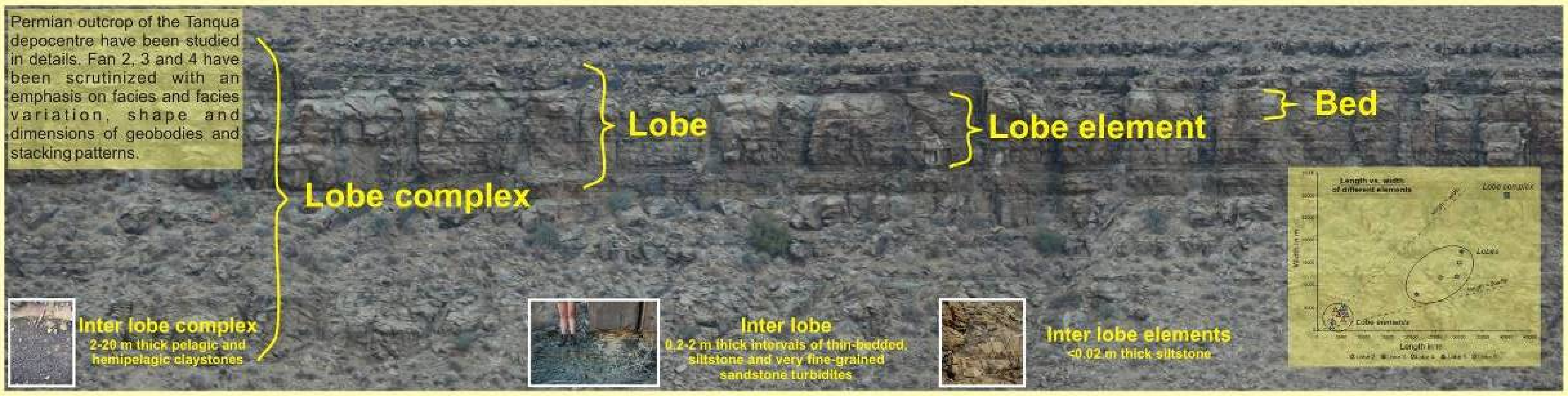

B. OUTCROP DATASET

Here, Digital Outcrop Models was built only after conceptual depositional models of the distributive systems had been developed (B). Outcrop data was used to narrow input parameters for a processed-based numerical model that was validated with the outcrop observations. The numerical model was used iteratively to test hypotheses and to refine the conceptual model (D). The refined conceptual depositional model and the quantitative data collected from the outcrops were used to construct 3D geological (reservoir) models, which can be used as a check on the conceptual model. Seismic data and physical model was not incorporated to refine the depositional model further.

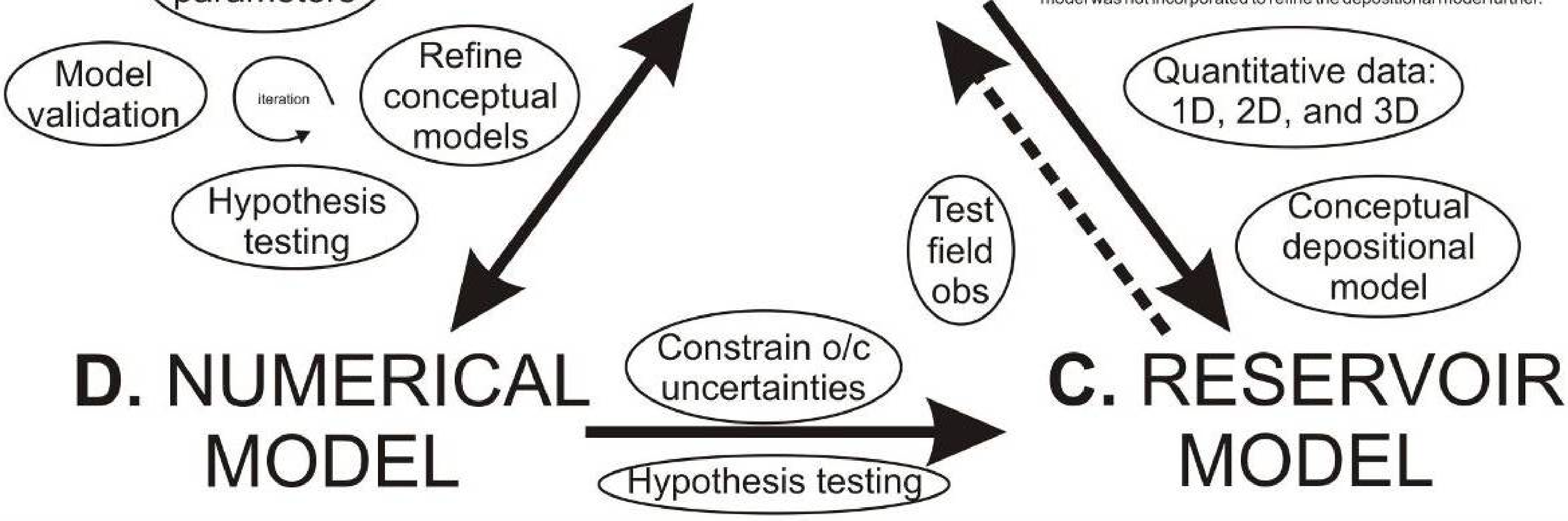

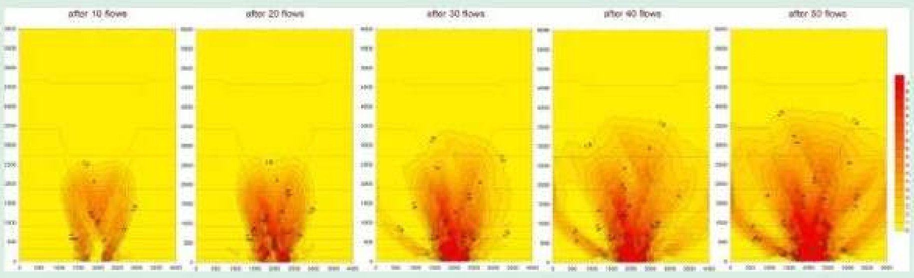

Outcrop studies give a good insight on turbidite reservoirs at interwells scale. However, the results obtained are mostly specific to the fan system under investigation, and extrapolation of findings to other fan systems often proves challenging. The 'process-based' approach focuses on the turbidity currents themselves. In addition, process-based numerical models provide a means to test and develop hypotheses developed from outcrop

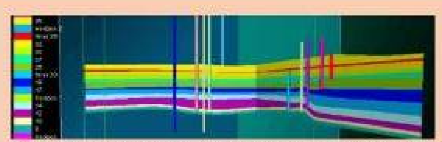

Intersection through the lower stratigraphic part of the zone model in the NB2 area. The left intersection is perpendicular to the Farm outcrop and crosses the Cliff outcrop. Vertical exaggeration is 20.

Example of lateral stacking driving by underlying depositional topography.

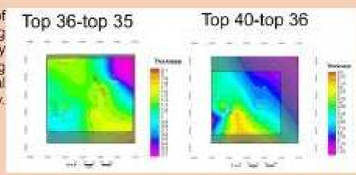

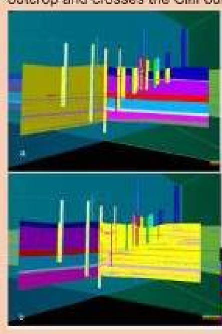

Cross-section of facies model of the NB2 model through the Cliff outcrop (a) and Gully outcrop (b).

The zone model for the NB2 area (built by Wieske Paulissen, TU Delft) represents several levels in the hierarchy of the lobe complex, and may provide insights into the trends of the zones and their stacking patterns. Since the NB2 model is based on a high-resolution field dataset it was possible to model a lobe element in one zone in the lower part of the stratigraphy and in one case even an individual bed (unit 36). Up stratigraphy, thicker packages were modelled in one zone which are lobes embedded in continuous siltstone- and mudstone-prone intervals.

E4. References

Fildani, A., Drinkwater, N.J., Weislogel, A., McHargue, T., Hodgson, D.M, Flint S.S. (2007) Age controls on the Tanqua and Laingsburg deep-water systems: New insights on the evolution and sedimentary fill of the Karoo basin, South Africa Source: Journal of sedimentary research, 77, 901 -908

Twichell DC, Schwab WC, Kenyon NH (1995) Geometry of sandy deposits at the distal edge of the Mississippi fan, Gulf of Mexico. In: Pickering KT, Hiscott RN, Kenyon NH, Ricci Lucchi F, Smith RDA (eds) Atlas of deep water environments: architectural style in turbidite systems. Chapman and Hall, London, pp 282–286

Wickens H de V (1994) Basin floor fan building turbidites of the southwestern Karoo Basin, Permian Ecca Group, South Africa. PhD Thesis, Univ Port Elisabeth, 233 pp

E5. Acknowledgments

The authors wish to thanks the LOBE consortium: Chevron, Maersk Oil, Petrobras, Petro SA, Shell, StatoilHydro and Total for sponsorising several studenships. Most of the reservoir modelling with Petrel® licences provided by Schlumberger, and the work was completed at PetroSA Cape Town and we are especially grateful for the help we received from Jody Frewin. Laura McAllister, Emily Parrott and John Kavanagh are thanks for field assistance.

Appendix B

PowerPoint presentation given at PetroSA on 18 June 2008.

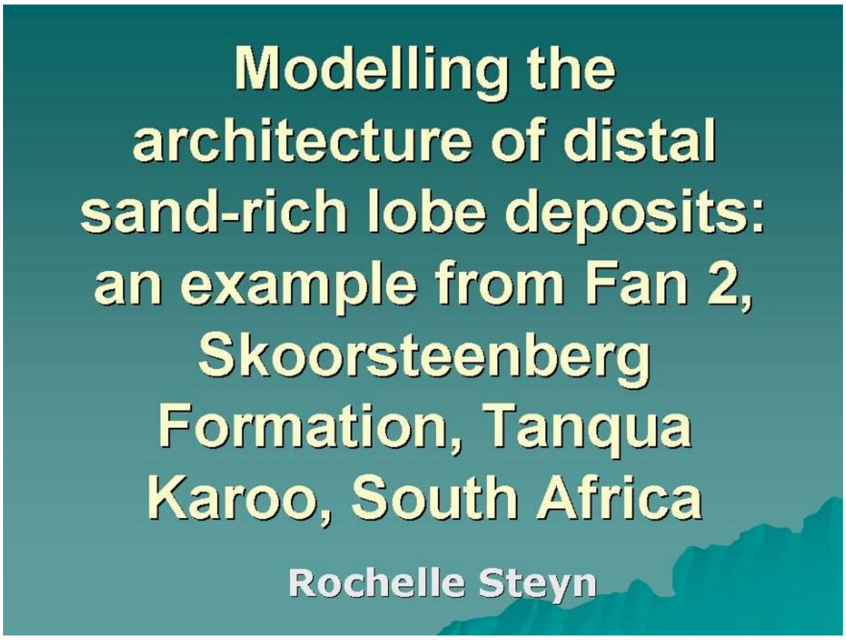

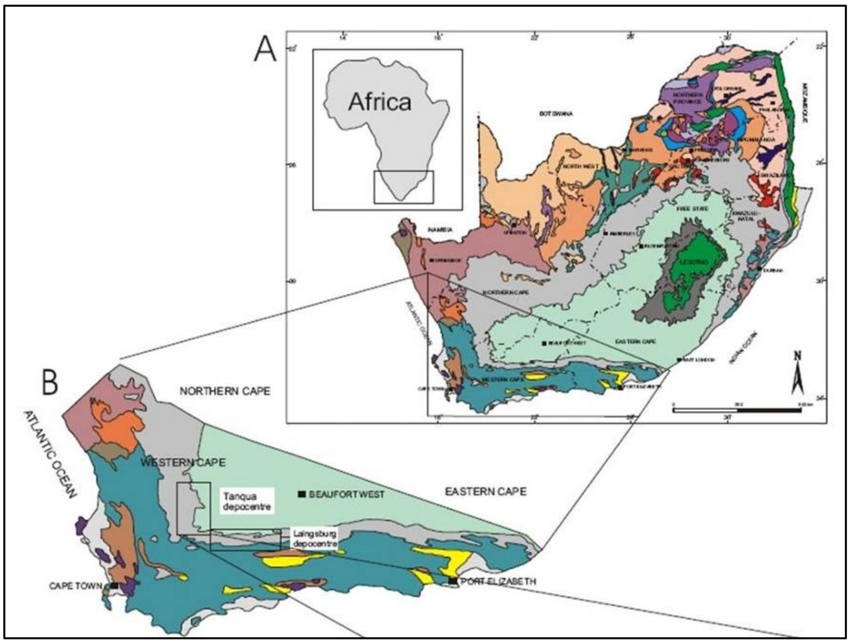

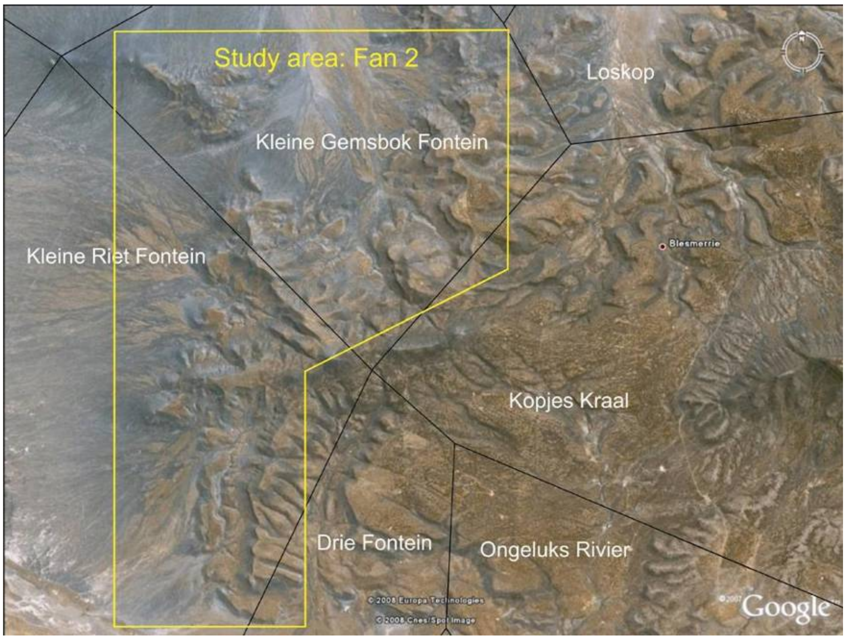

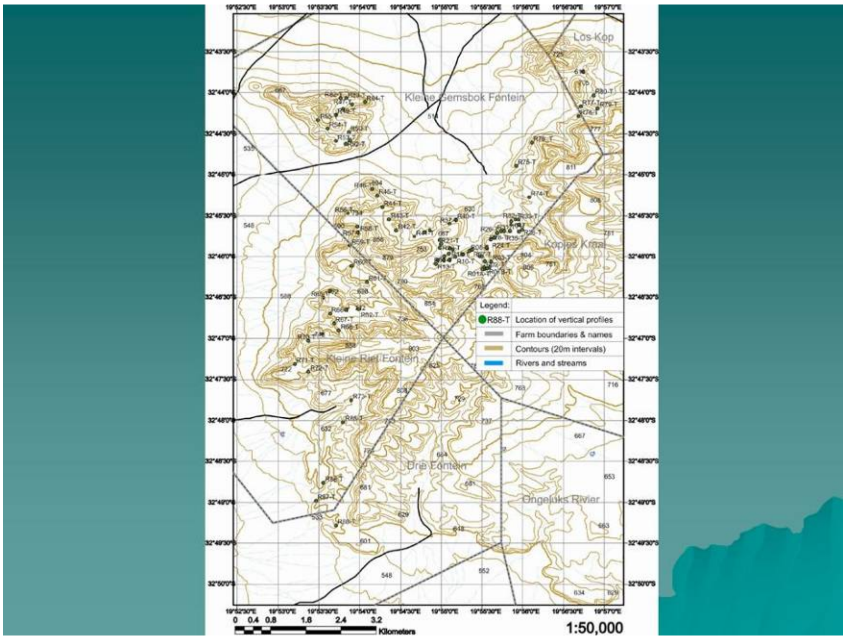

Aims

- Detailed vertical profiling in Middle Fan 2
- Detailed breakdown of lobe elements in Middle Fan 2
- Facies associations between distal turbidity current deposits and lateral pinchouts
- Dimensions of linked debrites
- Petrel data manipulation

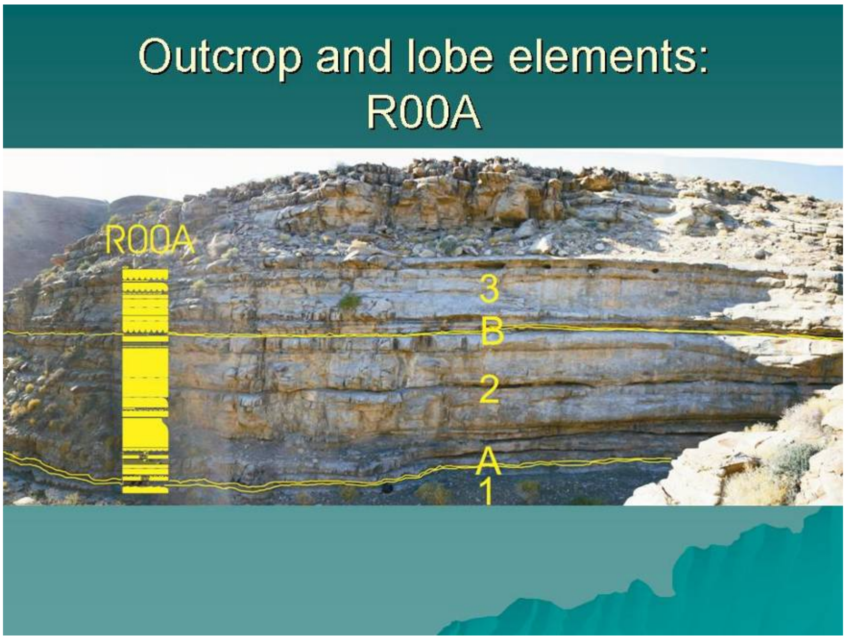
Outcrop and lobe elements:
R00A
R00A
3
B
2
A
1

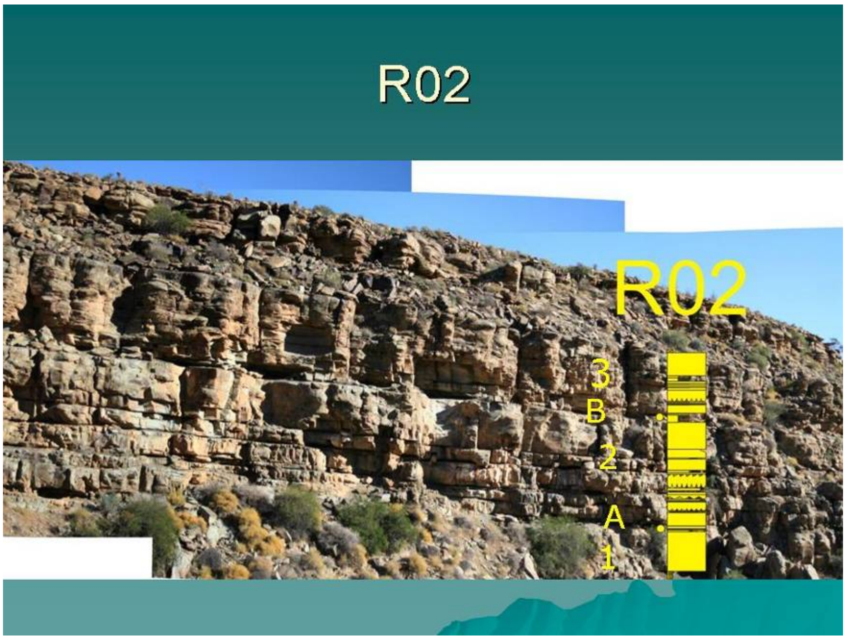
R02
R02
3
B
2
A
1

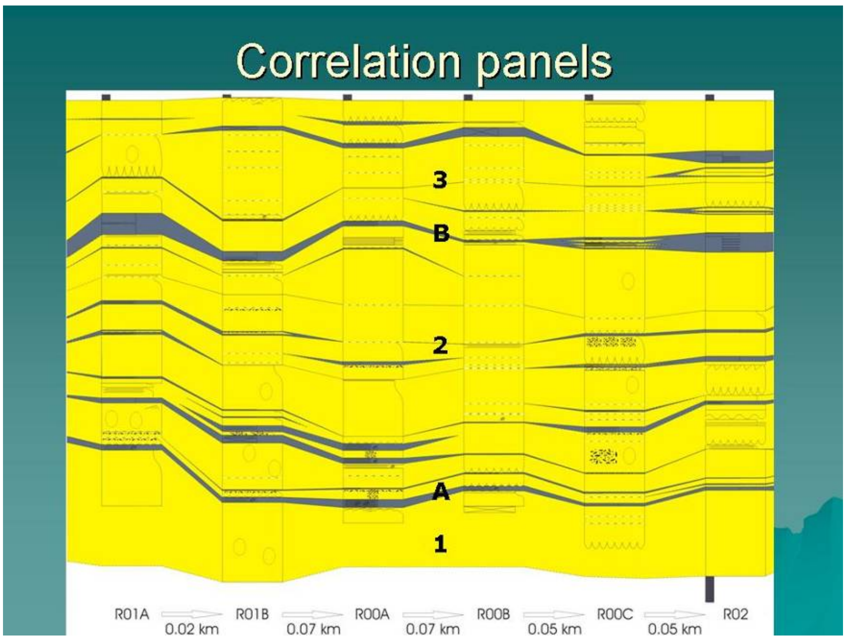
Correlation panels
3
B
2
A
1
R01A
0.02 km
R01B
0.07 km
R00A
0.07 km
R00B
0.05 km
R00C
0.05 km
R02

Chapter 3	Chapter 7.3.1	Chapter 7.3.6
Lithofacies description	DSL facies	Petrel facies associations
1) Massive sandstone	1) Structureless sandstone	1) Structureless sandstone
2) Ripple cross- and parallel-laminated sandstone	2) Structured sandstone 3) Sandstone - ripples/planar lamination	2) Structured sandstone
3) Siltstone 4) Ripple cross- and parallel-laminated siltstone	4) Siltstone/sandstone (>50% silt) 5) Sandstone/siltstone (>50% sand) 6) Laminated/rippled siltstone	3) Siltstone
5) Organic-rich debrite	7) Debrite (dominant sandstone with organics)	4) Other
6) Claystone	8) Mudstone 9) Mudstone/siltstone (>50% mud)	5) Background

	R00A		
Surfaces	X	Y	Z
Top 3	-32.7692	19.92548	649
	0.7		
	0.1		
	0.02		
	0.6		
	0.17		
	0.28		
	0.53		
	0.5		
	0.34		
Base 3/Top B	0.76	4	645
	0.15	0.15	644.85
Base B/Top 2	0.38		
	0.25		
	0.1		
	0.4		
	1.85		
	1.22		
	0.65		
	0.11		
	0.48		
	0.05		
	1.85		
	0.24		
	0.23		
	0.25		
	0.17		
	0.05		
	0.11		
	0.25		
	0.4		
	0.04		
Base 2/Top A	0.34	9.42	635.43
	0.27	0.27	635.16
Base A/Top 1	0.04		
	0.47	0.51	634.65
Base 1			

Rochelle Steyn: Top measured GPS coordinates

Rochelle Steyn: Measured thickness of sandstone lobe element

Rochelle Steyn: Measured thickness of siltstone intra-lobe element

Rochelle Steyn: Calculated GPS Z coordinate for surface Base 2/Top A

Rochelle Steyn: Bottom calculated GPS coordinate

	X	Y	Z	Z - Thickness	Base 3/Top B	Thickness	Z - Thickness	Base B/Top 2	Thickness	Z - Thickness	Base 2/Top A	Thickness
R00A-T	399360	6373789	649	645	Base 3/Top B	4	644.85	Base B/Top 2	0.15	635.43	Base 2/Top A	9.42
R00B-T	399319	6373788	646	641.38	Base 3/Top B	4.62	641.31	Base B/Top 2	0.07	633.19	Base 2/Top A	8.12
R00C-T	399356	6373839	663	658.42	Base 3/Top B	4.58	658.04	Base B/Top 2	0.38	649.62	Base 2/Top A	8.42
R01A-T	399461	6373834	641	637.26	Base 3/Top B	3.74	636.55	Base B/Top 2	0.71	629.59	Base 2/Top A	6.96
R01B-T	399413	6373810	643	637.95	Base 3/Top B	5.05	637.63	Base B/Top 2	0.32	629.81	Base 2/Top A	7.82
R02-T	399363	6373957	645	640.62	Base 3/Top B	4.38	639.97	Base B/Top 2	0.65	632.26	Base 2/Top A	7.71
R03-T	399485	6373960	645	639.68	Base 3/Top B	5.32	639.21	Base B/Top 2	0.47	636.11	Base 2/Top A	3.1
R04-T	399406	6374250	665	659.16	Base 3/Top B	5.84	658.56	Base B/Top 2	0.6	655.23	Base 2/Top A	3.33
R05A-T	399305	6374070	656	651.69	Base 3/Top B	4.31	651.16	Base B/Top 2	0.53	643.33	Base 2/Top A	7.83
R05B-T	399263	6374071	649	643.78	Base 3/Top B	5.22	643.7	Base B/Top 2	0.08	637.98	Base 2/Top A	5.72
R06-T	399398	6374267	671	665.18	Base 3/Top B	5.82	665.16	Base B/Top 2	0.02	661.01	Base 2/Top A	4.15
R07-T	399120	6374219	656	649.38	Base 3/Top B	6.62	649.2	Base B/Top 2	0.18	644.24	Base 2/Top A	4.96
R08-T	399071	6374194	668	661.56	Base 3/Top B	6.44	661.52	Base B/Top 2	0.04	657.07	Base 2/Top A	4.45
R09-T	398945	6374123	660	653.4	Base 3/Top B	6.6	653.34	Base B/Top 2	0.06	650.24	Base 2/Top A	3.1
R10-T	398799	6374055	663	656.84	Base 3/Top B	6.16	656.77	Base B/Top 2	0.07	653.88	Base 2/Top A	2.89
R11-T	398687	6373980	665	658.66	Base 3/Top B	6.34	658.58	Base B/Top 2	0.08	655.79	Base 2/Top A	2.79
R12-T	398577	6373981	667	661.53	Base 3/Top B	5.47	661.49	Base B/Top 2	0.04	658.51	Base 2/Top A	2.98
R13-T	398427	6373891	675	669.51	Base 3/Top B	5.49	669.47	Base B/Top 2	0.04	665.68	Base 2/Top A	3.79
R14-T	398468	6373977	673	667.695	Base 3/Top B	5.305	667.675	Base B/Top 2	0.02	662.395	Base 2/Top A	5.28
R15-T	398587	6374072	666	660.26	Base 3/Top B	5.74	660.22	Base B/Top 2	0.04	657.04	Base 2/Top A	3.18
R16-T	398670	6374131	658	651.32	Base 3/Top B	6.68	651.28	Base B/Top 2	0.04	648.43	Base 2/Top A	2.85
R17-T	398755	6374221	667	662.53	Base 3/Top B	4.47	662.49	Base B/Top 2	0.04	660	Base 2/Top A	2.49
R18-T	398692	6374249	662	658.48	Base 3/Top B	3.52	658.36	Base B/Top 2	0.12	655.79	Base 2/Top A	2.57
R19-T	398497	6374265	666	660.74	Base 3/Top B	5.26	660.69	Base B/Top 2	0.05	656.82	Base 2/Top A	3.87
R20-T	398521	6374348	669	664.6	Base 3/Top B	4.4	664.56	Base B/Top 2	0.04	659.79	Base 2/Top A	4.77
R21-T	398500	6374440	670	665.28	Base 3/Top B	4.72	665.21	Base B/Top 2	0.07	661.24	Base 2/Top A	3.97
R22-T	398780	6374535	680	675.26	Base 3/Top B	4.74	675.16	Base B/Top 2	0.1	671.23	Base 2/Top A	3.93
R23-T	398846	6374635	669	664.49	Base 3/Top B	4.51	664.43	Base B/Top 2	0.06	660.34	Base 2/Top A	4.09
R24-T	399472	6374454	660	654.61	Base 3/Top B	5.39	654.49	Base B/Top 2	0.12	650.15	Base 2/Top A	4.34
R25-T	399547	6374507	657	652.28	Base 3/Top B	4.72	651.99	Base B/Top 2	0.29	647.54	Base 2/Top A	4.45
R26-T	399593	6374607	653	647.87	Base 3/Top B	5.13	647.79	Base B/Top 2	0.08	643.99	Base 2/Top A	3.8
R27-T	399666	6374653	653	648.8	Base 3/Top B	4.2	648.52	Base B/Top 2	0.28	644.45	Base 2/Top A	4.07

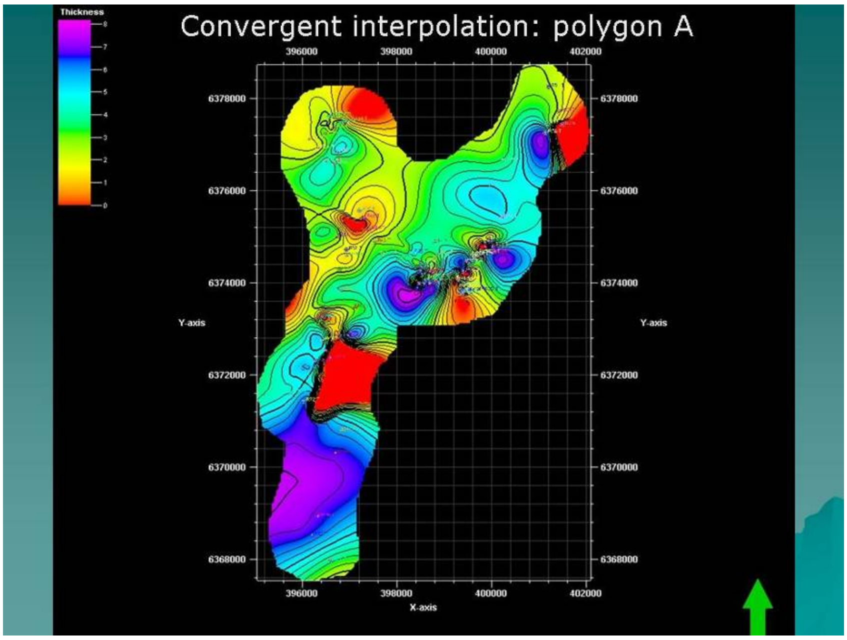
Thickness
Convergent interpolation: polygon A
396000
398000
400000
402000
6378000
6376000
6374000
6372000
6370000
6368000
Y-axis
X-axis

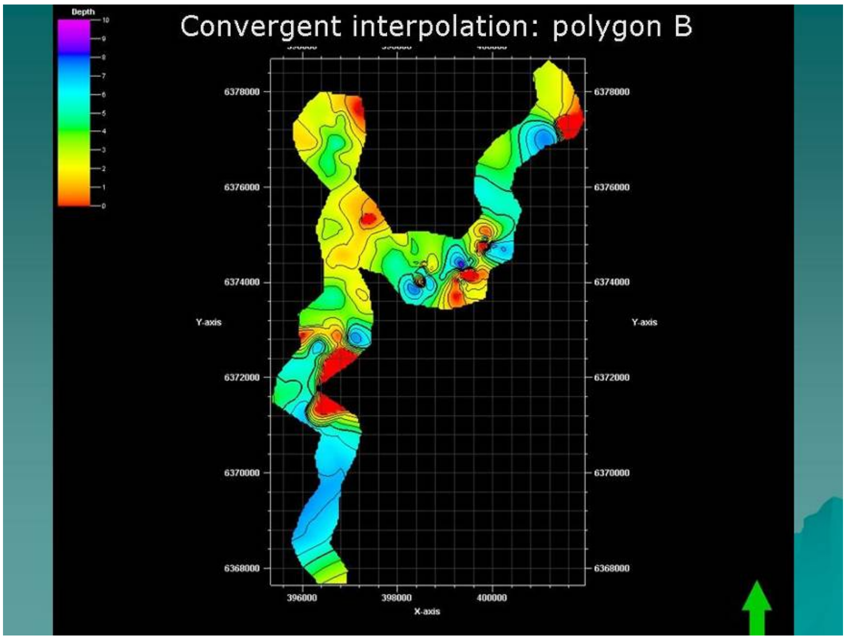
Depth
Convergent interpolation: polygon B
6378000
6376000
6374000
6372000
6370000
6368000
396000
398000
400000
Y-axis
X-axis

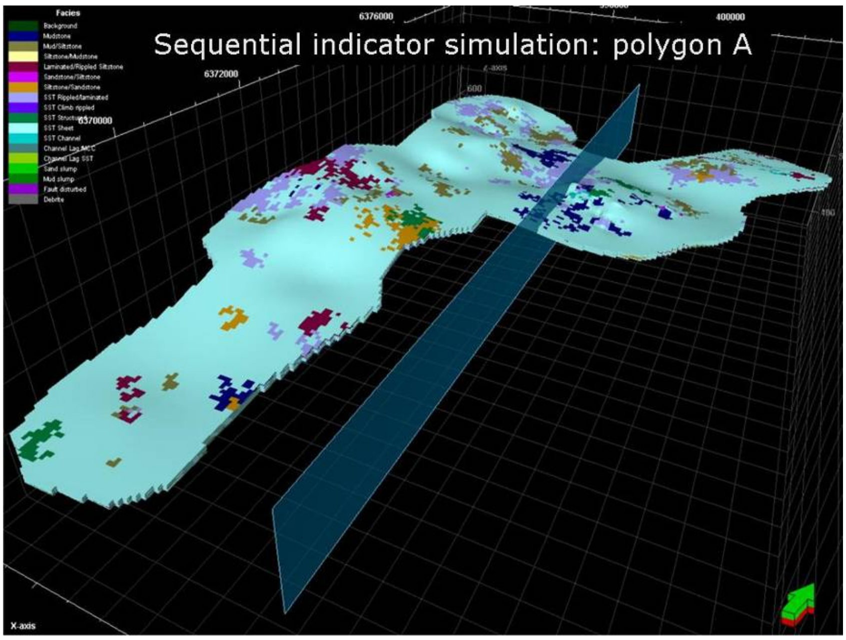
Facies
Background
Mudstone
Mud/Siltstone
Siltstone/Mudstone
Laminated/Rippled Siltstone
Sandstone/Siltstone
Siltstone/Sandstone
SST Rippled/laminated
SST Climb rippled
SST Sheet
SST Channel
Sand slump
Mud slump
Fault disturbed
Debrite
Sequential indicator simulation: polygon A
6376000
400000
6372000
6370000
X-axis

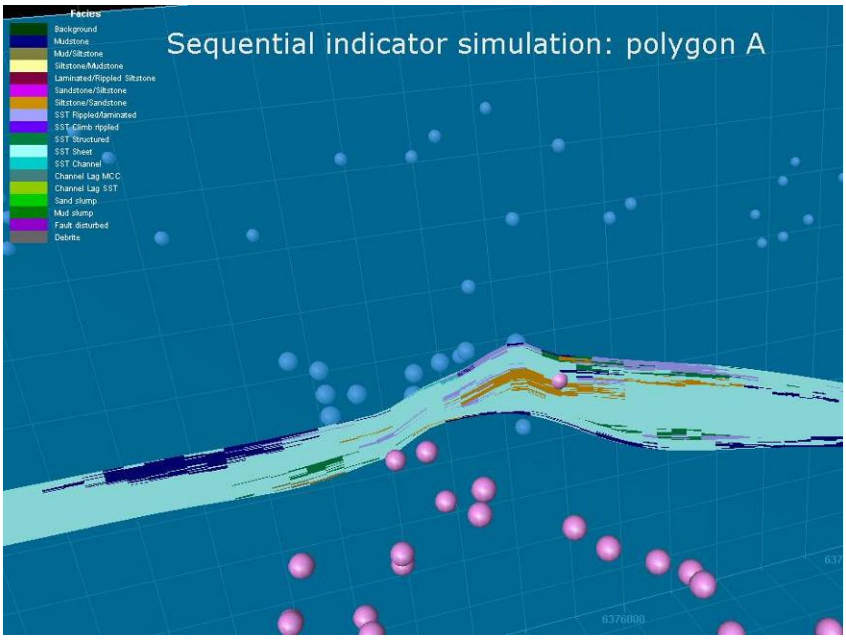
Facies
Background
Mudstone
Mud/Siltstone
Siltstone/Mudstone
Laminated/Rippled Siltstone
Sandstone/Siltstone
Siltstone/Sandstone
SST Rippled/laminated
SST Climb rippled
SST Structured
SST Sheet
SST Channel
Channel Lag MCC
Channel Lag SST
Sand slump
Mud slump
Fault disturbed
Debrite
Sequential indicator simulation: polygon A
6376000

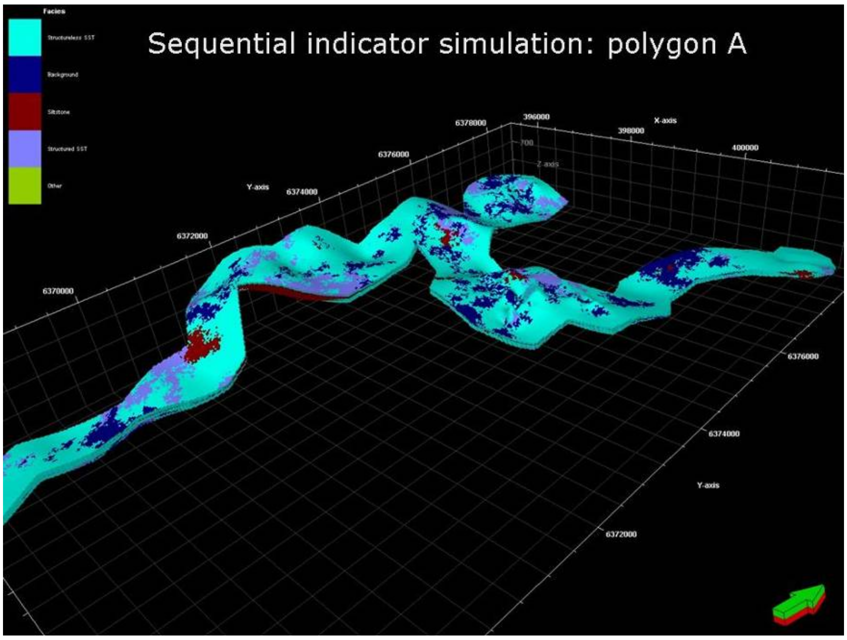
Facies
Structureless SST
Background
Siltstone
Structured SST
Other
Sequential indicator simulation: polygon A
6378000
396000
398000
400000
X-axis
Z-axis
6376000
Y-axis
6374000
6372000
6370000
6376000
6374000
Y-axis
6372000

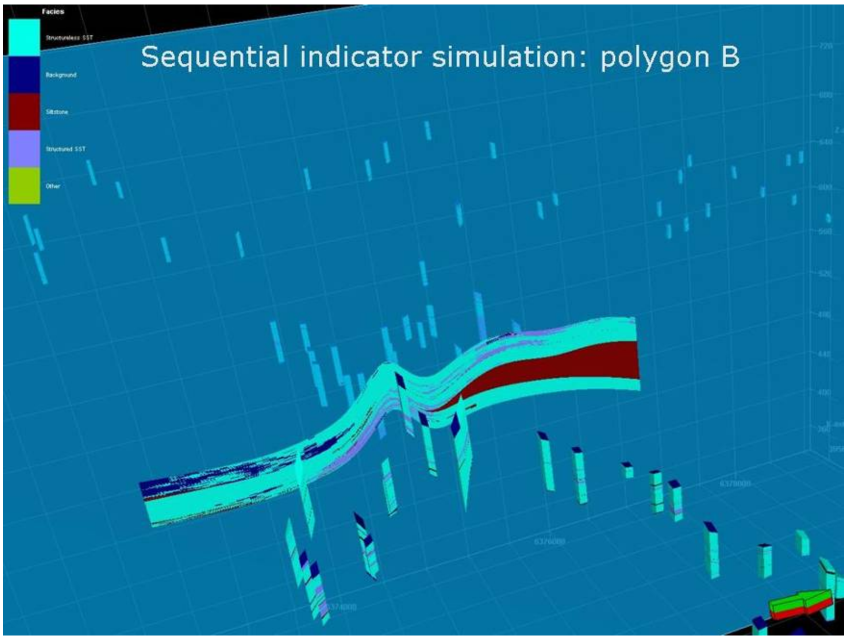
Facies
Structureless SST
Background
Siltstone
Structured SST
Other
Sequential indicator simulation: polygon B

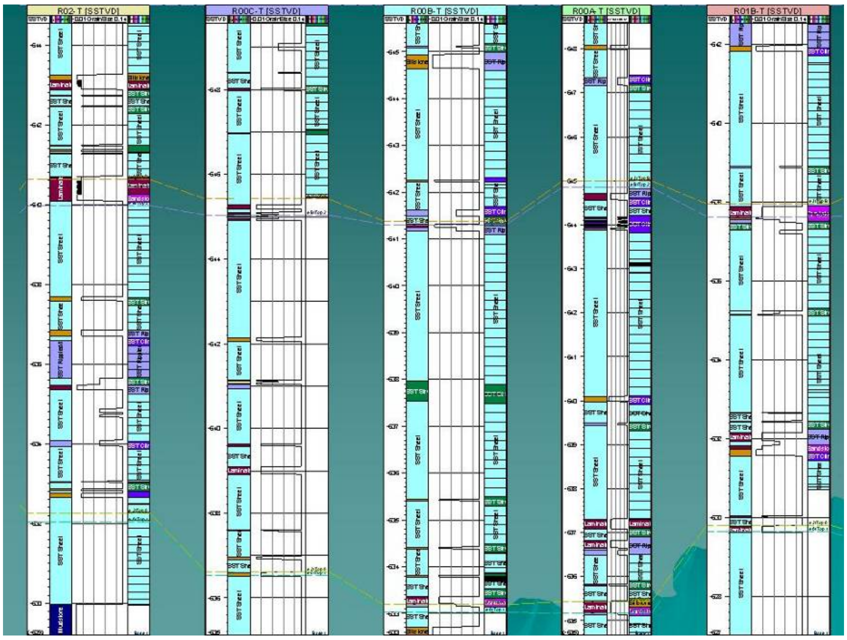

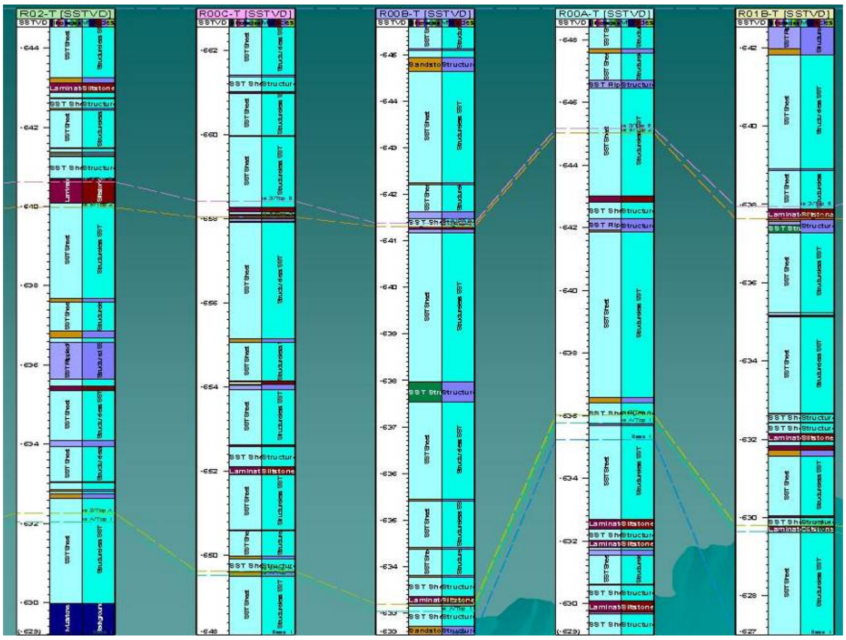

Conclusions

- Iterative process
- Official Petrel training needed
- Data not suitable?
- Hand-in: 1 September 2008

- Questions?

- Thank you

Appendix C

Isopach maps using the Kriging algorithm and convergent interpolation with polygon A (A and B on Figure 101 to Figure 105) and convergent interpolation with polygon B (C and D on Figure 101 to Figure 105).

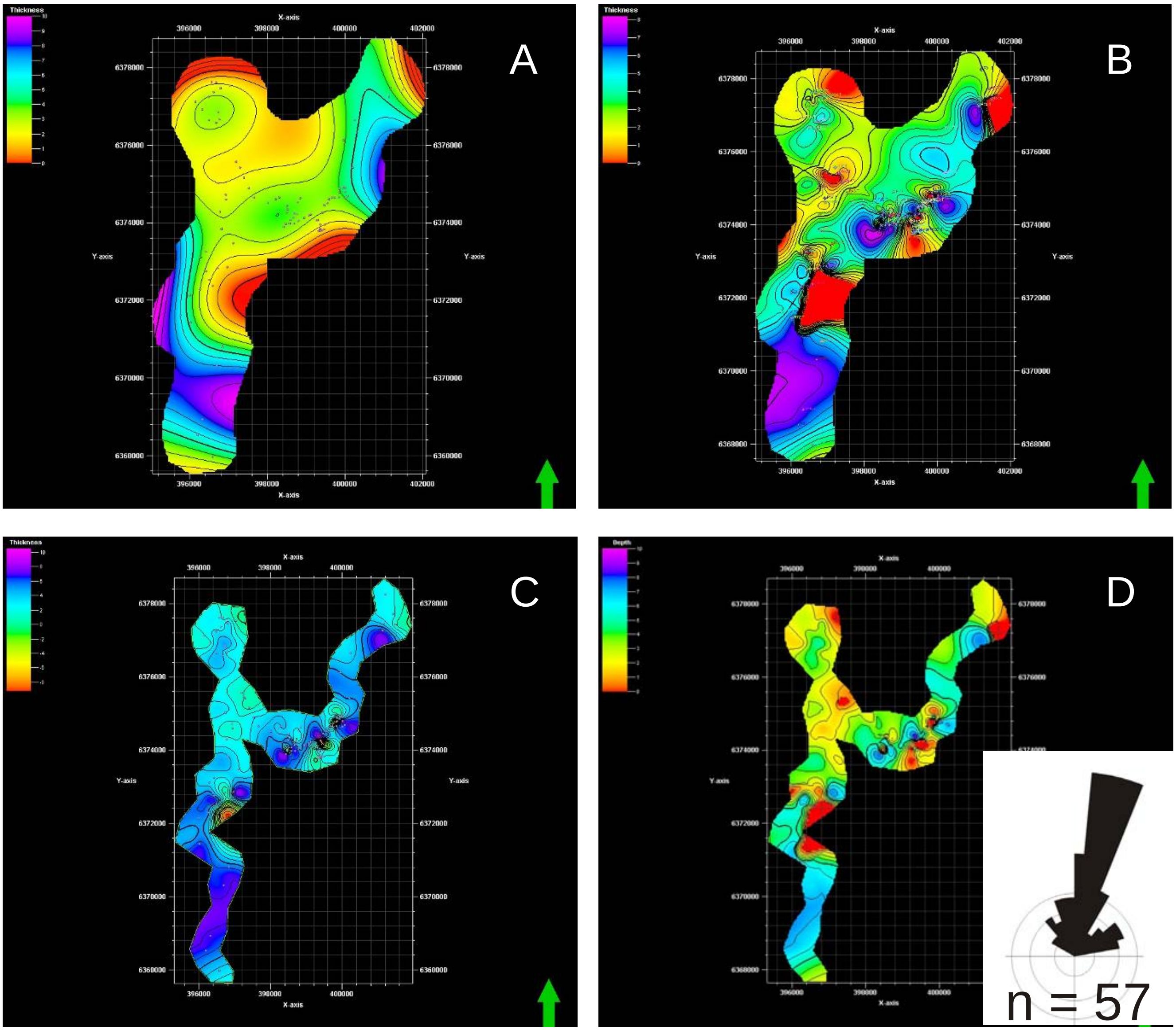

Figure 101: Isopach maps for sandstone-lobe element 1 using Kriging interpolation (A) and convergent interpolation (B) with polygon A, convergent interpolation with polygon B at a range of 50 metres (C), and convergent interpolation with polygon B at a range of 5 metres (D).

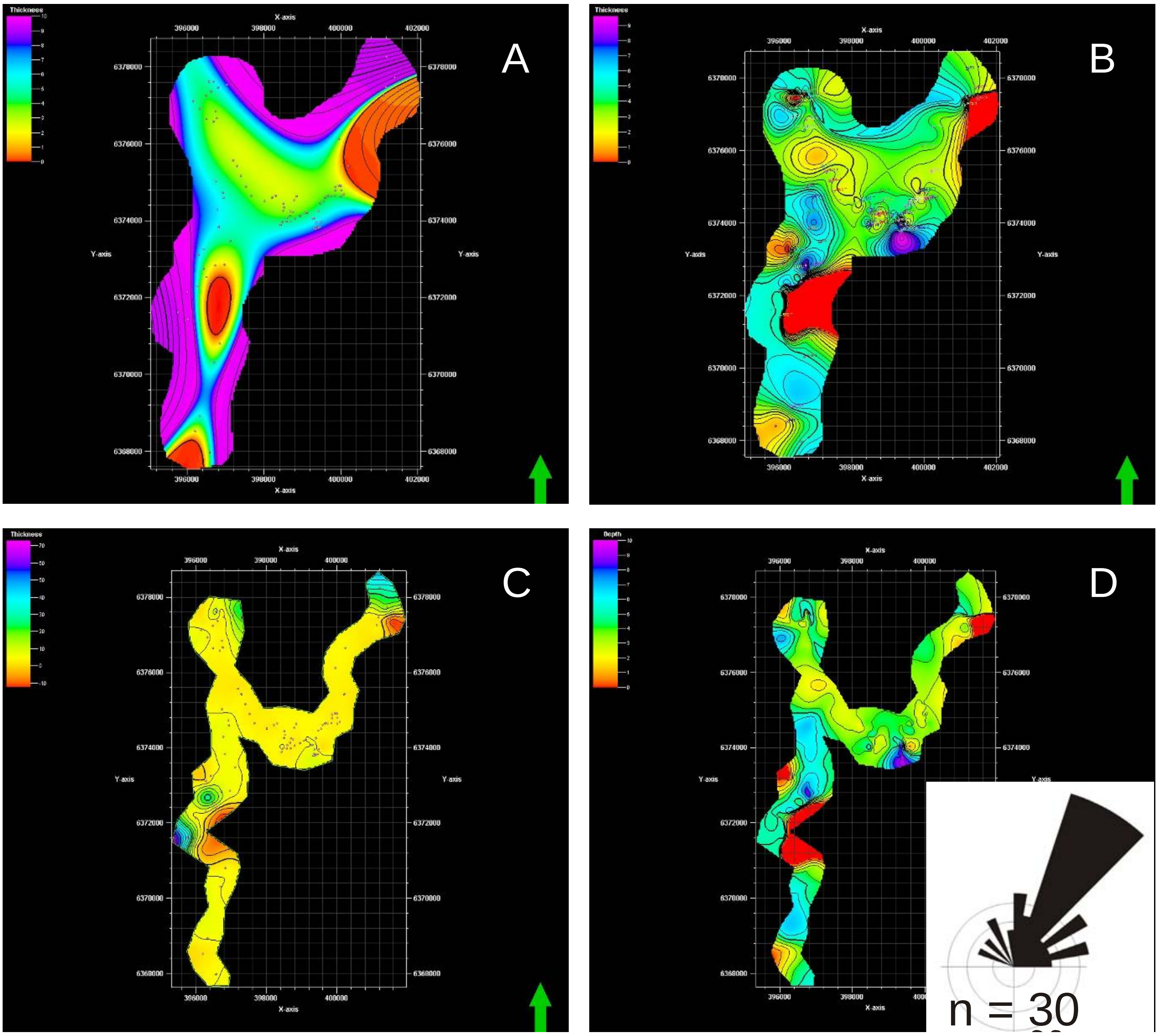

Figure 102: Isopach maps for sandstone-lobe element 2 using Kriging interpolation (A) and convergent interpolation (B) with polygon A, convergent interpolation with polygon B at a range of 50 metres (C), and convergent interpolation with polygon B at a range of 5 metres (D).

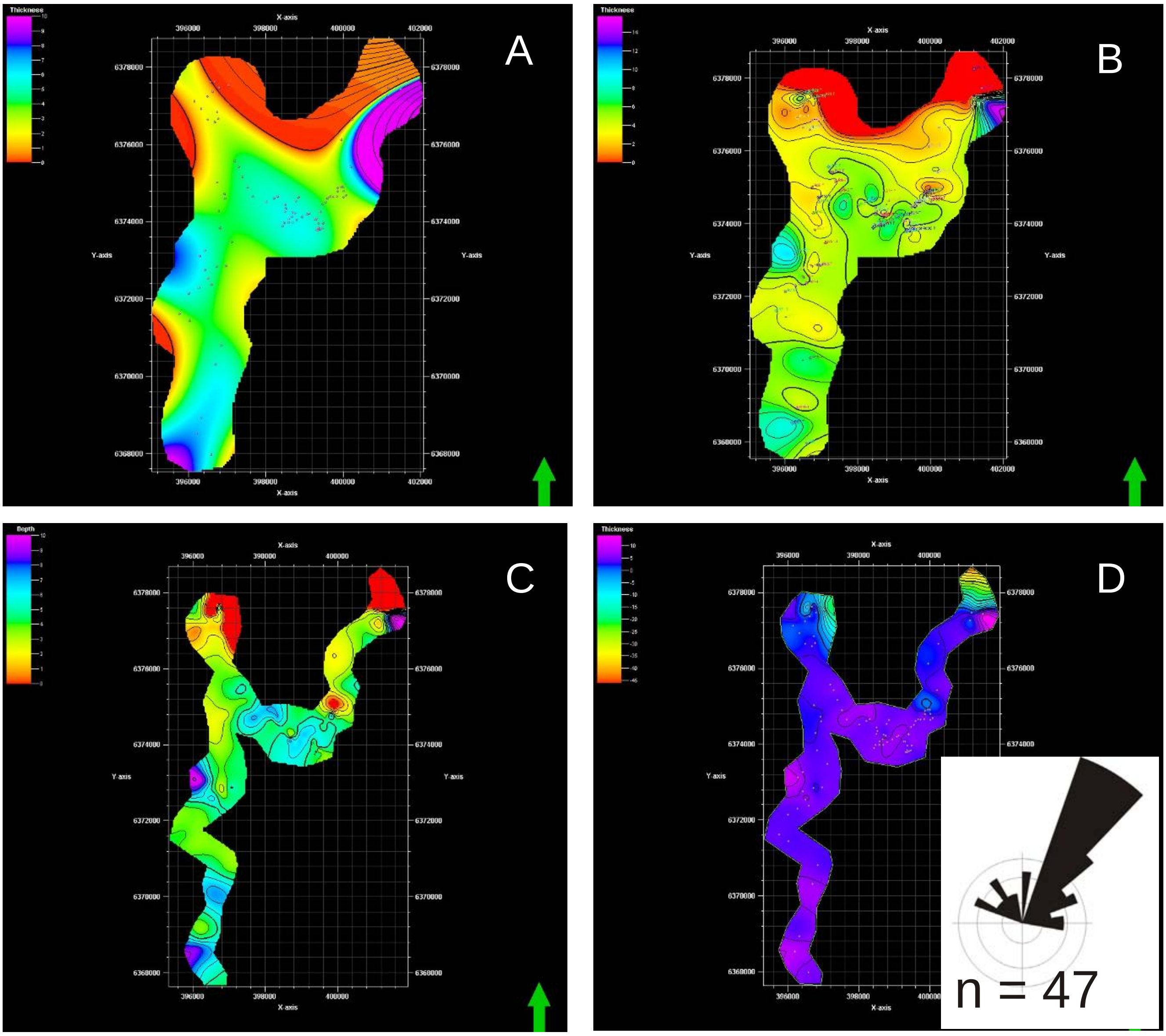

Figure 103: Isopach maps for sandstone-lobe element 3 using Kriging interpolation (A) and convergent interpolation (B) with polygon A, convergent interpolation with polygon B at a range of 50 metres (C), and convergent interpolation with polygon B at a range of 5 metres (D).

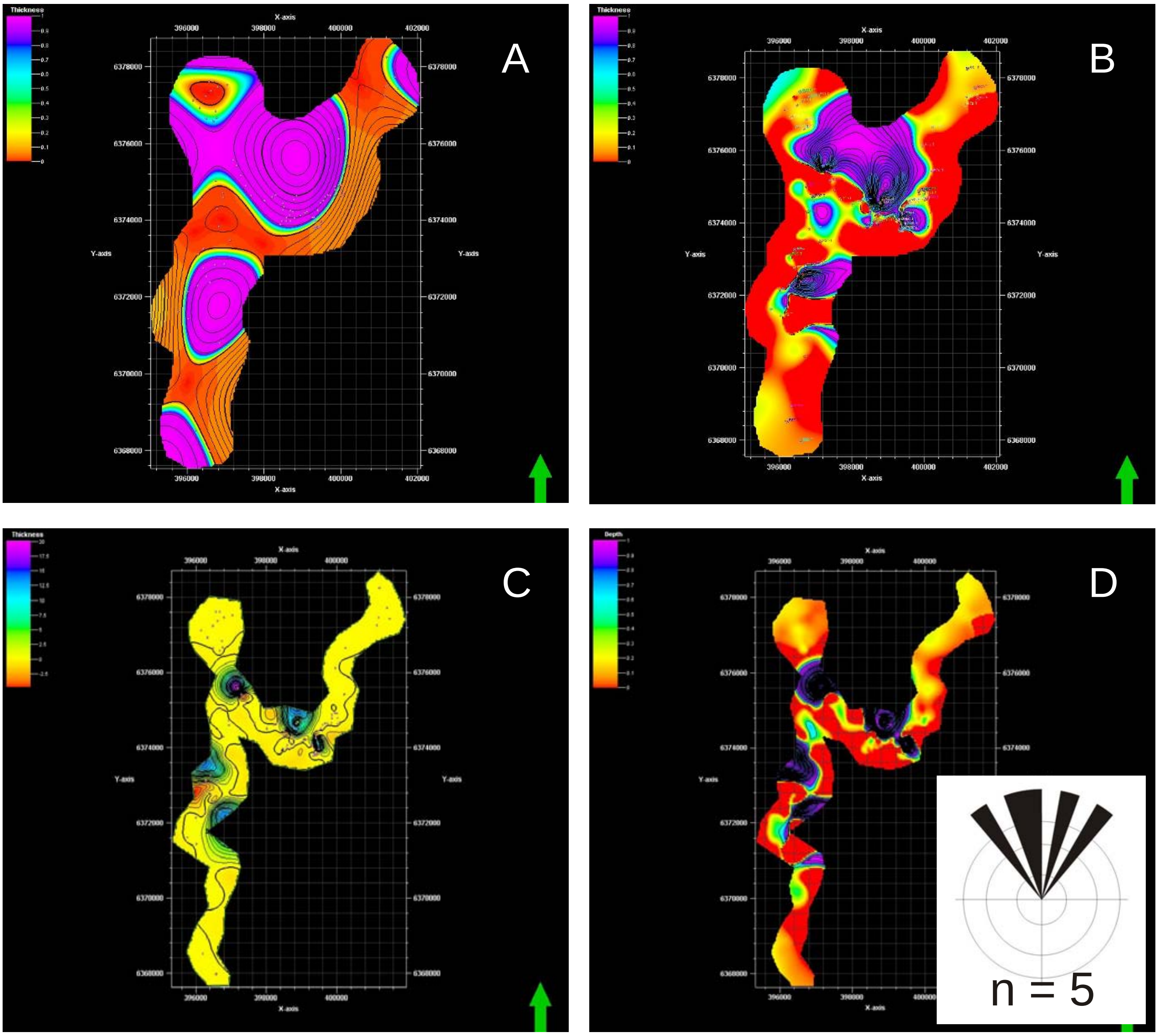

Figure 104: Isopach maps for siltstone intra-lobe element A using Kriging interpolation (A) and convergent interpolation (B) with polygon A, and convergent interpolation with polygon B at a range of 50 metres (C), and convergent interpolation with polygon B at a range of 5 metres (D).

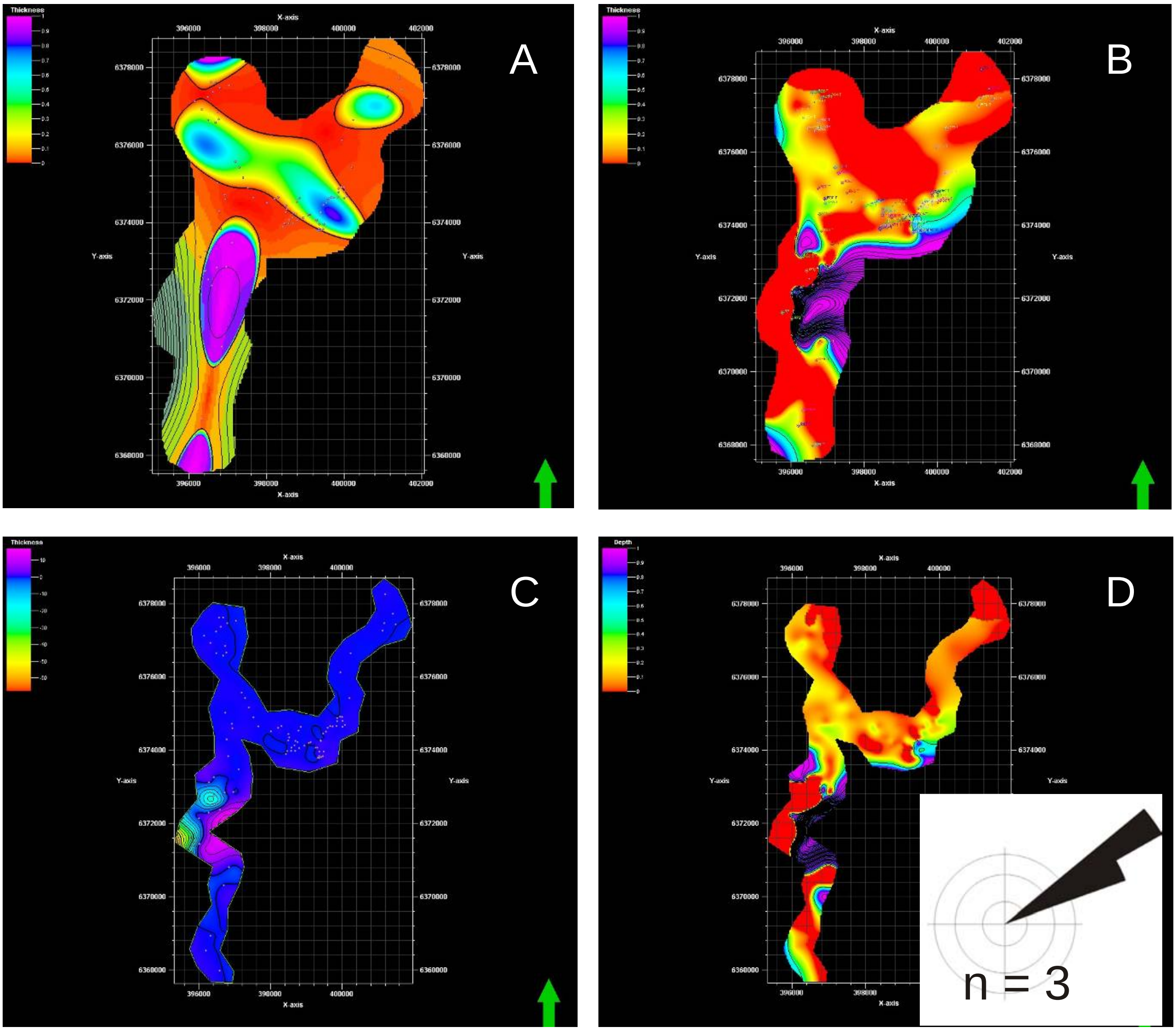

Figure 105: Isopach maps for siltstone intra-lobe element B using Kriging interpolation (A) and convergent interpolation (B) with polygon A, convergent interpolation with polygon B at a range of 50 metres (C), and convergent interpolation with polygon B at a range of 5 metres (D).